Efficient Calculation of Gluon Amplitudes with n Legs and An Implementation of Parton Showers Using the Dipole Formalism

Dissertation zur Erlangung des Grades
„Doktor der Naturwissenschaften“
am Fachbereich Physik, Mathematik und Informatik
der Johannes Gutenberg-Universität in Mainz

Marko Ternick

geboren in Lübben (Spreewald)

Mainz 2010

Erstgutachter: Prof. Dr. Stefan Weinzierl
Zweitgutachter: Prof. Dr. Hartmut Wittig
Datum der mündlichen Prüfung: 5. Oktober 2010
Dissertation Universität Mainz (D77)

Dedicated to Renate

Dum vivo spero

Summary

The conventional way to calculate hard scattering processes in perturbation theory using Feynman diagrams is not efficient enough to calculate all necessary processes – for example for the Large Hadron Collider – to a sufficient precision. Two alternatives to order-by-order calculations are studied in this thesis.

In the first part we compare the numerical implementations of four different recursive methods for the efficient computation of Born gluon amplitudes: Berends–Giele recurrence relations and recursive calculations with scalar diagrams, with maximal helicity violating vertices and with shifted momenta. From the four methods considered, the Berends–Giele method performs best, if the number of external partons is eight or bigger. However, for less than eight external partons, the recursion relation with shifted momenta offers the best performance. When investigating the numerical stability and accuracy, we found that all methods give satisfactory results.

In the second part of this thesis we present an implementation of a parton shower algorithm based on the dipole formalism. The formalism treats initial- and final-state partons on the same footing. The shower algorithm can be used for hadron colliders and electron–positron colliders. Also massive partons in the final state were included in the shower algorithm. Finally, we studied numerical results for an electron–positron collider, the Tevatron and the Large Hadron Collider.

Zusammenfassung

Die herkömmliche Möglichkeit harte Streuprozesse in der Störungstheorie mittels Feynman-Diagrammen zu berechnen, ist nicht effizient genug, um alle notwendigen Prozesse – beispielsweise für den Large Hadron Collider – mit ausreichender Präzision zu bestimmen. Zwei Alternativen zur Berechnung Ordnung für Ordnung werden in dieser Arbeit untersucht.

Im ersten Teil vergleichen wir die numerische Umsetzung von vier verschiedenen rekursiven Methoden zur effizienten Berechnung von Gluonamplituden auf Born-Niveau: die Berends-Giele-Rekursionsrelation sowie rekursive Berechnungen mit skalaren Diagrammen, mit maximal helizitätsverletzenden Vertices und mit verschobenen Impulsen. Von diesen vier Methoden liefert die Berends-Giele-Methode die beste Leistung, wenn die Anzahl der externen Partonen acht oder größer ist. Für weniger als acht externe Partonen ist dagegen die Rekursionsbeziehung mit verschobenen Impulsen die Beste. Bei Untersuchungen zur numerischen Stabilität und Genauigkeit fanden wir, dass alle Methoden gute Resultate liefern.

Im zweiten Teil präsentieren wir eine Implementierung eines Partonschaueralgorithmus', der auf dem Dipolformalismus basiert. Dieser Formalismus behandelt einlaufende und auslaufende Partonen gleich. Der Schaueralgorithmus kann sowohl für Hadronencollider als auch für Elektron-Positron-Collider verwendet werden. Auch massebehaftete auslaufende Partonen wurden im Algorithmus einbezogen. Außerdem studierten wir die numerischen Resultate für einen Elektron-Positron-Collider, für das Tevatron und für den Large Hadron Collider.

Contents

Preface

The Large Hadron Collider (LHC) at CERN, the largest machine in human history and the experiment the particle physicists community was waiting for, was built in the last years in Geneva, Switzerland. This proton–proton collider has a planned centre of mass energy of 14 TeV and a design peak luminosity of $10^{34}\,\mathrm{cm}^{-2}\,\mathrm{s}^{-1}$ which is about two orders of magnitude bigger than the peak luminosity of the Tevatron at Fermilab, Batavia, Illinois. The aim of the LHC is not only to test the Standard Model (SM) in energy ranges where it was not possible to test it before, but also to finally prove or disprove the existence of the predicted Higgs boson. The detection of this boson would be a great success in particle physics, because it is hunted since more than 40 years, when the model was first introduced. Other SM processes are also on the agenda, like top-quark physics, B-physics, the physics of $W^{\pm}$ and Z^0, and heavy-ion physics. Perhaps the second most prominent aim of LHC – after the Higgs – is the search for "new physics", such as supersymmetry (SUSY) – especially the search for the SUSY Higgs bosons and the lightest supersymmetric particle –, and additional spatial dimensions, so-called large extra dimensions. The Standard Model, the LHC and its physics programme are presented in section 1.1 of chapter 1.

The conventional way to calculate hard scattering processes in particle physics is to look at all permitted Feynman diagrams and use the Feynman rules to obtain the amplitude. Than one takes the squared absolute value of the sum of all amplitudes, and sums or averages over the polarisations (or any other degree of freedom). This way is not feasible for final states with many particles as they occur in colliders with very high energies like the LHC. In fact, this approach already reaches its limit at Born amplitudes for about five external partons. The problems are: there are too many diagrams, there are too many terms in each diagram and there are too many kinematic variables. It is a drawback of the method that intermediate results in the calculations are orders of magnitude more complicated than the final one.

In the 1980s, some new methods were developed to avoid these difficulties. One is the *spinor-helicity method*, another the *colour decomposition*. In the spinor-helicity method a new set of kinematical variables is introduced and the polarisation vectors are written in terms of these spinor products. The colour decomposition splits amplitudes into a trace over colour matrices and a so-called partial amplitude which contains the kinematical information. Both techniques develop their full power when combined with recurrence relations that construct the amplitudes recursively from smaller building blocks. The Berends–Giele recurrence relations were historically the first ones. In the 2000s, new methods for the calculation of helicity amplitudes in quantum chromodynamics (QCD) were contrived, inspired by a relationship of QCD amplitudes to twistor string theory. The Cachazo–Svrček–Witten approach constructs tree-level QCD amplitudes from vertices that are off-shell continuations of maximal helicity

violating (MHV) amplitudes connected by scalar propagators. Subsequently, a set of recursion relations has been found that involves only on-shell amplitudes with shifted, complex, external momenta. Schwinn and Weinzierl presented a method, which is close in spirit to the Berends–Giele recursion relations, but which involves only a set of primitive vertices and scalar propagators. In section 1.2 of chapter 1 these methods for the numerical computation of pure gluonic amplitudes in the Born approximation are introduced and in chapter 2 we compare the efficiency for different numbers of gluons.

High-energy SM events, as well as "new physics" events, will produce final states with high particle multiplicities. Especially at hadron colliders one has not only the hard interaction but also the so-called underlying event, which is the interaction of the coloured beam remnants. Since SM processes are background to "new physics", it is important to make precise theoretical SM predictions to compare with experimental results when they are available. For these predictions Monte Carlo event generators like PYTHIA, HERWIG, ISAJET and SHERPA were developed. They consist of different steps: at a high energy scale, the hard interaction of quarks or gluons from each of the incoming protons is taken into account, with initial momentum of the quarks or gluons given by the structure functions. This parton interaction is calculated in perturbative QCD. Then the coloured initial- and final-state particles from the scattering process radiate gluons and parton showers evolve. The shower evolution will go on until the energy is of the order of $\Lambda_{\mathrm{QCD}} \approx 200\,\mathrm{MeV}$. Afterwards hadronisation will collect the partons to form hadrons, which can subsequently decay into final-state particles observable in the detector. On top of that, the already mentioned underlying event is incorporated in event generators. In chapter 3 we present an implementation of a parton shower algorithm for hadron colliders and electron–positron colliders, based on the dipole factorisation formulæ. Chapters 2 and 3 can be read independent of each other.

Chapter 4 summarises the results. Useful formulæ are collected in the appendix. The bibliography and an acknowledgement conclude the thesis.

Chapter 1

Introduction

In the first section of this chapter we review the Standard Model of Particle Physics, some extensions of the Standard Model, the physics programme of the Large Hadron Collider, the machine and the detectors. The second section presents perturbation theory, Feynman diagrams and some more efficient methods that circumvent some of the drawbacks of Feynman diagrams, namely colour decomposition, the spinor-helicity method and the Berends–Giele recursion relations. The connection from twistor string theory to Yang–Mills perturbation theory is mentioned and the proof of the Britto–Cachazo–Feng–Witten recursion relation is shown. In the last section of this chapter, an introduction to parton showers is given.

1.1 The Standard Model and the Large Hadron Collider

1.1.1 The Standard Model

The Standard Model (SM) of Particle Physics (for a newer textbook see for example [1]) is a relativistic quantum field theory [2] and was developed in the 1960s and 1970s. It describes all the interactions (table 1.2) of subatomic particles, except gravity. The SM gauge group is $SU_c(3) \times SU_L(2) \times U_Y(1)$ containing the strong [3–7] as well as the weak and electromagnetic interactions [8–10]. $SU(n)$ is the special unitary group consisting of unitary $n \times n$ matrices with determinant 1 and $U(n)$ the group of unitary $n \times n$ matrices. The subscript c stands for colour, L means that only left-handed particles take part in the weak interactions and Y stands for the weak hypercharge $Y = 2(Q - I_3)$ [11–13], where Q is the electric charge and I_3 the third component of the weak isospin. The fundamental particles – quarks [14, 15] and leptons – are shown in table 1.1. Additionally, quarks carry a colour charge and for all particles there are corresponding antiparticles. Quarks can be combined to mesons, consisting of a quark and an antiquark, and baryons, made of three quarks. For properties of the fundamental particles as well as hadrons see the Review of Particle Physics [16].

The Standard Model Lagrangian density

$$\mathcal{L}_{\mathrm{SM}} = \mathcal{L}_{\mathrm{c}} + \mathcal{L}_{\mathrm{w}} + \mathcal{L}_{\mathrm{f}} + \mathcal{L}_{\mathrm{fH}} + \mathcal{L}_{\mathrm{fc}} + \mathcal{L}_{\mathrm{FPc}} + \mathcal{L}_{\mathrm{FPw}} \tag{1.1}$$

consists of a colour Lagrangian density $\mathcal{L}_{\mathrm{c}}$, describing the gluons of quantum chromodynamics and their mutual interactions, a weak Lagrangian density $\mathcal{L}_{\mathrm{w}}$, describing the vector

bosons and their interactions including the interactions with the Higgs system, a fermion Lagrangian density $\mathcal{L}_{\mathrm{f}}$, describing the interactions of the fermions with the weak vector bosons, a fermion–Higgs Lagrangian density $\mathcal{L}_{\mathrm{fH}}$, describing the interactions of fermions with the Higgs system, a fermion–colour Lagrangian density $\mathcal{L}_{\mathrm{fc}}$, describing the interactions of fermions with gluons, a Faddeev–Popov ghost [17] Lagrangian density $\mathcal{L}_{\mathrm{FPc}}$ of quantum chromodynamics and a Faddeev–Popov ghost Lagrangian density $\mathcal{L}_{\mathrm{FPw}}$ of the weak interactions. The full Standard Model Lagrangian density is given in appendix A.1.

	charge	Generation 1		Generation 2		Generation 3	
Quarks	$+2/3$	up	u	charm	c	top	t
	$-1/3$	down	d	strange	s	bottom	b
Leptons	0	electron neutrino	ν_e	muon neutrino	ν_μ	tau neutrino	ν_τ
	-1	electron	e	muon	μ	tau	τ

Table 1.1: *The elementary Standard Model fermions (spin=1/2).*

interaction	strong	electromagnetic	weak	gravity
force carrier	8 gluons	photon γ	$W^{\pm}$, Z^0	(graviton)
spin	1	1	1	2
mass in GeV	0	0	≈ 80.4, ≈ 91.2	0
relative strength	25	1	0.8	10^{-41}
acts on	colour charge	flavour	electric charge	mass, energy

Table 1.2: *The four fundamental forces. Gravity is not a part of the Standard Model and the graviton is not observed, yet. The strength of the forces is relative to the strength of the electromagnetic force for two up quarks at a distance of* 10^{-18} *m.*

The mixing in the quark sector manifests itself in the Cabibbo–Kobayashi–Maskawa (CKM) matrix [18, 19]:

$$V = \begin{pmatrix} c_{12}c_{13} & s_{12}c_{13} & s_{13}e^{-i\delta} \\ -s_{12}c_{23} - c_{12}s_{23}s_{13}e^{i\delta} & c_{12}c_{23} - s_{12}s_{23}s_{13}e^{i\delta} & s_{23}c_{13} \\ s_{12}s_{23} - c_{12}c_{23}s_{13}e^{i\delta} & -c_{12}s_{23} - s_{12}c_{23}s_{13}e^{i\delta} & c_{23}c_{13} \end{pmatrix}, \tag{1.2}$$

where $c_{ij} = \cos\theta_{ij}$ and $s_{ij} = \sin\theta_{ij}$ with the mixing angles θ_{ij} (θ_{12} is the Cabibbo angle). The phase δ is responsible for CP violation. The CKM matrix V transforms the weak eigenstates on the right-hand side into the mass eigenstates on the left-hand side:

$$\begin{pmatrix} d' \\ s' \\ b' \end{pmatrix} = \begin{pmatrix} V_{ud} & V_{us} & V_{ub} \\ V_{cd} & V_{cs} & V_{cb} \\ V_{td} & V_{ts} & V_{tb} \end{pmatrix} \begin{pmatrix} d \\ s \\ b \end{pmatrix}. \tag{1.3}$$

The corresponding matrix for the lepton sector is the Pontecorvo–Maki–Nakagawa–Sakata (PMNS) matrix [20–22] $U = V_\nu K$, where V_ν can be parametrised in the same way as the

CKM matrix in equation (1.2), and

$$K = \begin{pmatrix} e^{i\alpha_1/2} & 0 & 0 \\ 0 & e^{i\alpha_2/2} & 0 \\ 0 & 0 & 1 \end{pmatrix}. \tag{1.4}$$

The SM has in its simplest version (without neutrino mixing) 19 free parameters, which can be chosen as the three coupling constants of the gauge group $SU_c(3) \times SU_L(2) \times U_Y(1)$, the three lepton and six quark masses, the mass of the Z boson, the four parameters of the CKM matrix, a CP violating parameter associated with the strong interaction and the mass of the still undiscovered Higgs boson. Three light Majorana neutrinos would add at least nine new parameters: three masses, three mixing angles and three phases, resulting in 28 arbitrary parameters altogether, which have to be measured in experiment and cannot be predicted by theory – at least not within the Standard Model.

1.1.2 Some Extensions of the Standard Model

The Standard Model explains almost all particle physics data measured within one or two standard deviations σ. In some observables there are bigger deviations, but these could also be statistical fluctuations. Only future measurements can tell if, for example, the 2.5 σ difference [16, p. 134] of the experimental and theoretical values of the anomalous magnetic moment of the muon $\alpha_\mu = (g_\mu - 2)/2$ is a random fluctuation or a hint of "new physics".

Nevertheless, there are some important questions which are not answered by the SM, like: What is dark matter? What is dark energy? Why are there so many particles compared to antiparticles in the universe? What are the masses of the neutrinos? What is mass at all? Is there a Higgs boson? Why is the electroweak scale so much different from the Planck scale (hierarchy problem)? Why are there three generations of fundamental particles? Some of these questions are addressed by extensions of the SM.

In supersymmetric theories [23] there are superpartners for every particle in the Standard Model. For SM fermions there are supersymmetric bosons (squarks and sleptons) and for bosons there are fermionic superpartners (gluinos and gauginos). Additionally, there is not only one Higgs boson but five: h, H, A, $H^\pm$. The smallest possible supersymmetric extension of the Standard Model is called *Minimal Supersymmetric Standard Model* (MSSM) [24].

SUSY has some nice features: it stabilises the mass of the Higgs boson to radiative corrections, that are quadratically divergent in the Standard Model (naturalness). Within this model, the gauge couplings unite at a high scale, which they do not in the Standard Model. Moreover, the lightest supersymmetric particle (LSP) is a promising candidate for dark matter if R-parity is conserved. R is defined in such a way that it is $+1$ for all particles and -1 for all supersymmetric particles:

$$R = (-1)^{3(B-L)+2s}, \tag{1.5}$$

where B is the baryon number, L the lepton number and s the spin. A not so nice feature are about 100 new parameters (masses, mixing angles and phases) [25]. If supersymmetry were an exact symmetry, particles and their superpartners would have the same mass. Since there is so far no experimental evidence for supersymmetric partners, supersymmetry must be broken. If SUSY exists at the electroweak scale, it will be discovered at the LHC. A lot of squarks and

gluinos are expected, since their cross section should be a few pb at 1 TeV. Measurements of the masses of SUSY particles and the parameters will show which specific SUSY model is realised in nature. If nature is not supersymmetric, superstring theories – which incorporate supersymmetry – cannot be valid.

An alternative to the elementary Higgs mechanism of the Standard Model is the dynamical electroweak symmetry breaking by a composite field which is bound together by a new type of strong interaction called *technicolour* [26–29]. Technicolour is acting on massless technifermions at an energy scale of $\Lambda_{\mathrm{TC}} \approx v_{\mathrm{weak}} = 246$ GeV and it is asymptotically free. It solves the naturalness and the hierarchy problem. At LHC, especially, the decay of the technimeson $\rho_{\mathrm{TC}} \rightarrow WZ$ is interesting, since is has a very clean final state, namely $3l + \nu$, which is easier to distinguish from the Standard Model background than decays containing jets.

In ADD models [30–32], introduced by Arkani-Hamed, Dimopoulos and Dvali, additional dimensions of space were introduced. The Standard Model lives on a four-dimensional brane, whereas gravity can also propagate into the extra dimensions, which are large compared to the Planck length $l_P \approx 10^{-35}$ m. Another group of models with more than four spacetime dimensions was proposed by Randall and Sundrum [33, 34]. In these models all elementary particles are localised on a four-dimensional brane, only the graviton can propagate in the fifth dimension. To solve the hierarchy problem, extra dimensions with a fundamental scale of order TeV^{-1} are needed. Thus they should be observable at the LHC: Kaluza–Klein [35, 36] gravitons should show up as heavy resonances in the dielectron mass spectrum of the Drell–Yan process [37] $pp \rightarrow \gamma/Z \rightarrow e^+e^-$.

1.1.3 Physics Programme of the LHC

The multi purpose detectors at LHC, ATLAS and the Compact Muon Solenoid (CMS), plan a very rich physics programme [38, 39]. Both will test the Standard Model (SM) in energy ranges where it was not tested before and will search for "new physics". After a few years of data taking at nominal luminosity and energy they will be able to sieve out realistic models from the excess of theoretical possibilities.

LHC will be a *b*-quark factory, a top-quark factory, a Z factory, a W factory and even a Higgs and SUSY particle factory if these particles exist in the TeV range.

One of the main goals of the LHC is to understand the mechanism of electroweak symmetry breaking, may it be through the Higgs boson [40–43] or something else. The Higgs particle, a neutral scalar boson, spontaneously breaks the $SU(2) \times U(1)$ symmetry of electroweak interaction. Since it has a non-zero expectation value ($v_{\mathrm{weak}} = 246$ GeV), the $W^{\pm}$ and Z bosons acquire mass, while the photon remains massless. The detection of the Higgs boson would be a great success in particle physics – experimental and theoretical. The LHC will be able to finally answer the question if the predicted Standard Model Higgs boson exists or not, because in the whole allowed mass range it has a significance well above five standard deviations σ for Higgs signals and 100 fb^{-1} of integrated luminosity. The lower bound of the allowed region is fixed by the experimental limit of LEP at 114.4 GeV [44], and the upper bound of 186 GeV is sourced from radiative effects of the Higgs boson on electroweak observables [16, p. 452].

At the lower end of the allowed mass range the Higgs boson decays dominantly to ha-

drons. Due to the large QCD background these decay channels are difficult to use in the discovery of the Higgs. Instead of doing so, one prefers to look for isolated leptons and photons even though they have much smaller branching ratios. One of the most promising channels for low mass Higgs is the decay $H \to \gamma\gamma$. If the Higgs mass is around twice the mass of the W boson, the decay $H \to WW^* \to l\nu l\nu$ is important. One of the cleanest discovery channels for a Standard Model Higgs with a mass up to 600 GeV is $H \to ZZ^* \to 4l$, especially the final state with four muons.

Eight million top quark pairs are expected for an integrated luminosity of 10 fb^{-1}. With this huge number of top quarks a mass measurement with a precision of about 2 GeV is possible. Also cross section measurements and searches for many rare top decays are planned at the LHC. The number of produced $b\bar{b}$ pairs strides the number of top quark pairs by orders of magnitude: 10^{12} per years are expected even at low luminosity. This allows the investigation of CP violation in the B system as well as measurements of B_S^0 mixing and the decays of rare B mesons such as the B_c.

Precise constraints on the parton distribution functions (PDFs) are received from Drell–Yan production, W and Z boson production, production of direct photons and high p_T jets, heavy flavour and gauge boson pairs. About 300 million single W events will take place in one year of data taking, which will lower the uncertainty in the W mass to below 20 MeV. The measurement of the triple gauge boson couplings are planned with gauge boson pair production. The determination of the Cabibbo–Kobayashi–Maskawa matrix elements and heavy-ion physics are also part of the Standard Model physics programme.

Since the LHC will increase the maximal energy accessible at colliders by a factor of seven (compared to Tevatron), new discoveries are expected. At the energy frontier, signatures of physics beyond the Standard Model may be seen, like supersymmetric particles, new massive vector bosons, additional spatial dimensions, and others.

Of the superpartners, especially the searches for the SUSY Higgs bosons and the lightest supersymmetric particle (LSP) are interesting. If R-parity is conserved, decays of supersymmetric particles contain the lightest SUSY particle, which is supposed to interact very weakly and will lead to a significant missing transverse energy E_T^{miss} in the final state. There are lots of leptons and jets (particularly b- and/or τ-jets) in decays of supersymmetric particles.

The search for a new massive vector boson Z' is focussed on decays to e^+e^- and $\mu^+\mu^-$ with p_T in the order of TeV.

The signatures of additional spatial dimensions, so-called *large extra dimensions*, are different, depending on the characteristic energy scale M_D of quantum gravity, which is the analogue of the Planck mass in a D-dimensional theory. If the energy E is much less than M_D, signals involving the emission of gravitons escaping into extra dimensions are expected, leading to E_T^{miss}. If $E \approx M_D$, the expectation is model-dependent. In string-theory motivated models there are Z-like resonances with separations in the order of TeV in mass. If $E \gg M_D$, mini black holes are produced which decay with equal production rates to fundamental particles like leptons, photons, neutrinos, W, Z, etc.

The LHC also searches for more exotic models, like little Higgs models, technicolour, leptoquarks, new quarks and leptons, excited quarks, right-handed neutrinos, magnetic monopoles and evidence for composite quarks and leptons.

1.1.4 The Large Hadron Collider

The recently completed Large Hadron Collider (LHC) [45–47] at CERN is a superconducting hadron accelerator and collider. The LHC was built in the 26.7 km long tunnel of the Large Electron–Positron Collider (LEP), which was operating from 1989 till 2000. The CERN Council approved the LHC project in December 1994. At that time it was clear that, after completion, the LHC would be the collider with the highest centre of mass energy, since the construction of the Superconducting Super Collider (SSC) in the U.S. was stopped one year before. In the LHC tunnel there are two rings, for protons going clockwise and anti-clockwise, respectively. Contrary to the Tevatron, where protons and antiprotons are used, the LHC collides protons, because they are much easier to produce in the quantities that are needed to get the planned, extraordinary high luminosity. An unavoidable drawback of the proton–proton approach is the need of two rings with separate magnetic fields and vacuum chambers.
The planned centre of mass energy is 14 TeV and the design peak luminosity is $10^{34}\,\mathrm{cm}^{-2}\,\mathrm{s}^{-1}$, which is about two orders of magnitude bigger than the peak luminosity of Tevatron at Fermilab [48]. To be able to detect rare events, one has to maximise the number of events per second N_{event}, which is directly proportional to the luminosity L:

$$N_{\mathrm{event}} = L\sigma_{\mathrm{event}}\,, \tag{1.6}$$

where σ_{event} is the cross section of the specific event. The luminosity depends only on the beam parameters. For a Gaussian beam distribution it can be written as:

$$L = \frac{N_b^2 n_b f \gamma}{4\pi\varepsilon_n \beta^*} F\,, \tag{1.7}$$

where N_b is the number of particles per bunch (LHC nominal value: 1.15×10^{11} protons per bunch), n_b the number of bunches per beam (2 808), f the revolution frequency ($11\,245\,\mathrm{s}^{-1}$), γ the relativistic gamma factor (7 461), ε_n the normalised transverse beam emittance (3.75 μm), β^* the beta function at the collision point (0.55 m) and F the geometric luminosity reduction factor (0.836) due to the crossing angle at the interaction point.

$$F \approx \frac{1}{\sqrt{1 + \left(\frac{\theta_c \sigma_z}{2\sigma_*}\right)^2}}\,, \tag{1.8}$$

with θ_c the full crossing angle at the interaction point (285 μrad), σ_z the root mean square (RMS) bunch length (7.55 cm) and σ_* the transverse RMS beam size at the interaction point (16.7 μm). The integrated luminosity over one run is:

$$L_{\mathrm{int}} = L_0 \tau_L \left(1 - e^{-T_{\mathrm{run}}/\tau_L}\right)\,, \tag{1.9}$$

where L_0 is the design peak luminosity after filling the rings, τ_L is the so-called luminosity lifetime of about 15 hours for LHC and T_{run} is the total time of the luminosity run. For an assumed average time of 7 hours between the end of a luminosity run with an old beam and

a new beam at top energy, and an operation of 200 days per year, the optimum run time with one beam is 12.5 hours and the accumulated luminosity is 75 fb^{-1} per year.

After some time of running at the nominal luminosity, an upgrade to the so-called Super LHC or SLHC [49, 50] running at $10^{35}\,\mathrm{cm}^{-2}\,\mathrm{s}^{-1}$ is planned. Even without the upgrade, the LHC will be the collider with the highest luminosity and the largest energy for the next years. Other colliders, like the Very Large Hadron Collider (VLHC) [51] or the International Linear Collider (ILC) [52], the Compact Linear Collider (CLIC) [53] or the muon collider [54], are unlikely to be realised in the near future.

The other mode of operation of LHC uses ions to study quark–gluon plasma. Lead ions $^{208}\mathrm{Pb}^{82+}$ collide with a total centre of mass energy of 1150 TeV or 2.76 TeV per nucleon. This is more than one order of magnitude bigger than the 100 GeV per nucleon that were reached for gold ions in the Relativistic Heavy Ion Collider (RHIC) at Brookhaven National Laboratory (BNL) [55].

The machine, together with the CERN share of the detectors and computing sum up to about 6.5×10^9 Swiss francs and consumes 120 MW electrical power. The experiments at the four interaction points are described in the next subsection.

1.1.5 Experiments at the LHC

At the LHC there are two multi purpose experiments – ATLAS [56] and the *Compact Muon Solenoid* (CMS) [57] – with the highest luminosity of $10^{34}\,\mathrm{cm}^{-2}\,\mathrm{s}^{-1}$. The two low luminosity experiments are *Large Hadron Collider beauty* (LHCb) [58] for *B*-physics at a peak luminosity of $10^{32}\,\mathrm{cm}^{-2}\,\mathrm{s}^{-1}$ and *Total Elastic and Diffractive Cross Section Measurement* (TOTEM) [59] at a peak luminosity of $2 \times 10^{29}\,\mathrm{cm}^{-2}\,\mathrm{s}^{-1}$ with 156 bunches. The experiment especially dedicated to work with ion beams is *A Large Ion Collider Experiment* (ALICE) [60] – aiming at a peak luminosity of $10^{27}\,\mathrm{cm}^{-2}\,\mathrm{s}^{-1}$ for nominal lead–lead ion operation. In addition, there is the *Large Hadron Collider forward* (LHCf) [61], which is not resistant to hard radiation and will thus be removed when the luminosity reaches $10^{30}\,\mathrm{cm}^{-2}\,\mathrm{s}^{-1}$.

The principle aim of the multi purpose detectors is to identify secondary particles produced in collisions and to measure their ways through the detector, their charges, momenta and energies. The basic design is the following: as close as possible to the interaction point there is a radiation-hard tracking chamber measuring the path of electrically charged particles. A magnetic field bends the trajectories so that it is possible to determine the curvature and hence the momenta. In electromagnetic and hadron calorimeters the particles are stopped and the released energy is measured. The only charged particles that are able to pass the hadron calorimeters are muons, so the muon detector is located behind the calorimetry. Neutrinos and some of the particles of "new physics" theories beyond the Standard Model, like the lightest supersymmetric particle, cannot be detected directly. Only missing transverse energy E_T^{miss} shows that there were some undetected particles. A high granularity of the detector components is needed to have a low occupancy rate and to distinguish particle paths that are close to each other.

ALICE is a general purpose heavy-ion experiment to study quarks and gluons under very high temperature and extreme density. Due to the asymptotic freedom [6, 7] there will be a transition from hadronic matter to a plasma of deconfined quarks and gluons, a so-called

Detector	Size in m	Weight in tonnes	Material cost in million Swiss francs	Members of collaboration
ALICE	26×16×16	10 000	115	1 500
ATLAS	46×25×25	7 000	540	1 900
CMS	21×15×15	12 500	500	2 000
LHCb	21×10×13	5 600	75	650
LHCf	0.3×0.1×0.1	0.04		21
TOTEM	440×5×5	20	6.5	70

Table 1.3: *The six experiments at the LHC with their size in m, their weight in tonnes, their material cost in million Swiss francs and their numbers of collaboration members (as of May 2007) [46].*

quark–gluon plasma, a state of matter which existed in the early universe during the first 10^{-5} s after the big bang. ALICE will not only work with heavy ions (Pb–Pb) and lower-mass ions (to vary the energy density) but also with protons – pp as well as proton–nucleus – to obtain reference data for the nucleus–nucleus collisions. In addition, $\gamma\gamma$ collisions are of interest. (There is a large flux of virtual photons associated with the Coulomb fields of the interacting lead nuclei.) The detector itself has to digest the highest particle multiplicities, 8 000 charged particles per unit of pseudorapidity ($\eta = -\ln\tan(\theta/2)$, where θ is the angle of a particle relative to the beam axis). ALICE consists (from inside to outside) of an inner tracking system with six layers of high-resolution silicon tracking detectors, a cylindrical time projection chamber and a large area particle identification detector array of time of flight counters. Additionally, there is the small area electromagnetic calorimeter and an array of counters optimised for high-momentum inclusive particle identification, made up of either ring imaging Cherenkov detectors or time of flight counters. All this is embedded in the large magnet of the former L3 experiment with a weak solenoidal field of 0.2 T. Outside the magnet there is the forward muon spectrometer covering 2–10° (or a pseudorapidity of η =2.4–4).

ATLAS is a general purpose experiment to detect "new physics" signatures like SUSY and large extra dimensions, as well as Higgs decays and Standard Model processes. It consists (from inside to outside) of the inner detector, made of high-resolution semiconductor pixel and strip detectors near the interaction point and straw-tube tracking detectors in the outer parts. The inner detector is optimised to give good momentum and vertex measurements as well as electron identification. It covers a range in pseudorapidity of $|\eta| \leq 2.5$ and is embedded in a thin superconducting solenoid which produces a field of about 2 T. Outside the magnet there is the lead/liquid argon electromagnetic calorimeter, which is characterised by a good energy and position resolution, and the hadron calorimeter made of plastic scintillator plates embedded in an iron absorber. The electromagnetic and hadronic calorimeters provide a very good jet- and E_T^{miss}-performance and cover the pseudorapidity range of $|\eta| \leq 3.2$ whereas for the region $3.1 \leq |\eta| \leq 4.9$ there are special forward calorimeters. The detector is completed by a muon spectrometer with good momentum resolution in superconducting air-core toroids.

CMS is – like ATLAS – a general purpose detector to explore physics at the TeV scale and to study the mechanism of electroweak symmetry breaking – may it be through the Higgs boson or another mechanism. It is designed for the search for new particles, like SUSY partners of SM particles, and extra dimensions, as well as for precision tests of the Standard Model. Close to the interaction point there are three layers of pixel detectors to measure the position of secondary vertices and the impact parameter of charged-particle tracks. Together with the silicon tracker, consisting of ten layers of silicon microstrips, they form the inner detector, which is surrounded by the electromagnetic calorimeter. The EM calorimeter is made of lead tungstate ($PbWO_4$) crystals and covers a pseudorapidity range of $|\eta| \leq 3.0$. The same range is covered by the hadronic calorimeter made of brass and scintillators. The calorimeters are embedded in a huge superconducting solenoid with a magnetic field of 4 T to measure momenta of charged particles precisely. Outside the solenoid there are the muon detectors up to $|\eta| \leq 2.4$. In the very forward region ($|\eta| \leq 5.0$) special end-cap calorimeters are installed.

LHCb is a conical detector to study the CP violation in *B*-particles. The tip of the cone is the interaction point with a silicon vertex detector that allows to reconstruct a *B*-decay vertex with a very good resolution. The RICH (Ring Imaging Cherenkov) counters next to it identify charged particles and distinguish pions from kaons, for example. The tracking system, partially inside a dipole magnet with a maximal magnetic field of 1.1 T, is used for the efficient reconstruction and precise momentum measurement of charged tracks. The different trackers are located in front of and behind the first RICH detector; in front of, inside and behind the magnet as well as behind the second RICH detector. Then the calorimetry follows, which can distinguish electrons from hadrons and provides a measurement of energy and position. The electromagnetic calorimeter consists of lead and a polystyrene-based scintillator whereas the hadronic calorimeter is made of iron and scintillators. The last part of LHCb is the muon detector. The overall detector covers a range from 10 mrad to 250 mrad (or $2.1 \leq |\eta| \leq 5.3$). This geometry has been chosen because at high energies the *b*- and the $\bar{b}$-hadrons are predominantly produced in the same forward cone.

The LHCf experiment consists of two detectors next to ATLAS and covers the very forward region. Its aim is to test models used in estimating the primary energy of ultra high-energetic cosmic rays. To achieve this goal it uses two small sampling and imaging calorimeters and measures the forward production spectra of photons and neutral pions as well as the leading particle spectrum.

The TOTEM detector, installed in the forward region of CMS, measures the total pp cross section and studies elastic scattering and diffractive dissociation. Therefore, tracking detectors are installed inside the end caps of the CMS muon detectors close to the beam pipe, and behind the CMS end-cap calorimeters covering a pseudorapidity interval $3 \leq |\eta| \leq 6.8$. In addition, there are two sets of silicon detectors, $\pm 147\,\text{m}$ and $\pm 220\,\text{m}$ from the interaction point.

1.2 Feynman Rules and Some More Efficient Alternatives

1.2.1 Perturbation Theory

Perturbation theory in general is a method to find an approximate solution to a problem which is not solvable analytically at all or not solvable analytically in a reasonable amount of time. It is only applicable if the problem can be formulated as a small deviation from a similar but simpler and exactly solvable problem. The general procedure is: *(i)* ignore effects that make the process complicated, *(ii)* calculate the simplified process analytically, *(iii)* add the ignored effects as a small perturbation of the simplified process, *(iv)* calculate the solution, order by order, in terms of a power series in a small parameter which describes the deviation from the exactly solvable problem. The first term in the power series is the exact solution of the simplified problem. Further terms approximate the solution of the hard problem better and better. These terms are usually called Leading Order (LO), Next to Leading Order (NLO), Next to Next to Leading Order (NNLO) and so on. This can formally be written as:

$$x = x_0 + g x_1 + g^2 x_2 + \dots \tag{1.10}$$

If g is small and the x_n do not grow too fast, the terms in this series become successively smaller (on the other hand, the calculation of the x_n usually becomes successively more complex). So the first few terms are enough to compare theoretical predictions with experimental data. As experiments become more and more precise, the theorists have to calculate more and more orders.

Perturbation theory is used for example in celestial mechanics, quantum mechanics and quantum field theories. Especially in the latter, problems occur: there are infrared and ultraviolet divergences. Infrared divergences occur in integrals over a momentum k in the case of vanishing momentum, $k \to 0$. These divergences are cancelled if the summation over the initial and final degenerate states is carried out (Kinoshita–Lee–Nauenberg theorem) [62, 63]. Ultraviolet divergences occur in integrals over a momentum k in the case of momentum going to infinity, $k \to \infty$. They can be removed by regularisation and renormalisation.

Regularisation is a mathematical method of dealing with these divergences. In dimensional regularisation [64–67] all calculations are done in $d = 4 - 2\varepsilon$ dimensions and not in $d = 4$ dimensions, where the integrals are divergent. By this trick, the singularities are parametrised in poles like $1/\varepsilon$ and $1/\varepsilon^2$ and form a Laurent series in the regularisation parameter. One could also avoid the infinities by changing the upper integration boundary to a finite value $k = k_{\max}$, which is called cutoff regularisation. In Pauli–Villars regularisation [68] one introduces fictitious heavy particles to separate finite from divergent terms.

Renormalisation is a formalism of redefinition of physical quantities like mass and charge as well as the fields. For example, in charge renormalisation, there is a difference between quantities in the formulæ, like the Lagrangian density, and physical constants measured in the laboratory. The first one is called *bare* charge e_0 and the second one *physical* charge $e = \sqrt{Z_3} e_0$ with the renormalisation constant Z_3. The physical charge takes into account the contribution of virtual particle–antiparticle pairs.

The first renormalised perturbation theory was quantum electrodynamics (QED) [69–74]. Two of the first successful applications were the calculations of the Lamb shift by Bethe [75]

and the anomalous magnetic moment of the electron by Schwinger [76]. Today the anomalous magnetic moment of the electron is one of the best understood quantities in nature: the experimental value agrees with the theoretical one within nine significant digits.

Even though perturbation theory gives an amazingly good result in this case, the perturbation series is in general divergent [77–81]. The absolute magnitude of the first terms of the series decreases, but the factorial growth of the perturbative coefficients x_n in equation (1.10) overcompensates the additional coupling factors of higher orders in perturbation theory, and the series finally diverges.

1.2.2 Feynman Rules

From the Lagrangian density $\mathcal{L}$ of a given theory, say QED or QCD, one can derive Feynman rules. For example, every term in $\mathcal{L}$ with a product of fields $\phi_1, \ldots, \phi_n$ will lead to a vertex with these external fields. Some of the Standard Model Feynman rules are given in appendix A.4. Feynman diagrams, also called Feynman graphs, are pictorial representations of the perturbation series and they are composed according to the Feynman rules.

The classical way to calculate hard scattering processes in particles physics is, firstly, to draw all permitted Feynman diagrams. These are all diagrams that are not forbidden by conservation laws and have the required initial and final states. Secondly, one uses the Feynman rules to get a mathematical expression – called amplitude – for every single graph. Thirdly, one adds up the amplitudes of all graphs, and, fourthly, squares the absolute value of the sum. After that one has to sum or average over the polarisations (or any other degree of freedom). To get the cross section one finally integrates over the phase space volume. The cross sections for virtual and real emissions are both divergent, the divergences cancel when virtual and real contributions are added to give a physical meaningful result.

There are computer programs for the different parts of this calculation. For example, for the generation of Feynman rules in field theory, there is the program LanHEP [82]. Programs for the automated generation and computation of Feynman diagrams are FeynArts [83] and GEFICOM [84]. A review can be found in reference [85].

1.2.3 Limits of the Feynman Approach

The Feynman diagram approach is not feasible for final states with many particles as they occur in very high-energy colliders. There are too many diagrams and the number of diagrams increases very fast, as the number of external particles rises (see table 1.4). There are too many terms in each diagram. Especially in QCD calculations many terms appear due to the structure of non-Abelian vertices. Additionally, many kinematic variables complicate the calculations.

Intermediate results of the calculations tend to be orders of magnitude more complicated than the final one.

The limits of this approach in numbers of loops and legs are compiled in figure 1 in reference [86]: the technique is well established for two loops up to two legs, for one loop up to five legs and for zero loops up to eight legs. Partial results or special cases were calculated for three loops up to two legs, for two loops up to four legs, for one loop up to six legs and for zero loops up to ten legs. To bring the theoretical predictions to the expected precision for the ILC, even more loops and legs are needed, at least the leading effects of that.

number of gluons n	3	4	5	6	7	8	9	10
Feynman diagrams	1	4	25	220	2 485	34 300	559 405	10 525 900
factorial $n!$	6	24	120	720	5 040	40 320	362 880	3 628 800
partial amplitudes $(n-2)!$	1	2	6	24	120	720	5 040	40 320

Table 1.4: *The number of Feynman diagrams at tree-level contributing to a scattering process with n gluons ($gg \to (n-2)g$). The number of diagrams grows faster than the factorial, which is given for comparison. In the last row the number of independent partial amplitudes is shown [87].*

1.2.4 More Efficient Methods

In the 1980s new methods were developed to avoid the difficulties described in the preceding subsection. These methods are the colour decomposition, the spinor-helicity method and recurrence relations.

Colour Decomposition

The colour decomposition [88, 89] splits Feynman amplitudes into a colour part and a Lorentz part. The former contains a trace over colour matrices and the latter, called partial amplitude, contains the kinematical information. For a tree-level amplitude with n external gluons this reads:

$$\mathcal{A}_n(k_1^{\lambda_1},\ldots,k_n^{\lambda_n}) = g^{n-2} \sum_{\sigma\in S_n/Z_n} 2\,\mathrm{Tr}\,(T^{a_{\sigma(1)}}\ldots T^{a_{\sigma(n)}})\, A_n\left(k_{\sigma(1)}^{\lambda_{\sigma(1)}},\ldots,k_{\sigma(n)}^{\lambda_{\sigma(n)}}\right). \tag{1.11}$$

S_n is the set of all permutations of n objects and Z_n is the subset of cyclic permutations, which preserve the trace. Thus the sum runs over all non-cyclic permutations of the external gluon legs. In this formula, k_j denotes the four-momentum of the j-th gluon and λ_j its helicity, g stands for the strong coupling constant and T^a are the colour matrices, normalised such that $\mathrm{Tr}(T^aT^b) = 1/2\,\delta^{ab}$. The partial amplitudes A_n contain the kinematic information. They are colour-ordered, i. e. only diagrams with a particular cyclic ordering of the gluons contribute. This way one can reduce the number of diagrams to be calculated. Hence, the calculation of partial amplitudes is more efficient than calculating all conventional Feynman diagrams. In addition, partial amplitudes satisfy several identities which further reduce the number of independent partial amplitudes, see equation (2.4) and the following equations.

The proof of the colour decomposition is very simple [90]. In any tree-level purely gluon Feynman diagram we pick any vertex and replace the colour structure constants defined in equation (A.32) by $f^{abc} = -2i\,\mathrm{Tr}(T^aT^bT^c - T^bT^aT^c)$. If a leg attached to this vertex is external, there are no colour terms. If a leg is internal it leads to another vertex, whose structure constants can be replaced by traces over matrices T^a. The product of a structure constant and a matrix T^a can be replaced using equation (A.32). This procedure can be continued until all vertices have been treated in this manner. Then we have the desired colour decomposition (1.11).

Spinor-Helicity Method

The spinor-helicity method [90–96] introduces a new set of kinematical variables and the polarisation vectors are written in terms of these spinor products (for more details see appendix A.2).

The advantage is, that many terms vanish, like $k\varepsilon_{\pm}^{\mu}(k,q) = 0$ and $\varepsilon_{\pm}^{\mu}(k_i,q)\,\varepsilon_{\pm}^{\mu}(k_j,q) = 0$. To make use of this, it is particularly useful to choose the reference momenta of gluons with the same helicity to be identical and equal to the external momentum of one of the gluons of opposite helicity. In this way one can reduce the number of terms per diagram significantly. Since different helicity configurations do not interfere, it is sufficient to sum incoherently over the squares of all possible helicity amplitudes contributing to a given process, to obtain the full cross section. For processes with n Feynman diagrams one classically had to calculate $n(n+1)/2$ interference terms. In the spinor-helicity formalism the number of amplitudes to calculate is usually much smaller. In the process $e^+e^- \to e^+e^-\gamma\gamma$ for example there are 80 Feynman diagrams, thus 3240 interference terms, but only 64 helicity amplitudes. Because of parity conjugation (equation 2.4), which flips all helicities, one has to calculate only 32 (short) expressions, compared to 3240 (long) ones [97]. This is a major step towards more efficiency.

Berends–Giele Recurrence Relations

The colour decomposition and the spinor-helicity method demonstrate their full power when combined with recurrence relations that construct the amplitudes recursively from smaller building blocks. The Berends–Giele recurrence relations [98, 99] were historically the first ones.

Pure gluonic processes are calculated recursively, because they play a special role among all parton processes. In hadron collisions the gluons have the largest parton cross section and when one has techniques to calculate gluon processes, it is relatively easy to add a single quark–antiquark pair. To calculate the partial amplitudes A_n one first removes the polarisation vector of the n-th gluon and multiplies with an off-shell propagator term. This so arisen auxiliary quantity is called *off-shell current* J_{n-1}, because the n-th leg is off-shell (all other legs are on-shell). Since J is an off-shell quantity, it is gauge dependent. For that reason, reference momenta for the on-shell gluons, which J depends on, have to be kept fixed until after one has extracted an on-shell result. The off-shell current for $n-1$ gluons can then be related to off-shell currents with less gluons. This recursion step is repeated until we reach J_1, which is defined as the polarisation vector of the gluon. In this way J_{n-1} is constructed and to get the partial amplitudes A_n we only have to multiply with the inverse propagator as well as the polarisation vector of the n-th gluon.

The recurrence relations automatically take into account all Feynman diagrams and allow to prove certain properties of partial amplitudes.

1.2.5 Twistor Approach

In Penrose's twistor theory [100–102] the usual background spacetime is replaced by a background space of twistors. The known physical phenomena are to be reinterpreted in this new

twistor space to gain new insight. This is analogous to introducing momentum space and using the Fourier transform to change from spacetime to momentum space and vice versa. A twistor space $\mathbb{T}$ is a four-dimensional complex vector space $\mathbb{C}^4$. A twistor is an element $Z^\alpha = (Z^0, Z^1, Z^2, Z^3)$ in this vector space. Theoretical physicists work in twistor space to better understand various classical field equations and modern relativistic and gauge field equations. One of the initial aims of twistor theory was to provide a formalism for the unification of general relativity and quantum theory. However, it is also interesting from a purely mathematical point of view.

In 2003 Witten introduced a string theory in twistor space [103, 104], later called *twistor string theory*, which is dual to a weakly coupled gauge theory. This duality shed new light on Yang–Mills perturbation theory and led to new methods for computing Yang–Mills scattering amplitudes. The perturbative expansion in the gauge theory is related to *D*-instanton expansion in string theory (the string theory in question is a topological open string *B*-model on a Calabi–Yau supermanifold $\mathbb{CP}^{3|4}$, which is a supersymmetric generalisation of Penrose's twistor space). The relationship to QCD amplitudes inspired new methods for the calculation of helicity amplitudes in field theories. The Cachazo–Svrček–Witten (CSW) approach [105, 106] constructs tree-level QCD amplitudes from vertices that are off-shell continuations of maximal helicity violating (MHV) amplitudes [107], connected by scalar propagators.

Subsequently, a set of recursion relations has been found [108–111] that involve only on-shell amplitudes with shifted, complex, external momenta.

1.2.6 The BCFW Recursion Relation

In this subsection we prove the recursion relation with shifted momenta, following the ideas of Britto, Cachazo, Feng and Witten [104, 108, 109], because this proof is constructive and the same technique can be, and has been, applied to many other problems [112–114]. The idea of the relation is as follows: one holds two gluons fixed and sums over products of subamplitudes with r external gluons on one side, connected by an internal gluon to $n-r$ external gluons on the other side. The two fixed gluons are on opposite sides. The sum is over all possible decompositions with one fixed gluon on each side. The momentum of the internal gluon is k and its helicity λ. The momenta are shifted in such a way that the internal gluon, as well as the external gluons, are on-shell.

In other words: we prove that any gluonic tree-level amplitude can be constructed from two subamplitudes with fewer gluons times a Feynman propagator. The subamplitudes are physical, on-shell amplitudes with shifted momenta. The recursion relation can be written as:

$$A_n = \sum_{r,\lambda} A^{\lambda}_{r+1} \frac{1}{k_r^2} A^{-\lambda}_{n-r+1}\,, \tag{1.12}$$

where A_n is the tree-level scattering amplitude for n cyclically ordered gluons.

The proof uses the spinor-helicity formalism mentioned in subsection 1.2.4. The spinors of the i-th gluon are called κ_i and $\tilde{\kappa}_i$. Thus we can write $k_i^{a\dot{a}} = \kappa_i^a \tilde{\kappa}_i^{\dot{a}}$ for the null-vector k_i. Now two gluons' momenta are changed by introducing a complex variable z in the following

manner (without loss of generality these can be chosen as l and n, if we use cyclic symmetry):

$$k_l(z) = \kappa_l\left(\tilde{\kappa}_l - z\tilde{\kappa}_n\right), \quad k_n(z) = \left(\kappa_n + z\kappa_l\right)\tilde{\kappa}_n, \tag{1.13}$$

which is the transition:

$$\tilde{\kappa}_l \to \tilde{\kappa}_l - z\tilde{\kappa}_n, \quad \kappa_n \to \kappa_n + z\kappa_l, \tag{1.14}$$

with fixed κ_l and $\tilde{\kappa}_n$. The momenta of all the other gluons stay unaltered. The changed momenta $k_l(z)$ and $k_n(z)$ are on-shell for all z. Using these we can define the auxiliary function:

$$A(z) = A\big(k_1, \ldots, k_{l-1}, k_l(z), k_{l+1}, \ldots, k_{n-1}, k_n(z)\big), \tag{1.15}$$

which is a physical on-shell amplitude for all z. All momenta are on-shell and momentum conservation is fulfilled. Without loss of generality, we assume that the helicities λ_l and λ_n are $-$ and $+$, respectively. The proof for other helicity configurations can be done in a similar manner.

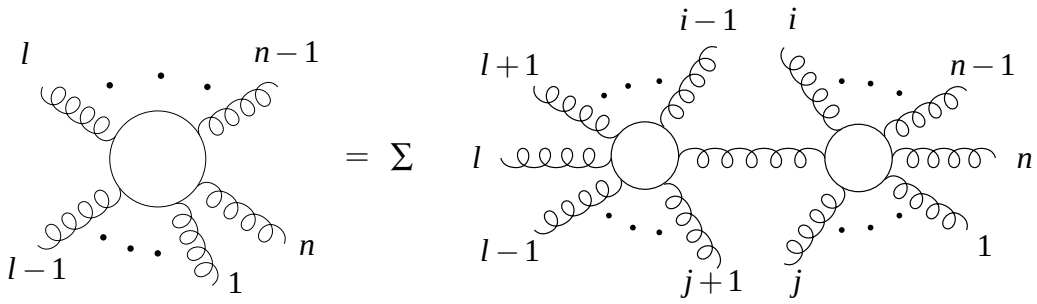

Figure 1.1: *Pictorial representation of the BCFW recursion relation. The momenta of gluons n and l are changed according to equation (1.13). The sum runs over all cyclically ordered gluons with at least two gluons on each side and over the two choices of helicity for the internal gluon connecting the two subamplitudes.*

If we can show that $A(z)$ is a rational function, it has only simple poles and it vanishes for $z \to \infty$, we are basically done, because it can then be written as:

$$A(z) = \sum_{p \in \{\text{poles}\}} \frac{c_p}{z - z_p}, \tag{1.16}$$

where c_p is the residue at the pole p. It will turn out, that c_p is proportional to amplitudes with fewer legs than $A(z)$ which leads to the desired recursion relation. Let us start with the proof of these three statements about A.

Since the original tree-level amplitude is a rational function of spinor products and the z-dependence only enters via equations (1.14), $A(z)$ is also a rational function in z.

$A(z)$ is constructed out of Feynman diagrams and can only have singularities from propagator terms. Since $A(z)$ is colour-ordered, all propagators are of the form $1/K_{ij}^2$, where $K_{ij} = k_i + k_{i+1} + \ldots + k_j$. K_{ij} is independent of z if $l, n \notin \{i, \ldots, j\}$, but also if $l, n \in \{i, \ldots, j\}$, since $k_l(z) + k_n(z) = \kappa_l\tilde{\kappa}_l + \kappa_n\tilde{\kappa}_n$ is z-independent. For $l \in \{i, \ldots, j\}$ and $n \notin \{i, \ldots, j\}$ we

use momentum conservation to replace $k_i + \ldots + k_j$ by $-(k_{j+1} + \ldots + k_{i-1})$. Then we are left with the last remaining case $l \notin \{i, \ldots, j\}$ and $n \in \{i, \ldots, j\}$. In this case $K_{ij}(z) = K_{ij} + z\kappa_l\tilde{\kappa}_n$. Using the fact that the shift of k_n is a null-vector, we have:

$$K_{ij}^2(z) = K_{ij}^2 + z\langle\kappa_l|K_{ij}|\tilde{\kappa}_n\rangle\,, \tag{1.17}$$

where the product is defined by $\langle\kappa|k|\tilde{\kappa}\rangle = -k_{a\dot{a}}\kappa^a\tilde{\kappa}^{\dot{a}}$. Hence, the propagator $1/K_{ij}^2(z)$ has only one single simple pole at:

$$z_{ij} = \frac{K_{ij}^2}{\langle\kappa_l|K_{ij}|\tilde{\kappa}_n\rangle}\,. \tag{1.18}$$

The z_{ij} for different pairs of i and j are distinct and they are the only singularities of $A(z)$. Accordingly, $A(z)$ has only simple poles.

Now we show that of $A(z)$ vanishes for $z \to \infty$. Any Feynman diagram contributing to $A(z)$ is linear in the polarisation vectors $\varepsilon_{a\dot{a}}$ of the external gluons, that can be written as:

$$\varepsilon^-_{a\dot{a}} = \frac{\kappa_a\tilde{\mu}_{\dot{a}}}{[\tilde{\kappa},\tilde{\mu}]}, \quad \varepsilon^+_{a\dot{a}} = \frac{\mu_a\tilde{\kappa}_{\dot{a}}}{\langle\mu,\kappa\rangle}, \tag{1.19}$$

where μ and $\tilde{\mu}$ are fixed reference spinors. The only z-dependent polarisation vectors are the ones of gluons l and n. The spinor κ_l does not depend on z, and $\tilde{\kappa}_l$ is linear in z. Since the helicity of λ_l is negative, it follows that ε_l^- goes to zero like $1/z$ for $z \to \infty$. The same can be shown for ε_n^+. The other terms in Feynman diagrams are propagators (which are constant or vanish in the limit $z \to \infty$) and vertices. Since vertices with four gluons do not have any momentum factors, we only have to show that contributions from three-gluon vertices vanish like $1/z$ for $z \to \infty$. In a tree diagram the z-dependence flows from gluon l to gluon n along a unique path of propagators. Each of them gives a factor $1/z$. If there are r of these propagators there can be at most $r+1$ cubic vertices along the path. Vertices and propagators together give a factor that grows at most linearly in z for large z. Since the product of polarisation vectors vanishes like $(1/z)^2$, $A(z)$ vanishes like $1/z$ for $z \to \infty$.

Equation (1.16) can now be rewritten with the residues c_{ij} of $A(z)$ at the pole $z = z_{ij}$ as:

$$A(z) = \sum_{i,j} \frac{c_{ij}}{z - z_{ij}}\,, \tag{1.20}$$

where the sum over i and j runs over all pairs in such a way that n is in the range from i to j, while l is outside this range. To get the recursion relation we now calculate the residues c_{ij}. If there is a pole at $K_{ij}^2(z) = 0$, a tree diagram is divided into two parts by a propagator. The first part, the subamplitude on the right-hand side of figure 1.1, contains all external gluons inside the range from i to j, whereas the second part, the left subamplitude, contains the external gluons outside this range. The connecting internal line has momentum $K_{ij}(z)$. We have to sum over the helicities $\lambda = \pm$ at the left-hand side (the helicity of the right-hand side is always opposite). The contributions of such diagrams near the pole $z = z_{ij}$ are:

$$\sum_\lambda \frac{A_L^\lambda(z)A_R^{-\lambda}(z)}{K_{ij}^2(z)}\,, \tag{1.21}$$

where $A_L^{\lambda}(z)$ and $A_R^{-\lambda}(z)$ are the contributions of the particular sides. The denominator $K_{ij}^2(z)$ is linear in z. To obtain the function $c_{ij}/(z-z_{ij})$ in equation (1.20), we set $z = z_{ij}$. In doing so, the internal line becomes on-shell and the numerator becomes a product of physical on-shell scattering amplitudes. Thus we have:

$$\begin{aligned} A_R^{-\lambda}(z_{ij}) &= A\big(-K_{ij}^{-\lambda}(z_{ij}), k_i, \ldots, k_n(z_{ij}), \ldots, k_j\big)\,, \\ A_L^{\lambda}(z_{ij}) &= A\big(k_{j+1}, \ldots, k_l(z_{ij}), \ldots, k_{i-1}, K_{ij}^{\lambda}(z_{ij})\big)\,. \end{aligned} \tag{1.22}$$

Using this, we can rewrite equation (1.20) as:

$$A(z) = \sum_{i,j}\sum_{\lambda} \frac{A_L^{\lambda}(z_{ij})A_R^{-\lambda}(z_{ij})}{K_{ij}^2(z_{ij})}\,. \tag{1.23}$$

We set $z = 0$ in the denominator, without changing the numerator, to obtain the physical scattering amplitude $A(1,2,\ldots,n)$:

$$A(1,2,\ldots,n) = \sum_{i,j}\sum_{\lambda} \frac{A_L^{\lambda}(z_{ij})A_R^{-\lambda}(z_{ij})}{K_{ij}^2}\,, \tag{1.24}$$

which is the BCFW recursion relation.

1.3 Parton Showers

This section gives an introduction to parton showers [115].

With present techniques, our limited ability to calculate perturbative corrections in QCD allows analytical predictions only for the first few orders in α_s. Since the size of calculations grows roughly factorially with the order of α_s, without new ideas, not many higher orders results can be expected in the near future. Nevertheless, higher order terms are important for some regions in phase space, such as collinear parton emission in deep inelastic scattering. Also at high thrust [116, 117]:

$$T = \frac{\max\limits_{\vec{n}} \sum\limits_i |\vec{p}_i \cdot \vec{n}|}{\sum\limits_i |\vec{p}_i|} \to 1 \tag{1.25}$$

in electron–positron annihilation, fixed order predictions are unreliable, since for each power of α_s there is an extra factor of $\ln^2(1-T)$ which spoils the calculation.

For these regions in phase space, there is a different approach: not a precise calculation to some fixed order in the perturbation series, but an approximate result for all orders. This approach is called *parton showers*. The shower gives an approximate perturbative result at scales of momentum-transfer squared t greater than some infra-red cut-off t_0, typically of the order of 1 GeV^2. Combined with a non-perturbative hadronisation model at scales $t < t_0$, one obtains two of the main ingredients for a QCD event generator, a computer program to simulate interaction and production of hadrons with similar final states (average and fluctuations)

as those observed in experiment. To this end, the parton distribution functions of the initial state, the hard interaction itself, other semi-hard processes and beam remnants with colour connection (the so-called underlying event), as well as the decay of hadrons, have to be taken into account. Since quantum mechanics is probabilistic, a generator has to produce the events randomly. For this reason, event generators are Monte Carlo programs [118].

Generator	latest version	hadronisation	references
PYTHIA	6.4 (Fortran)	string model	[119]
	8.135 (C++)		[120]
HERWIG	6.510 (Fortran)	cluster model	[121]
HERWIG++	2.4.2 (C++)	cluster model	[122, 123]
ISAJET	7.80 (Fortran)	independent fragmentation	[124]
SHERPA	1.2.1 (C++)	string & cluster	[125]

Table 1.5: *The main hadronic event generators. For special purposes there are a lot more programs available, e. g.* ARIADNE *[126] for parton showers or* ALPGEN *[127] for multi-parton processes in hadronic collisions.*

1.3.1 Splitting Functions

We will now derive the unregularised gluon splitting function as an example of a splitting function. Let a be an outgoing gluon, branching into gluons b and c like in the right-hand side of figure 1.2. This is a time-like branching, since $t = p_a^2 > 0$. The opening angle is $\theta = \theta_b + \theta_c$. The energy fraction z is defined by:

$$z = \frac{E_b}{E_a} = \frac{E_a - E_c}{E_a} = 1 - \frac{E_c}{E_a} \,. \tag{1.26}$$

For momenta parametrised as:

$$\begin{aligned} p_a &= (E_a + \frac{p_a^2}{4E_a}, 0, 0, E_a - \frac{p_a^2}{4E_a}) \,, \\ p_b &= (E_b, +E_b \sin\theta_b, 0, E_b \cos\theta_b) \,, \\ p_c &= (E_c, -E_c \sin\theta_c, 0, E_c \cos\theta_c) \end{aligned} \tag{1.27}$$

and in the approximation of small angles, we obtain:

$$t = p_a^2 = (p_b + p_c)^2 = 2E_b E_c (1 - \cos\theta) \approx z(1-z) E_a^2 \theta^2 \,. \tag{1.28}$$

Using transverse momentum conservation, we get:

$$\theta = \frac{1}{E_a} \sqrt{\frac{t}{z(1-z)}} = \frac{\theta_b}{1-z} = \frac{\theta_c}{z} \,. \tag{1.29}$$

For the matrix element $\mathcal{M}$ there is a factor proportional to $1/t$ from the propagator of gluon a, and the vertex of the three gluons gives a factor:

$$V_{ggg} = ig f^{abc} \varepsilon_a^\alpha \varepsilon_b^\beta \varepsilon_c^\gamma \left[g_{\alpha\beta}(p_a - p_b)_\gamma + g_{\beta\gamma}(p_b - p_c)_\alpha + g_{\gamma\alpha}(p_c - p_a)_\beta \right] \,, \tag{1.30}$$

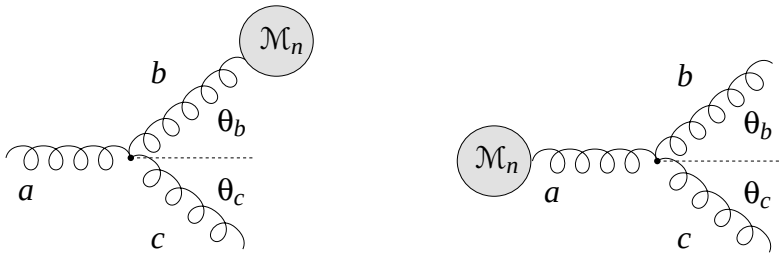

Figure 1.2: *The incoming branching (left) is space-like, $p_b^2 = t < 0$, whereas the outgoing branching (right) is time-like, $p_a^2 = t > 0$.*

where ε_i^μ is the polarisation vector for gluon i. All momenta of the gluons are defined as outgoing, so that $p_a + p_b + p_c = 0$. Using $\varepsilon_i \cdot p_i = 0$, we get:

$$V_{ggg} = -2ig f^{abc}\big((\varepsilon_a \cdot \varepsilon_b)(\varepsilon_c \cdot p_b) - (\varepsilon_b \cdot \varepsilon_c)(\varepsilon_a \cdot p_b) - (\varepsilon_c \cdot \varepsilon_a)(\varepsilon_b \cdot p_c)\big)\,. \tag{1.31}$$

The gluons are almost on-shell. Hence, we can take their polarisation vectors to be purely transverse. These can be written as superpositions of a polarisation vector in the plane, which is spanned by the three gluons, and a polarisation vector perpendicular to this plane. Polarisation states of the first kind are labelled as $\varepsilon_i^{\text{in}}$, the latter ones as $\varepsilon_i^{\text{out}}$. The following relations are fulfilled:

$$\begin{aligned} \varepsilon_i^{\text{in}} \cdot \varepsilon_j^{\text{in}} &= \varepsilon_i^{\text{out}} \cdot \varepsilon_j^{\text{out}} = -1\,, \\ \varepsilon_i^{\text{in}} \cdot \varepsilon_j^{\text{out}} &= \varepsilon_i^{\text{out}} \cdot p_j \;\; = 0\,. \end{aligned} \tag{1.32}$$

For small θ, when terms of order θ^2 are neglected, one has:

$$\begin{aligned} \varepsilon_c^{\text{in}} \cdot p_b &= -E_b\theta \;\; = -zE_a\theta\,, \\ \varepsilon_a^{\text{in}} \cdot p_b &= -E_b\theta_b = -z(1-z)E_a\theta\,, \\ \varepsilon_b^{\text{in}} \cdot p_c &= +E_c\theta \;\; = (1-z)E_a\theta\,. \end{aligned} \tag{1.33}$$

We see that every term in the three-gluon vertex is proportional to θ. With the propagator is proportional to $1/t \sim 1/\theta^2$, it follows that the amplitude has a $1/\theta$ singularity. The matrix element is:

$$\mathcal{M}_{n+1} \sim V_{ggg}\frac{1}{t}\mathcal{M}_n\,. \tag{1.34}$$

Squaring $\mathcal{M}_{n+1}$ and inserting θ from equation (1.29), gives:

$$|\mathcal{M}_{n+1}|^2 \sim \frac{4g^2}{t}N_c F(z;\varepsilon_a,\varepsilon_b,\varepsilon_c)|\mathcal{M}_n|^2\,, \tag{1.35}$$

where the colour factor $N_c = 3$ for SU(3) comes from the product of the structure functions

f^{abc}. The functions $F(z;\varepsilon_a,\varepsilon_b,\varepsilon_c)$ are given by:

$$\begin{aligned}
F(z;\varepsilon_a^{\text{in}},\,\varepsilon_b^{\text{in}},\,\varepsilon_c^{\text{in}}) &= \frac{1-z}{z}+\frac{z}{1-z}+z(1-z)\,,\\
F(z;\varepsilon_a^{\text{in}},\,\varepsilon_b^{\text{out}},\varepsilon_c^{\text{out}}) &= z(1-z)\,,\\
F(z;\varepsilon_a^{\text{out}},\varepsilon_b^{\text{in}},\,\varepsilon_c^{\text{out}}) &= \frac{1-z}{z}\,,\\
F(z;\varepsilon_a^{\text{out}},\varepsilon_b^{\text{out}},\varepsilon_c^{\text{in}}) &= \frac{z}{1-z}\,.
\end{aligned} \tag{1.36}$$

All other polarisation combinations vanish. Averaging over the polarisations of a and summing over the polarisations of b and c lead to:

$$\langle F\rangle = \frac{1}{2}\sum_{\mu_a=\text{in,out}}\sum_{\mu_b=\text{in,out}}\sum_{\mu_c=\text{in,out}} F(z;\varepsilon_a^{\mu_a},\varepsilon_b^{\mu_b},\varepsilon_c^{\mu_c}) = \frac{1-z}{z}+\frac{z}{1-z}+z(1-z)\,. \tag{1.37}$$

The unregularised gluon splitting function is defined as:

$$\hat{P}_{gg}(z) = N_c\langle F\rangle = N_c\left[\frac{1-z}{z}+\frac{z}{1-z}+z(1-z)\right]. \tag{1.38}$$

The branching probability $\hat{P}_{gg}(z)$ for gluons is related to the corresponding Altarelli–Parisi kernel [128] and diverges for $z\to 0$ (if gluon b is soft) and $z\to 1$ (if gluon c is soft). As can be seen from equation (1.36) the divergences are correlated to the emission of a soft gluon polarised in the plane of branching. To get the regularised splitting function we use the *plus prescription*, also called *plus distribution*, defined by:

$$\int_0^1 f(x)\big(g(x)\big)_+\,\mathrm{d}x = \int_0^1 \big(f(x)-f(1)\big)g(x)\,\mathrm{d}x\,, \tag{1.39}$$

where $f(x)$ is a smooth test function and $g(x)$ is singular at $x=1$. Thus we finally obtain:

$$P(z) = \hat{P}(z)_+\,. \tag{1.40}$$

1.3.2 Evolution Equations

To get the DGLAP evolution equation [128–130] we look at multiple small-angle gluon emissions from a space-like quark (see figure 1.3). The quark from hadron A has, in the beginning, a low virtual mass-squared $t_0<0$ and a high fraction x_0 of the hadron's momentum. With every emitted gluon it moves to a more virtual mass $t_i<t_{i-1}$ and a lower momentum fraction $x_i<x_{i-1}$. After emitting n gluons, the quark takes part in a hard scattering process via an exchange of a photon of virtual mass-squared $q^2=-Q^2$.

To get a better understanding of the evolution, it is helpful to imagine every sequence of branchings as a path in (t,x)-space, as in figure 1.4. The path starts at (t_0,x_0) and follows a parallel to the t-axis until a branching occurs at (t_1,x_0). Then there is a step downwards from x_0 to x_1 at constant t_1, where t_1 is equal to the virtual mass-squared after the branching.

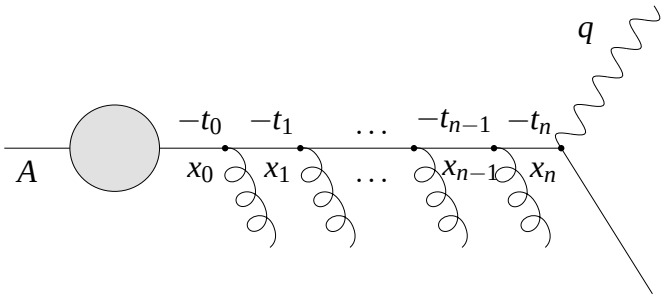

Figure 1.3: *Initial-state branching: multiple small-angle gluon emissions from a space-like quark.*

The cross-section of the hard scattering process depends on the scale Q^2 and on the momentum fraction distribution of the partons seen by the virtual photon at this scale, $D(x,Q^2)$. We derive an evolution equation for the scale-dependence of this distribution by the help of the pictorial representation introduced above. At $t = t_0$ the paths have a distribution $D(x_0,t_0)$ characteristic for the hadron A at this scale. The parton distribution $D(x,t)$ at scale t is the x-distribution of paths at this scale. When t is increased to $t+\delta t$, the change in the distribution of partons is the number of paths arriving in the element $(\delta t,\delta x)$ minus the number of paths leaving, divided by δx. We integrate the branching probability times the parton density over all momentum fractions $x' = x/z$ higher than x to get the total number of arriving paths:

$$\delta D_{\text{in}}(x,t) = \frac{\delta t}{t}\int_x^1 dx' \int_0^1 dz \frac{\alpha_s}{2\pi}\hat{P}(z)D(x',t)\delta(x-zx') = \frac{\delta t}{t}\int_0^1 \frac{dz}{z}\frac{\alpha_s}{2\pi}\hat{P}(z)D(x/z,t)\ . \qquad (1.41)$$

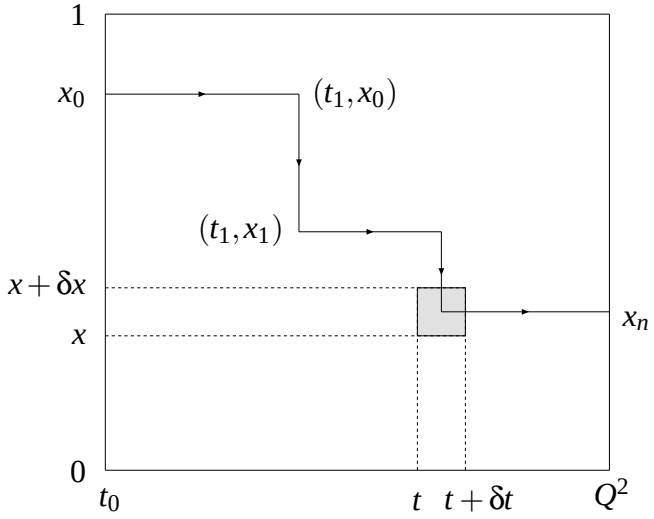

Figure 1.4: *Parton branching for a space-like parton as a path in* (t,x)*-space.*

The number of leaving paths can be obtained in a similar way by integrating over all momentum fractions $x' = xz$ lower than x:

$$\delta D_{\text{out}}(x,t) = \frac{\delta t}{t} D(x,t) \int_0^x dx' \int_0^1 dz \frac{\alpha_s}{2\pi} \hat{P}(z) \delta(x' - xz) = \frac{\delta t}{t} D(x,t) \int_0^1 dz \frac{\alpha_s}{2\pi} \hat{P}(z) \,. \tag{1.42}$$

The difference of them gives the net change of paths:

$$\delta D(x,t) = \delta D_{\text{in}}(x,t) - \delta D_{\text{out}}(x,t) = \frac{\delta t}{t} \int_0^1 dz \frac{\alpha_s}{2\pi} \hat{P}(z) \left[\frac{1}{z} D(x/z, t) - D(x,t) \right] \,. \tag{1.43}$$

Using this, we can write down the DGLAP evolution equation with the regularised splitting function:

$$t \frac{\partial}{\partial t} D(x,t) = \int_x^1 \frac{dz}{z} \frac{\alpha_s}{2\pi} P(z) D(x/z, t) \,. \tag{1.44}$$

The lower limit of the z-integration can be chosen as zero or x because the integrand vanishes for $z < x$. The function $D(x,t)$ is the distribution of parton momentum fractions inside the incoming hadron A at the scale t. For more than one type of partons this can be generalised to:

$$t \frac{\partial}{\partial t} D_i(x,t) = \sum_j \int_x^1 \frac{dz}{z} \frac{\alpha_s}{2\pi} P_{ij}(z) D_j(x/z, t) \,, \tag{1.45}$$

where $P_{ij}(z)$ is the regularised $i \to j$ splitting function and $D_i(x,t)$ is the distribution of partons of type i.

1.3.3 Sudakov Form Factors

There is a way to eliminate the plus prescription from the evolution equation by introducing a so-called Sudakov form factor [131]:

$$\Delta(t) = \exp\left(- \int_{t_0}^t \frac{dt'}{t'} \int dz \frac{\alpha_s}{2\pi} \hat{P}(z) \right) \,. \tag{1.46}$$

With that definition we can rewrite equation (1.43) as:

$$t \frac{\partial}{\partial t} D(x,t) = \int \frac{dz}{z} \frac{\alpha_s}{2\pi} \hat{P}(z) D(x/z, t) + \frac{D(x,t)}{\Delta(t)} t \frac{\partial}{\partial t} \Delta(t) \tag{1.47}$$

and

$$t \frac{\partial}{\partial t} \left(\frac{D}{\Delta} \right) = \frac{1}{\Delta} \int \frac{dz}{z} \frac{\alpha_s}{2\pi} \hat{P}(z) D(x/z, t) \,. \tag{1.48}$$

This has a form similar to the DGLAP equation (1.44). Integrating gives an equation for $D(x,t)$ in terms of the initial parton distribution $D(x,t_0)$:

$$D(x,t) = \Delta(t)D(x,t_0) + \int_{t_0}^{t} \frac{dt'}{t'} \frac{\Delta(t)}{\Delta(t')} \int \frac{dz}{z} \frac{\alpha_s}{2\pi} \hat{P}(z) D(x/z, t) \,. \tag{1.49}$$

This equation can be interpreted using the paths in (t,x)-space from figure 1.4: the first term on the right-hand side is the contribution of the path from t_0 until the first branching occurs at t. Thus the Sudakov factor is the probability of evolving from t_0 to t without branching. The second term gives the contribution from all paths which have their last branching at t', whereas the quotient $\Delta(t)/\Delta(t')$ stands for the probability of evolving from t' to t without branching. If there is more than one parton, each parton species i has its own Sudakov factor $\Delta_i(t)$. Additionally, if there is more than one possible type of branching, the sum over all allowed processes $i \to j$ has to be taken. In this case we get a generalised Sudakov form factor:

$$\Delta_i(t) = \exp\left(-\sum_j \int_{t_0}^{t} \frac{dt'}{t'} \int dz \frac{\alpha_s}{2\pi} \hat{P_{ji}}(z) \right) \,. \tag{1.50}$$

With the same generalisation, equation (1.48) becomes:

$$t\frac{\partial}{\partial t}\left(\frac{D_i}{\Delta_i}\right) = \frac{1}{\Delta_i} \sum_j \int \frac{dz}{z} \frac{\alpha_s}{2\pi} \hat{P_{ij}}(z) D_j(x/z, t) \,. \tag{1.51}$$

The infrared singularity of the unregularised splitting function at $z = 1$ can be removed by introducing an infrared cutoff $z < 1-\varepsilon(t)$. Branchings with $z > 1-\varepsilon(t)$ involve the emission of an undetectable soft parton and are not taken into account. The Sudakov factor with this cutoff gives the probability of evolving from t_0 to t without any resolvable branching.

The formulation of parton branching in terms of the Sudakov form factor is suitable for computer implementation. The task for the program is to generate values (t_2, x_2) for a given virtual mass scale t_1 and a given momentum fraction x_1. The value of t_2 can be obtained from

$$\frac{\Delta(t_2)}{\Delta(t_1)} = r_1 \,, \tag{1.52}$$

where r_1 is a uniformly distributed random number in the interval $[0,1]$. Since the left-hand side of this equation gives the probability of evolving from t_1 to t_2 without any resolvable branching, t_2 can be generated with the correct probability distribution in this way. If the t_2 determined in this way is bigger than Q^2, there is no further branching. If t_2 is smaller than Q^2, a value of the momentum fraction is generated. This is done according to a probability distribution proportional to $P(z)\alpha_s/(2\pi)$, by solving the equation:

$$\int_{\varepsilon}^{z} dz' \frac{\alpha_s}{2\pi} P(z') = r_2 \int_{\varepsilon}^{1-\varepsilon} dz' \frac{\alpha_s}{2\pi} P(z') \tag{1.53}$$

for another random number $r_2 \in [0,1]$, where ε is the infrared cut-off for resolvable branchings. If there are no further constraints, the azimuthal angle ϕ of the emitted parton is generated within the range $[0, 2\pi]$. With the given values of t_2, z and ϕ the momentum of the emitted parton can be calculated.

For branchings of partons with time-like momentum, t evolves downwards in the direction of the cut-off value t_0, instead of upwards towards Q^2 like in the case considered above. Then the equation to determine t_2 reads:

$$\frac{\Delta(t_1)}{\Delta(t_2)} = r_1 \,. \tag{1.54}$$

Since $\Delta(t_0) = 1$, this equation has no solution for $t_2 > t_0$ if $r_1 < \Delta(t_1)$, which correctly generates the probability for no resolvable branching. The momentum fraction z is generated like in the space-like case. The successive time-like branchings form a cascade of partons, called a *parton shower*, until the partons generate no additional branchings.

After the parton shower has terminated, we are left with a set of partons with virtual masses squared of the order of the cut-off scale t_0. Then perturbation theory is not applicable any more and hadronisation – also called fragmentation – sets in, converting the partons into observable hadrons. For the hadronisation process different models are used.

The simplest model supposes that each parton fragments independently [132, 133]. A quark, for example, is combined with an antiquark from a $q\bar{q}$ pair created out of the vacuum, to give a meson with energy fraction z. The remaining quark with energy fraction $1-z$ from the $q\bar{q}$ pair fragments in the same way, until the leftover energy falls below some cut-off. Every gluon is assumed to split into a $q\bar{q}$ pair before the described hadronisation process sets in.

In the simplest example of the *Lund string model* [134–137] a quark–antiquark pair moving apart in opposite directions losing energy to the colour field which collapses into a string-like configuration between them. Since the string has an uniform energy per unit length, the total energy rises until it eventually breaks apart through spontaneous $q\bar{q}$ production. Each of the separate strings can undergo further break-ups. In this model gluons produce kinks on the string [138] which leads to a different angular distribution compared to the independent fragmentation.

In the *cluster model* [139, 140] colour-singlet clusters of partons form after the partons in the shower stop branching. The clusters of typical masses of two or three times $\sqrt{t_0}$ decay into the observed hadrons.

1.3.4 Backward Evolution and Angular Ordering

In the previous subsections we discussed forward evolution. The initial momentum fraction x_0 of the emitting parton is known and the final value x_n is calculated. This is convenient in time-like evolution. For space-like showers it is more convenient and more efficient to start with the momentum fraction x_n of the final parton, because this parton takes part in the hard scattering. From x_n the preceding momentum fractions $x_{n-1}, \ldots, x_0$ are generated through backward evolution [141, 142].

An example is Drell–Yan production of a vector boson in hadron–hadron collisions. A quark with momentum fraction x_q and an antiquark with $x_{\bar{q}}$ coming from different hadrons

interact to produce a boson of mass M, where $M^2 \approx x_q x_{\bar{q}} s$ and $\sqrt{s}$ is the hadron–hadron centre-of-mass energy. The product of the final x_n's of the two space-like partons should have the right value to produce this particular boson. If the showers would be generated forwards, in most cases the product would not have the needed value. Thus the contributions to the cross-section would be negligible and the efficiency very low. In backward evolution we can choose the x_n's in the region where the contributions to the cross-section are big gaining a bigger efficiency.

The form factor in the case of backward evolution is modified:

$$\Delta(t_i) \to \frac{\Delta(t_i)}{D(x,t_i)}. \tag{1.55}$$

The probability of evolving backwards from (t_2,x) to (t_1,x) reads:

$$\Pi(t_1,t_2,x) = \frac{D(x,t_1)\Delta(t_2)}{D(x,t_2)\Delta(t_1)}. \tag{1.56}$$

The value of t_1 can be obtained from equating $\Pi(t_1,t_2,x)$ with a random number uniformly distributed in the interval $[0,1]$. To get the corresponding value for the momentum fraction, we generate $z = x_2/x_1$ with a probability distribution proportional to

$$\frac{\alpha_s}{2\pi}\frac{P(z)}{z} D(x_2/x_1,t_1)\,, \tag{1.57}$$

where $P(z)$ is the appropriate splitting function. The extra factor of $D(x_2/x_1,t_1)$ will be divided out in the next backward step in t. The generation of x can be done in a similar way like in forward evolution in equation (1.53).

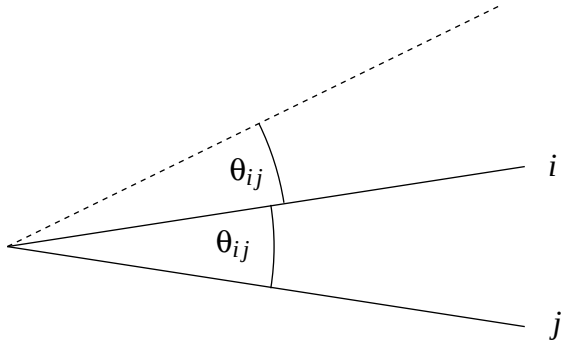

Figure 1.5: *Angular ordering: soft gluons from parton i are emitted inside a cone centred around the path of i with opening angle* $2\theta_{ij}$.

An investigation of the angular distribution of emitted soft gluons shows that gluons emitted by parton i are confined into a cone centred around the path of parton i with an opening angle $2\theta_{ij}$, where θ_{ij} is the angle between the trajectories of partons i and j. The cone of emitted gluons of parton j is centred around line j and has the same opening angle. After the emission of gluon k at angle $\theta_{ik} < \theta_{ij}$ the next gluon will be emitted within the angle θ_{ik}. The property of decreasing angles $\theta_{ij} > \theta_{ik} > \theta_{il} > \ldots$ is called *angular ordering*.

The analogue in electrodynamics is called Chudakov effect. The soft photon emission of an electron–positron pair is suppressed at angles larger than the opening angle of the pair. A simple explanation of this effect is that photons at larger angles do not see the individual charges of the electron and the positron, but only the net charge, which is zero, implying no emission.

Chapter 2

Born Gluon Amplitudes

In this chapter we compare four different methods for the numerical computation of pure gluonic amplitudes in the Born approximation [143]. These methods are Berends–Giele recurrence relations, recursive calculations with scalar diagrams, with maximal helicity violating (MHV) vertices and with shifted momenta. We investigate the efficiency of these methods for an increasing number of external particles and the numerical accuracy in critical phase space regions.

2.1 Four Different Methods

Using colour decomposition the tree-level amplitude with n external gluons can be written as

$$\mathcal{A}_n(k_1^{\lambda_1},\ldots,k_n^{\lambda_n}) = g^{n-2} \sum_{\sigma\in S_n/Z_n} 2\,\mathrm{Tr}\,(T^{a_{\sigma(1)}}\ldots T^{a_{\sigma(n)}})\, A_n\left(k_{\sigma(1)}^{\lambda_{\sigma(1)}},\ldots,k_{\sigma(n)}^{\lambda_{\sigma(n)}}\right), \tag{2.1}$$

where the sum runs over all non-cyclic permutations of the external gluon legs. In this formula k_j denotes the four-momentum of the j-th gluon and λ_j its helicity, while g stands for the strong coupling constant and T^a the colour matrices, which are normalised such that $\mathrm{Tr}(T^a T^b) = 1/2\,\delta^{ab}$. The gauge invariant partial amplitudes A_n contain the kinematic information and are invariant under cyclic permutations. They are colour-ordered, i. e. only diagrams with a particular cyclic ordering of the gluons contribute. In the computation of observables and cross sections enters the squared amplitude summed over all helicities and colour degrees of freedom

$$|\mathcal{A}_n|^2 = 2^{2-n} g^{2n-4} N_c^n \sum_{\lambda_1,\ldots,\lambda_n} \sum_{\sigma\in S_n/Z_n} \left|A_n\left(k_{\sigma(1)}^{\lambda_{\sigma(1)}},\ldots,k_{\sigma(n)}^{\lambda_{\sigma(n)}}\right)\right|^2 + \mathcal{O}\left(\frac{1}{N_c^2}\right). \tag{2.2}$$

Here $N_c = 3$ is the number of colours. The interference terms between partial amplitudes of different colour-orderings are colour-suppressed (of $\mathcal{O}(N_c^{-2})$). In the following we examine partial amplitudes A_n summed over all helicities (but not over the colour structures)

$$\mathcal{M}_n = \sum_{\lambda_1,\ldots,\lambda_n} \left|A_n\left(k_1^{\lambda_1},\ldots,k_n^{\lambda_n}\right)\right|^2. \tag{2.3}$$

$\mathcal{M}_n$ gives the leading-colour contribution to equation (2.2) and depends only on the kinematical information. It is used to study the efficiency of various methods to calculate the partial amplitudes A_n. Since parity relates a partial amplitude to the one with all helicities reversed, we only have to calculate half of the helicity configurations:

$$A_n\left(k_1^{\lambda_1},\ldots,k_n^{\lambda_n}\right) = -A_n\left(k_1^{-\lambda_1},\ldots,k_n^{-\lambda_n}\right)^* . \tag{2.4}$$

The partial amplitude is also invariant under cyclic permutation of its arguments and satisfies a reflection identity

$$A_n\left(k_n^{\lambda_n},\ldots,k_1^{\lambda_1}\right) = (-1)^n A_n\left(k_1^{\lambda_1},\ldots,k_n^{\lambda_n}\right)^* . \tag{2.5}$$

With the shorthand notation

$$A_n(1,2,\ldots,n) = A_n\left(k_1^{\lambda_1},k_2^{\lambda_2},\ldots,k_n^{\lambda_n}\right) \tag{2.6}$$

we can write down the cyclicity property:

$$A_n(1,2,\ldots,n) = A_n(2,3,\ldots,n,1) \tag{2.7}$$

and the identity:

$$A_n(1,2,3,\ldots,n)+A_n(2,1,3,\ldots,n)+A_n(2,3,1,\ldots,n)+\ldots+A_n(2,3,\ldots,1,n) = 0\ , \tag{2.8}$$

which is called photon decoupling equation [144] or dual Ward identity [90] or subcyclic property [87]. Partial amplitudes with all helicities plus (minus) as well as partial amplitudes with all helicities plus (minus) and only one minus (plus) vanish:

$$\begin{aligned} A_n\left(k_1^{\pm},k_2^{+},\ldots,k_n^{+}\right) &= 0 \\ A_n\left(k_1^{\pm},k_2^{-},\ldots,k_n^{-}\right) &= 0\ . \end{aligned} \tag{2.9}$$

The first non-vanishing amplitudes are those with all but two of the same helicity. A closed-form expression for this was found by Parke and Taylor [107]:

$$A_n(k_1^+,\ldots,k_{j-1}^+,k_j^-,k_{j+1}^+,\ldots,k_{k-1}^+,k_k^-,k_{k+1}^+,\ldots,k_n^+) = i\frac{\langle jk\rangle^4}{\langle 12\rangle\langle 23\rangle\ldots\langle n1\rangle}\ . \tag{2.10}$$

Kosower gave an expression for an amplitude with three negative helicities and the remaining ones positive [99]. The formula would fill half a page.

We also investigate the numerical accuracy of the various methods in critical phase space regions, i. e. regions where one or more partons become unresolved (soft or collinear). In the limit where gluon j becomes soft, the partial amplitudes behave as:

$$\begin{aligned} A_{n+1}(k_1,\ldots,k_j^+,\ldots,k_{n+1}) &\overset{k_j\ soft}{\longrightarrow} \sqrt{2}\frac{\langle k_{j-1}k_{j+1}\rangle}{\langle k_{j-1}k_j\rangle\langle k_jk_{j+1}\rangle}\,A_n(k_1,\ldots,k_{n+1}), \\ A_{n+1}(k_1,\ldots,k_j^-,\ldots,k_{n+1}) &\overset{k_j\ soft}{\longrightarrow} \sqrt{2}\frac{[k_{j+1}k_{j-1}]}{[k_{j+1}k_j][k_jk_{j-1}]}\,A_n(k_1,\ldots,k_{n+1}). \end{aligned} \tag{2.11}$$

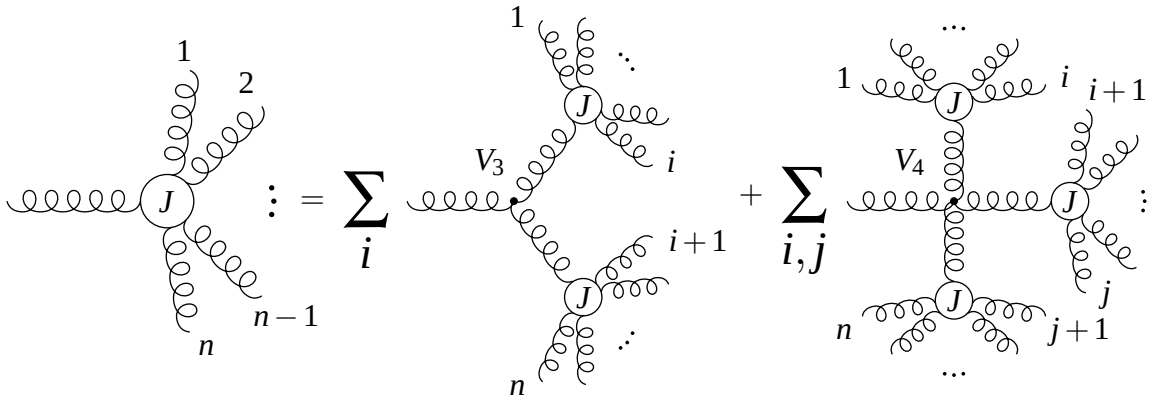

Figure 2.1: *Pictorial representation of the Berends–Giele recurrence relation. The gluons 1 to n are on-shell and the others off-shell.*

The spinor products $\langle k_i k_j \rangle$ and $[k_i k_j]$ are defined in appendix A.2. The quantity $\mathcal{M}_n$ factorises in the soft limit as:

$$\mathcal{M}_{n+1}(k_1,\ldots,k_j,\ldots,k_{n+1}) \xrightarrow{k_j \, soft} 2\,\frac{(2k_{j-1}k_{j+1})}{(2k_{j-1}k_j)(2k_jk_{j+1})}\,\mathcal{M}_n(k_1,\ldots,k_{n+1}). \tag{2.12}$$

In the collinear limit tree-level partial amplitudes factorise according to:

$$A_{n+1}(\ldots,k_a,k_b,\ldots) \xrightarrow{k_a||k_b} \sum_{\lambda=+/-} \mathrm{Split}_{-\lambda}(k_a^{\lambda_a},k_b^{\lambda_b})A_n(\ldots,K^{\lambda},\ldots), \tag{2.13}$$

where k_a and k_b are the momenta of two adjacent legs, $K = k_a + k_b$, $k_a = zK$ and $k_b = (1-z)K$. The corresponding helicities are denoted by λ, λ_a and λ_b. The splitting functions are listed in appendix A.3. In the collinear limit the quantity $\mathcal{M}_n$ behaves as [145–148]:

$$\mathcal{M}_{n+1}(\ldots,k_a,k_b,\ldots) \xrightarrow{k_a||k_b} \frac{2}{2k_ak_b}\left(\frac{2}{1-z}+\frac{2}{z}-4\right)\mathcal{M}_n(\ldots,K^{\lambda},\ldots)+\frac{8}{(2k_ak_b)^2}\mathcal{S}_n, \tag{2.14}$$

where the spin correlation is given by:

$$\mathcal{S}_n = \sum_{\lambda_1,\ldots,\lambda_{a-1},\lambda_{b+1},\ldots,\lambda_n} \left| EA_n\left(k_1^{\lambda_1},\ldots,K^{+},\ldots,k_n^{\lambda_n}\right) + E^*A_n\left(k_1^{\lambda_1},\ldots,K^{-},\ldots,k_n^{\lambda_n}\right)\right|^2 \tag{2.15}$$

and

$$E = z\frac{\langle k_b^+|k_a|K^+\rangle}{\sqrt{2}[Kk_b]}. \tag{2.16}$$

2.1.1 Berends–Giele Recurrence Relations

Berends–Giele type recurrence relations [98, 99] were introduced in 1987 by F. A. Berends and W. T. Giele. Pedagogical introductions can be found in references [90, 149, 150]. These

kinds of recurrence relations build partial amplitudes from smaller building blocks, so-called colour-ordered off-shell currents. Off-shell currents have n on-shell legs and one additional off-shell leg. They are not gauge-invariant.

Recurrence relations relate off-shell currents with n legs to off-shell currents with fewer legs. The recursion starts with $n = 1$:

$$J^\mu(k_1) = \varepsilon^\mu(k_1, q) \,. \tag{2.17}$$

The variable ε^μ is the polarisation vector of the gluon and q is an arbitrary light-like reference momentum. For positive and negative polarisation this vector looks like:

$$\varepsilon^+_\mu(k,q) = \frac{\langle q^-|\gamma_\mu|k^-\rangle}{\sqrt{2}\langle q^-|k^+\rangle}\,, \quad \varepsilon^-_\mu(k,q) = \frac{\langle q^+|\gamma_\mu|k^+\rangle}{\sqrt{2}\langle k^+|q^-\rangle}\,. \tag{2.18}$$

A gluon couples to other gluons only via the three- or four-gluon vertices. Therefore the recursive relation can be written in the following form:

$$\begin{aligned} J^\mu(k_1^{\lambda_1},\ldots,k_n^{\lambda_n}) = \frac{-i}{K_{1,n}^2}\Bigg[&\sum_{j=1}^{n-1} V_3^{\mu\nu\rho}(-K_{1,n},K_{1,j},K_{j+1,n}) J_\nu(k_1^{\lambda_1},\ldots,k_j^{\lambda_j}) J_\rho(k_{j+1}^{\lambda_{j+1}},\ldots,k_n^{\lambda_n}) \\ &+ \sum_{j=1}^{n-2}\sum_{l=j+1}^{n-1} V_4^{\mu\nu\rho\sigma} J_\nu(k_1^{\lambda_1},\ldots,k_j^{\lambda_j}) J_\rho(k_{j+1}^{\lambda_{j+1}},\ldots,k_l^{\lambda_l}) J_\sigma(k_{l+1}^{\lambda_{l+1}},\ldots,k_n^{\lambda_n})\Bigg]\,, \end{aligned} \tag{2.19}$$

where

$$K_{i,j} = \sum_{l=i}^{j} k_l = k_i + k_{i+1} + \ldots + k_j \tag{2.20}$$

and V_3 and V_4 are the colour-ordered three-gluon and four-gluon vertices

$$\begin{aligned} V_3^{\mu\nu\rho}(k_1,k_2,k_3) &= i\Big(g^{\mu\nu}\left(k_1^\rho - k_2^\rho\right) + g^{\nu\rho}\left(k_2^\mu - k_3^\mu\right) + g^{\rho\mu}\left(k_3^\nu - k_1^\nu\right)\Big), \\ V_4^{\mu\nu\rho\sigma} &= i\left(2g^{\mu\rho}g^{\nu\sigma} - g^{\mu\nu}g^{\rho\sigma} - g^{\mu\sigma}g^{\nu\rho}\right). \end{aligned} \tag{2.21}$$

Since gluon current J_μ is conserved:

$$\left(\sum_{i=1}^{n} k_i^\mu\right) J_\mu = K_{1,n}^\mu J_\mu = 0, \tag{2.22}$$

terms proportional to $K_{1,j}^\nu$ and to $K_{j+1,n}^\rho$ can be dropped in equation (2.19). Using momentum conservation, we get

$$V_3^{\mu\nu\rho}(k_1,k_2,k_3) = V_3^{\mu\nu\rho}(k_2,k_3) = i\left(g^{\nu\rho}(k_2-k_3)^\mu + 2g^{\rho\mu}k_3^\nu - 2g^{\mu\nu}k_2^\rho\right) \tag{2.23}$$

for the three gluon vertex in equation (2.19). With the shorthand notation

$$J^\mu(1,2,\ldots,n) = J^\mu\left(k_1^{\lambda_1},k_2^{\lambda_2},\ldots,k_n^{\lambda_n}\right) \tag{2.24}$$

we can write down the decoupling equation for off-shell currents J^μ (similar to equation 2.8):

$$J^\mu(1,2,3,\ldots,n)+J^\mu(2,1,3,\ldots,n)+J^\mu(2,3,1,\ldots,n)+\ldots+J^\mu(2,3,\ldots,n,1)=0 \quad (2.25)$$

and the reflection identity (similar to equation 2.5):

$$J^\mu(1,2,3,\ldots,n)=(-1)^{n+1}J^\mu(n,\ldots,3,2,1). \quad (2.26)$$

The partial amplitude $A_n(k_1^{\lambda_1},\ldots,k_n^{\lambda_n})$ can be obtained from the gluonic off-shell current $J^\mu(k_1^{\lambda_1},\ldots,k_{n-1}^{\lambda_{n-1}})$ by multiplying by the inverse gluon propagator and contracting with the polarisation vector for gluon n:

$$A_n\big(k_1^{\lambda_1},\ldots,k_n^{\lambda_n}\big)=\varepsilon_\mu^{\lambda_n}\big(k_n,q\big)\cdot\big(iK_{1,n-1}^2\big)J^\mu\big(k_1^{\lambda_1},\ldots,k_{n-1}^{\lambda_{n-1}}\big). \quad (2.27)$$

In some cases it is possible to give a closed form expression for the current:

$$J^\mu(1^+,2^+,\ldots,n^+)=\frac{\langle q^-|\gamma^\mu \not{K}_{1,n}|q^+\rangle}{\sqrt{2}\langle q1\rangle\langle 12\rangle\ldots\langle n-1,n\rangle\langle nq\rangle}, \quad (2.28)$$

$$J^\mu(1^-,2^+,\ldots,n^+)=\frac{\langle 1^-|\gamma^\mu \not{K}_{2,n}|1^+\rangle}{\sqrt{2}\langle 12\rangle\ldots\langle n1\rangle}\sum_{m=3}^{n}\frac{\langle 1^-|\not{k}_m \not{K}_{1,m}|1^+\rangle}{K_{1,m-1}^2K_{1,m}^2}, \quad (2.29)$$

where the reference momenta for equation (2.29) are $q_1=k_2$ and $q_2=\ldots=q_n=k_1$. With the help of equation (A.22) one can show, that the corresponding partial amplitude for the current in equation (2.28) vanishes (see equation 2.9).

In the recursion relation equation (2.19) only the quantities $J^\mu(k_i^{\lambda_i},\ldots,k_{j-1}^{\lambda_{j-1}})$ which respect the original order need to be calculated. Therefore an efficient implementation stores a list of four-momenta

$$[k_1,k_2,\ldots,k_n] \quad (2.30)$$

and a list of helicities

$$[\lambda_1,\lambda_2,\ldots,\lambda_n] \quad (2.31)$$

in memory and passes to the subroutine just two integers i and j, indicating that the quantity

$$J^\mu(k_i^{\lambda_i},\ldots,k_{j-1}^{\lambda_{j-1}}) \quad (2.32)$$

should be computed.

2.1.2 Recursive Calculation with Scalar Diagrams

The recursive calculation with scalar diagrams is a modification of the Berends–Giele recursion relation [99, 151, 152]. In this approach all summations over Lorentz indices are replaced by a sum over the two physical polarisations. This reduces the number of multiplications needed for a contraction from four to two. The resulting recurrence relation consists of scalar propagators and a set of primitive vertices.

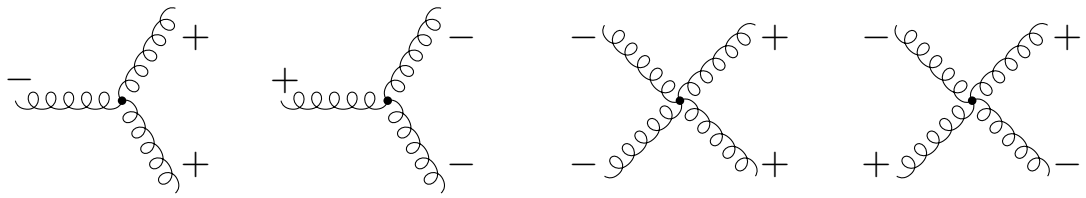

Figure 2.2: *The non-vanishing gluon amplitudes are the building blocks for recursive calculations with scalar diagrams. The mathematical expressions can be found in appendix A.4.3. A pictorial representation of the recursive calculation with scalar diagrams would look similar to the one of the Berends–Giele relation in figure 2.1.*

Let q be a null-vector, which will be kept fixed throughout the discussion. Using q, any massive vector k can be written as a sum of two null-vectors $k^\flat$ and q [153]:

$$k = k^\flat + \frac{k^2}{2kq} q. \tag{2.33}$$

Obviously, if $k^2 = 0$, we have $k = k^\flat$. Note further that $2kq = 2k^\flat q$. Using equation (2.33) we may associate a massless four-vector $k^\flat$ to any four-vector k. Using the projection onto $k^\flat$ we define the off-shell continuation of Weyl spinors as:

$$\begin{aligned} |k^\pm\rangle &\to |k^{\flat\pm}\rangle, \\ \langle k^\pm| &\to \langle k^{\flat\pm}|. \end{aligned} \tag{2.34}$$

We are going to use the following abbreviations:

$$\begin{aligned} \langle ij\rangle &= \left\langle k_i^{\flat-} | k_j^{\flat+} \right\rangle, \\ [ij] &= \left\langle k_i^{\flat+} | k_j^{\flat-} \right\rangle, \\ \left\langle i^- | j \pm k | l^- \right\rangle &= \left\langle k_i^{\flat-} \left| \not{k}_j^\flat \pm \not{k}_k^\flat \right| k_l^{\flat-} \right\rangle. \end{aligned} \tag{2.35}$$

In spinor products, the projections $k^\flat$ are always used. Let us define an *off-shell amplitude*:

$$O_n\left(k_1^{\lambda_1}, k_2^{\lambda_2}, \ldots, k_n^{\lambda_n}\right), \tag{2.36}$$

depending on n external momenta k_i and helicities λ_i. The momenta need not to be on-shell, but momentum conservation is imposed:

$$\sum_{j=1}^{n} k_j = 0. \tag{2.37}$$

By definition, the off-shell amplitudes O_n are calculated from all Feynman diagrams contributing to the cyclic-ordered partial amplitude A_n, by using the off-shell continuation equation (2.34) for all external spinors and polarisation vectors, and by using the axial gauge for

all internal gluon propagators. Compared to off-shell currents, which are used in recurrence relations of Berends–Giele type, an off-shell amplitude may have more than one leg off-shell. By construction, if all external particles are on-shell, the off-shell amplitude O_n coincides with the physical amplitude A_n. We have the following recurrence relation:

$$\begin{aligned} O_n\left(k_1^{\lambda_1},\ldots,k_n^{\lambda_n}\right) &= \sum_{\lambda,\lambda'=\pm}\sum_{j=2}^{n-1} V_3(K_{1,j-1}^{\lambda},K_{j,n-1}^{\lambda'},k_n^{\lambda_n}) \\ &\times\frac{i}{K_{1,j-1}^2}O_j(k_1^{\lambda_1},\ldots,k_{j-1}^{\lambda_{j-1}},(-K_{1,j-1})^{-\lambda})\frac{i}{K_{j,n-1}^2}O_{n-j+1}(k_j^{\lambda_j},\ldots,k_{n-1}^{\lambda_{n-1}},(-K_{j,n-1})^{-\lambda'}) \\ &+\sum_{\lambda,\lambda',\lambda''=\pm}\sum_{j=2}^{n-2}\sum_{l=j+1}^{n-1} V_4\left(K_{1,j-1}^{\lambda},K_{j,l-1}^{\lambda'},K_{l,n-1}^{\lambda''},k_n^{\lambda_n}\right)\frac{i}{K_{1,j-1}^2}O_j(k_1^{\lambda_1},\ldots,k_{j-1}^{\lambda_{j-1}},(-K_{1,j-1})^{-\lambda}) \\ &\times\frac{i}{K_{j,l-1}^2}O_{l-j+1}(k_j^{\lambda_j},\ldots,k_{l-1}^{\lambda_{l-1}},(-K_{j,l-1})^{-\lambda'})\frac{i}{K_{l,n-1}^2}O_{n-l+1}(k_l^{\lambda_l},\ldots,k_{n-1}^{\lambda_{n-1}},(-K_{l,n-1})^{-\lambda''}), \end{aligned} \tag{2.38}$$

where we define the two-point amplitude to be the inverse propagator:

$$O_2(k_j^{\pm},-K_{j,j}^{\mp}) = -ik_j^2. \tag{2.39}$$

The partial amplitude A_n coincides with O_n, if all gluons are on-shell:

$$A_n(k_1^{\lambda_1},\ldots,k_n^{\lambda_n}) = O_n(k_1^{\lambda_1},\ldots,k_n^{\lambda_n}). \tag{2.40}$$

There is only a limited number of non-zero vertices, which are listed in appendix A.4.3. This allows for a high degree of optimisation in the calculation of theses vertices. The double and triple sums over the intermediate helicities in equation (2.38) reduce in all cases to three non-vanishing terms.

On the other hand it should be pointed out, that in this approach the four-valent vertices depend (as do the three-valent vertices) on the momenta attached to these vertices. This should be compared to the standard Feynman rules, which enter the Berends–Giele recurrence relations, where the four-gluon vertex in equation (2.21) is independent of the momenta.

As in the Berends–Giele recurrence relations, an efficient implementation stores the sequence of four-momenta and helicities in a central place and just passes two integers i and j to the implementation of the recurrence relation, indicating the starting and ending points.

2.1.3 Recursive Calculation with MHV Vertices

In the Cachazo–Svrček–Witten (CSW) construction [105], tree-level QCD amplitudes are constructed from vertices that are off-shell continuations of maximal helicity violating (MHV) amplitudes, connected by scalar propagators. In maximal-helicity-violating amplitudes all gluons but two have the same helicity. Compact formulæ for these amplitudes have been known for a long time [107]. Using the off-shell continuation equation (2.34) the MHV-

amplitudes serve as new vertices:

$$V_n(k_1^+,\ldots,k_{j-1}^+,k_j^-,k_{j+1}^+,\ldots,k_{k-1}^+,k_k^-,k_{k+1}^+,\ldots,k_n^+) = i\left(\sqrt{2}\right)^{n-2}\frac{\langle jk\rangle^4}{\langle 12\rangle\langle 23\rangle\ldots\langle n1\rangle}, \quad (2.41)$$

$$V_n(k_1^-,\ldots,k_{j-1}^-,k_j^+,k_{j+1}^-,\ldots,k_{k-1}^-,k_k^+,k_{k+1}^-,\ldots,k_n^-) = i\left(\sqrt{2}\right)^{n-2}\frac{[kj]^4}{[1n][n(n-1)]\ldots[21]}.$$

Each MHV vertex has exactly two lines carrying negative helicity and at least one line carrying positive helicity.

Bena, Bern and Kosower [154] derived a recursive formulation, which allows to obtain vertices with more gluons of negative helicity from simpler building blocks:

$$V_n(k_1^{\lambda_1},\ldots,k_n^{\lambda_n}) = \frac{1}{(n_{\text{neg}}-2)}\sum_{j=1}^{n}\sum_{l=j+1}^{j-3}\frac{i}{K_{j,l}^2}V_{(l-j+2) \bmod n}(k_j^{\lambda_j},\ldots,k_l^{\lambda_l},(-K_{j,l})^-) \times V_{(j-l) \bmod n}(k_{l+1}^{\lambda_{l+1}},\ldots,k_{j-1}^{\lambda_{j-1}},(-K_{(l+1),(j-1)})^+), \quad (2.42)$$

where n_{neg} is the number of negative helicity gluons. The recursion starts if n_{neg} is less than two. For $n_{\text{neg}}=0$ or $n_{\text{neg}}=1$ the quantity $V_n(k_1^{\lambda_1},\ldots,k_n^{\lambda_n})$ vanishes. For $n_{\text{neg}}=2$ it is given by equation (2.41). Again, the partial amplitude A_n coincides with V_n, if all gluons are on-shell:

$$A_n(k_1^{\lambda_1},\ldots,k_n^{\lambda_n}) = V_n(k_1^{\lambda_1},\ldots,k_n^{\lambda_n}). \quad (2.43)$$

There are two points which should be noted: first of all, there is a double sum in equation (2.42), which over-counts each contribution $(n_{\text{neg}}-2)$ times. This over-counting is compensated by the explicit factor $1/(n_{\text{neg}}-2)$ in front. Secondly, it is no longer possible to work with a static list of four-vectors and helicities, as it was the case for the first two methods. The recursion relation equation (2.42) inserts the four-momenta $-K_{j,l}$ and $-K_{(l+1),(j-1)}$ into the cyclic order. Therefore the lists of momenta and helicities have to be updated at each step of the recursion. This is best implemented by a double-linked list, which allows for the insertion of the new elements without copying the remaining ones.

2.1.4 Recursive Calculation with Shifted Momenta

Britto, Cachazo and Feng [108] gave a recursion relation for the calculation of the n-gluon amplitude, which involves only on-shell amplitudes. To describe this method it is best to view the partial amplitude A_n not as a function of the four-momenta k_j^μ, but to replace each four-vector by a pair of two-component Weyl spinors. In detail this is done as follows: each four-vector K_μ has a bispinor representation, given by:

$$K_{A\dot{B}} = K_\mu \sigma^\mu_{A\dot{B}}, \qquad K_\mu = \frac{1}{2}K_{A\dot{B}}\bar{\sigma}_\mu^{\dot{B}A}. \quad (2.44)$$

For null-vectors this bispinor representation factorises into a dyad of Weyl spinors:

$$k_\mu k^\mu = 0 \Leftrightarrow k_{A\dot{B}} = k_A k_{\dot{B}}. \quad (2.45)$$

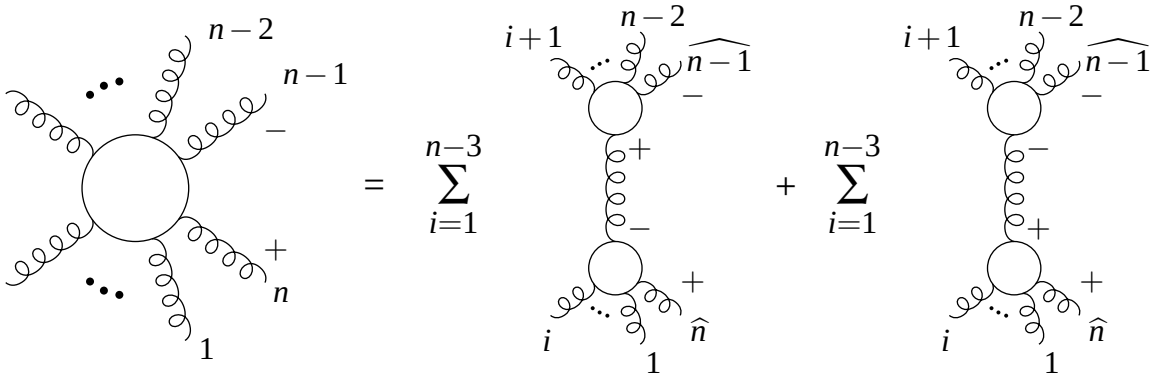

Figure 2.3: *Pictorial representation of the recursive calculation with shifted momenta.*

The equations (2.44) and (2.45) allow us to convert any light-like four-vector into a dyad of Weyl spinors and vice versa. Therefore the partial amplitude A_n, being originally a function of the momenta k_j and helicities λ_j, can equally be viewed as a function of the Weyl spinors k_A^j, $k_{\dot{B}}^j$ and the helicities λ_j:

$$A_n\big(k_1^{\lambda_1},\ldots,k_n^{\lambda_n}\big) = A_n\big(k_A^1,k_{\dot{B}}^1,\lambda_1,\ldots,k_A^n,k_{\dot{B}}^n,\lambda_n\big). \tag{2.46}$$

Note that for an arbitrary pair of Weyl spinors, the corresponding four-vector will in general be complex valued. If $(\lambda_n,\lambda_1)\neq(+,-)$ we have the following recurrence relation:

$$\begin{aligned} A_n\big(k_A^1,k_{\dot{B}}^1,&\lambda_1,\ldots,k_A^n,k_{\dot{B}}^n,\lambda_n\big) = \\ &\sum_{j=3}^{n-1}\sum_{\lambda=\pm} A_j\big(\hat{k}_A^1,k_{\dot{B}}^1,\lambda_1,k_A^2,k_{\dot{B}}^2,\lambda_2,\ldots,k_A^{j-1},k_{\dot{B}}^{j-1},\lambda_{j-1},i\hat{K}_A,i\hat{K}_{\dot{B}},-\lambda\big) \\ &\times\frac{i}{K_{1,j-1}^2}A_{n-j+2}\big(\hat{K}_A,\hat{K}_{\dot{B}},\lambda,k_A^j,k_{\dot{B}}^j,\lambda_j,\ldots,k_A^{n-1},k_{\dot{B}}^{n-1},\lambda_{n-1},k_A^n,\hat{k}_{\dot{B}}^n,\lambda_n\big). \end{aligned} \tag{2.47}$$

If $(\lambda_n,\lambda_1)=(+,-)$ we can always cyclic permute the arguments, such that $(\lambda_n,\lambda_1)\neq(+,-)$. This is possible, since on-shell amplitudes, where all gluons have the same helicity, vanish. In equation (2.47) the shifted spinors $\hat{k}_A^1$, $\hat{k}_{\dot{B}}^n$, $\hat{K}_A$ and $\hat{K}_{\dot{B}}$ are given by:

$$\begin{aligned} \hat{k}_A^1 &= k_A^1 - zk_A^n, \quad \hat{K}_A = \frac{K_{A\dot{B}}k_1^{\dot{B}}}{\sqrt{\langle 1^+|K|\,n^+\rangle}}, \\ \hat{k}_{\dot{B}}^n &= k_{\dot{B}}^n + zk_{\dot{B}}^1, \quad \hat{K}_{\dot{B}} = \frac{k_n^A K_{A\dot{B}}}{\sqrt{\langle 1^+|K|\,n^+\rangle}}, \end{aligned} \tag{2.48}$$

where

$$K_{A\dot{B}} = \sum_{l=1}^{j-1} k_A^l k_{\dot{B}}^l, \quad K_{1,j-1}^2 = \det K_{A\dot{B}}, \tag{2.49}$$

and

$$z = \frac{K^2_{1,j-1}}{\langle 1^+ | K | n^+ \rangle}. \tag{2.50}$$

The recurrence relation starts with $n = 3$. The only non-vanishing amplitudes are:

$$\begin{aligned} A_3\left(k^1_A, k^1_{\dot{B}}, -, k^2_A, k^2_{\dot{B}}, -, k^3_A, k^3_{\dot{B}}, +\right) &= i\sqrt{2}\frac{\langle 12\rangle^4}{\langle 12\rangle\langle 23\rangle\langle 31\rangle}, \\ A_3\left(k^1_A, k^1_{\dot{B}}, +, k^2_A, k^2_{\dot{B}}, +, k^3_A, k^3_{\dot{B}}, -\right) &= i\sqrt{2}\frac{[21]^4}{[32][21][13]} \end{aligned} \tag{2.51}$$

and the ones with cyclic permutations of the helicities. It should be noted that due to our choice of shifting the spinors, the three point function with $\hat{k}^1_A$ vanishes, if the helicities are a cyclic permutation of $(-,-,+)$. Similar, the three-point function involving $\hat{k}^n_{\dot{B}}$ vanishes, if the helicities are a cyclic permutation of $(+,+,-)$. To speed up the computation the Parke–Taylor formulæ in equation (2.41) may be used for $n \geq 4$.

As in the previous method we have to update at each step in the recursion the list of Weyl spinors and the helicities.

2.2 Comparison

In this section we study numerical implementations of recursive methods for the computation of Born gluon amplitudes. These amplitudes (together with corresponding ones, where additional quarks or vector bosons are involved), are relevant for LHC physics. They enter numerical NLO or LO program codes. As these calculations are based on Monte Carlo integration over the phase space, the efficiency of the computation has a direct impact on the running time of the Monte Carlo program.

From the four methods considered, we found the Berends–Giele method performs best, as the number of external partons increases ($n \geq 8$). However, for a not so large number of external partons ($n < 8$), the on-shell recursion relation (BCFW) offers the best performance.

We also investigated the numerical stability and accuracy. Here, all methods give satisfactory results.

2.2.1 Performance

We have implemented all four methods into a numerical program. All methods give identical results within an accuracy of 10^{-12} for randomly chosen non-exceptional phase space points and up to 12 external particles. To investigate the performance in terms of CPU time we study the quantity $\mathcal{M}_n$ defined in equation (2.3):

$$\mathcal{M}_n = \sum_{\lambda_1,\ldots,\lambda_n} \left| A_n\left(k^{\lambda_1}_1, \ldots, k^{\lambda_n}_n\right)\right|^2. \tag{2.52}$$

It is clear from the algorithms that the first two methods (Berends–Giele and scalar diagrams) need a constant amount of CPU time for each helicity configuration, whereas the last two

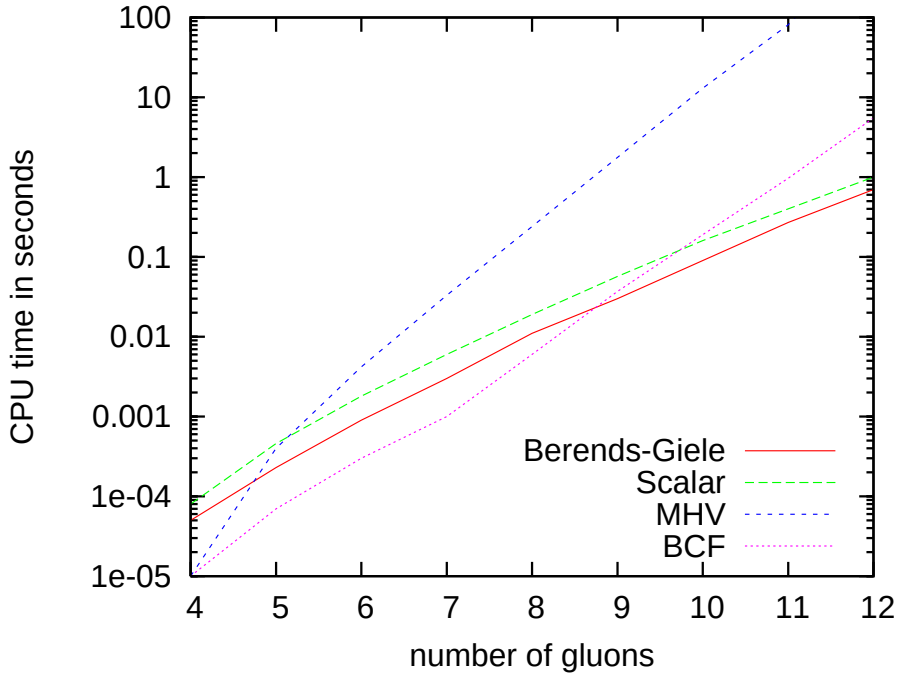

Figure 2.4: *CPU time in seconds for the computation of the n-gluon amplitude on a standard PC (Pentium IV with 2 GHz), summed over all helicities.*

methods (MHV and BCFW) are very efficient if the helicities are predominately all plus or all minus, but take more CPU time, if the helicity configuration contains roughly the same number of plus and minus helicities. To compare the different methods, the quantity $\mathcal{M}_n$ sums over all helicity configurations. This corresponds to the situation encountered in the calculation of cross sections and observables. Table 2.1 shows the CPU time needed for the computation of $\mathcal{M}_n$ as n varies from 4 to 12. The test was done on a standard PC with a Pentium IV processor with 2 GHz.

n	4	5	6	7	8	9	10	11	12
Berends–Giele	0.00005	0.00023	0.0009	0.003	0.011	0.030	0.09	0.27	0.7
Scalar	0.00008	0.00046	0.0018	0.006	0.019	0.057	0.16	0.4	1
MHV	0.00001	0.00040	0.0042	0.033	0.24	1.77	13	81	—
BCFW	0.00001	0.00007	0.0003	0.001	0.006	0.037	0.19	0.97	5.5

Table 2.1: *CPU time in seconds for the computation of the n-gluon amplitude on a standard PC (Pentium IV with 2 GHz), summed over all helicities.*

As can be seen from the table 2.1 and from figure 2.4, the Berends–Giele type recurrence relation is the fastest method, as the number of external gluons increases. In the second place comes the method with scalar diagrams, which has approximately the same slope. As already discussed in the presentation of the algorithms, these two methods are fast due to the fact that they can work with a static list of four-momenta and helicities. This avoids copying

large amounts of data at each step of the recursion. The scalar diagram technique allows for a higher degree of optimisation in the subroutines, but this is out-weighted by the fact, that in the Berends–Giele method each three- or four-valent vertex is called exactly once, whereas in the scalar diagram method each vertex is called three times with different helicity configurations. For smaller n up to circa eight the BCFW method is the fastest, but it has a steeper slope than the Berends–Giele recurrence relation and the scalar diagram technique, so that the latter both overtake the method of BCFW.

n	13	14	15	16	17	18	19	20
Berends–Giele	2	4	11	27	64	149	367	831
Scalar	3	6	15	36	85	195	465	1043

Table 2.2: *Continuation of table 2.1 for n in the range from* 13 *to* 20 *for the Berends–Giele method and the scalar diagram method. The settings are as in table 2.1.*

Table 2.2 shows the timings for the Berends–Giele method and the scalar diagram method for the computation of $\mathcal{M}_n$ as n varies from 13 to 20. It should be noted that for $n = 20$ the results of the two methods agree within 10^{-11}. It can be seen from table 2.1 and 2.2 that the CPU time for the scalar diagram method grows slower than the one for the Berends–Giele method as the number n of external particles increases.

The MHV method is rather slow compared to the other three methods. This is related to the double sum appearing in equation (2.42), which explicitly over-counts each contribution. In addition, the look-up tables we used to speed up the calculation are in this case rather memory-intensive. That is the reason why we were not able to compute the 12-gluon amplitude within this approach.

The BCFW method is faster than the Berends–Giele method as long as the number of external particles is below 9. For applications towards three- or four-jet rates at LHC the BCFW recurrence relations are therefore an improvement in efficiency.

2.2.2 Numerical Stability

We have shown, that all methods give identical results for randomly chosen non-exceptional phase space points within an accuracy of 10^{-12}. In this subsection we study the numerical stability near exceptional phase space points, e. g. near singular configurations where one or more partons become unresolved. We limit ourselves to single unresolved configurations, where an external momentum becomes soft, or two external momenta become collinear. In these cases the quantity $\mathcal{M}_n$ exhibits an infrared singularity and factorises into a singular function and a lower-point amplitude, as described by the equations (2.12) and (2.14). The singular behaviour can cause problems with the numerical stability of amplitude calculations. To investigate this problem, we evaluated $\mathcal{M}$ for configurations approaching each kind of singular limit. To illustrate the stability, we have plotted in figures 2.5 and 2.6 the ratio of a $\mathcal{M}_7$ to its factorised form $\mathcal{M}_7^{(f)}$ as given by the right-hand sides of equations (2.12) and (2.14). The soft limit (figure 2.5) is described by $x \to 0$ where x is the fraction of total energy carried by the soft gluon. The onset of instability is at $x \simeq 10^{-12}$. The collinear limit (figure 2.6)

is described by $p_T/E \to 0$ where p_T is the transverse momentum involved in the collinear splitting (with $z = 1/2$). Instability occurs when the dimensionless variable $p_T/E \simeq 10^{-7}$.

In addition to these physical singularities, spurious singularities might occur. An example can be found in the on-shell recursion relation. The shift in the spinors introduces sandwiches of the form $\langle p_i^- | p_k + p_l | p_j^- \rangle$ in the denominator. For example, the analytical formula for the six-gluon partial amplitude $A_6(1^+,2^+,3^+,4^-,5^-,6^-)$ reads:

$$A_6(1^+,2^+,3^+,4^-,5^-,6^-) = \\ 4i\left[\frac{\langle 6^-|1+2|3^-\rangle^3}{\langle 61\rangle\langle 12\rangle[34][45]s_{126}\langle 2^-|1+6|5^-\rangle} + \frac{\langle 4^-|5+6|1^-\rangle^3}{\langle 23\rangle\langle 34\rangle[56][61]s_{156}\langle 2^-|1+6|5^-\rangle}\right]. \quad (2.53)$$

This introduces unphysical singularities when sums of external momenta become collinear. Of course, these cancel exactly in the final result, but can lead to problems when the recursion relation is evaluated numerically. An example of this is shown in figure 2.7. Here we consider an amplitude of the form shown in equation (2.53), in the limit that $p_1 + p_6$ becomes collinear to $p_2 + p_5$. We have plotted the fractional error in the on-shell results by comparing to those of the Berends–Giele recursion relation. The onset of instability occurs when the transverse momentum is of the order of $10^{-7}E$.

The other recurrence relations can also exhibit spurious singularities, as each require an arbitrary light-like *reference* vector q to be specified, and various quantities diverge if this vector becomes collinear to one of the external momenta. For the Berends–Giele recurrence relations this vector is needed to define the polarisation vectors in equation (2.18), and for the scalar diagram and MHV vertex approaches it is needed to fix the on-shell projection in equation (2.33). The dependence of our results on q as q becomes collinear to an external momentum k is illustrated in figure 2.8. The scalar and MHV approaches become unstable when $\sqrt{k\cdot q} \simeq 10^{-7}E$, whereas the Berends–Giele relation is stable down to $\sqrt{k\cdot q} \simeq 10^{-12}E$.

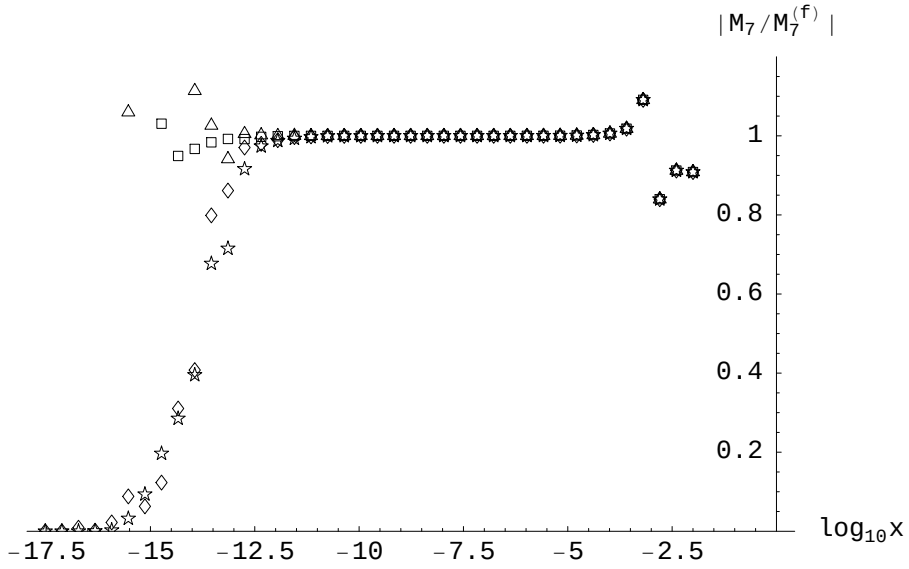

Figure 2.5: *Ratio of the helicity amplitude to its factorised form for a set of seven-gluon configurations where one gluon becomes soft. Here x is the energy fraction of the soft gluon. Key: ◇ Berends–Giele, ⋆ scalar diagrams, △ MHV rules, □ on-shell.*

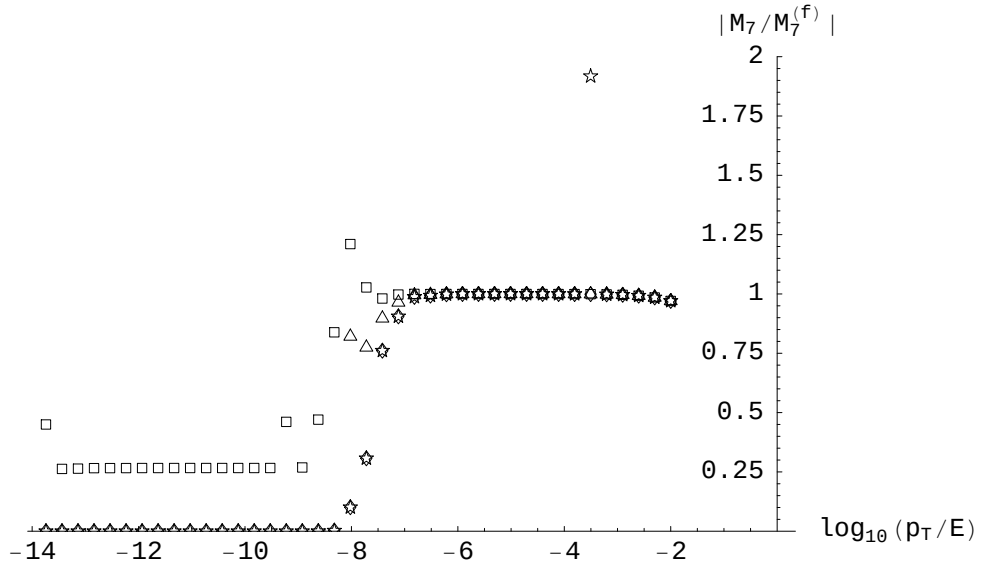

Figure 2.6: *Ratio of the helicity amplitude to its factorised form for a set of seven-gluon configurations where two gluons becomes collinear. Here p_T/E is the transverse momentum of the pair of gluons, normalised to the total energy. Key: ◇ Berends–Giele, ⋆ scalar diagrams, △ MHV rules, □ on-shell.*

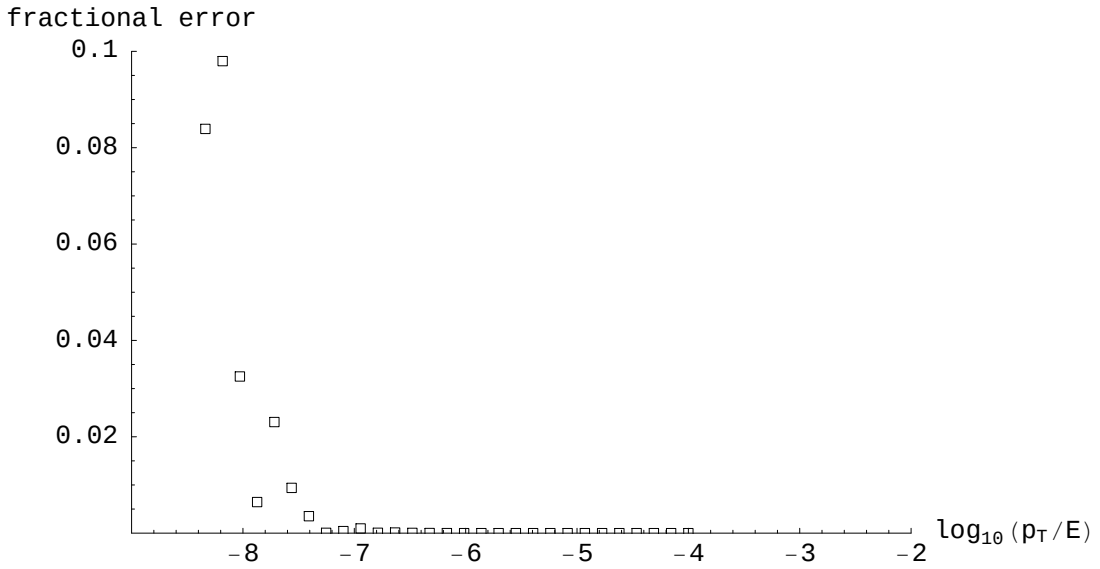

Figure 2.7: *Fractional error in the sum of squared helicity amplitudes computed with the on-shell recursion relations for a set of six-gluon configurations where $k_1 + k_2$ becomes collinear to $k_3 + k_4$. Here p_T/E is the transverse momentum between the two pairs of gluons, normalised to the total energy.*

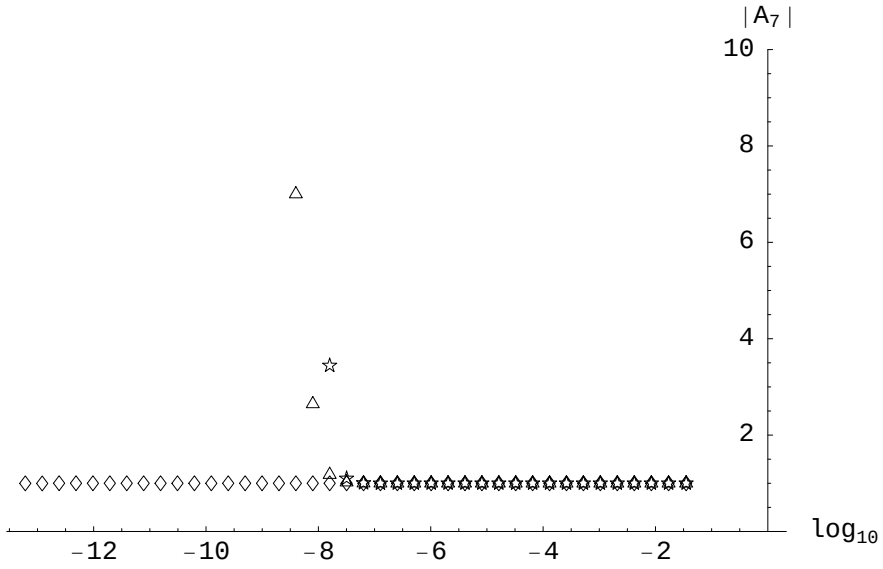

Figure 2.8: *Fractional error in the sum of squared helicity amplitudes as the reference vector (q) used in the definition of each recursion relation becomes collinear with an external momentum (k). Key: $\diamond$ Berends–Giele, $\star$ scalar diagrams, $\triangle$ MHV rules.*

Chapter 3

Shower Algorithm Using the Dipole Formalism

In this chapter we present an implementation of a parton shower algorithm for hadron colliders and electron–positron colliders based on the dipole factorisation formulæ [155]. The algorithm treats initial-state partons on equal footing with final-state partons. We implemented the algorithm for massless and massive partons.

3.1 Introduction

Event generators like PYTHIA [119, 120], HERWIG [121–123] or SHERPA [125] are a standard tool in high-energy particle physics. In these tools the physics of particle collisions is modelled by a simulation with different stages – hard scattering, parton showering, hadronisation – to name the most important ones. The hard scattering process is calculable in perturbation theory. The same holds – in theory at least – for the parton showering process, the relevant scales are still large enough for perturbation theory to be applicable. In practice however, one is forced into approximations due to the large parton multiplicities. These approximations are derived from the behaviour of the matrix elements in singular regions. The matrix elements become singular in phase space regions corresponding to the emission of collinear or soft particles. The first showering algorithms started from the collinear factorisation of the matrix elements and approximated colour interference effects through angular ordering [156, 157]. An exception is the algorithm implemented in ARIADNE [126, 158–161], which is based on a dipole cascade picture. Most shower algorithms are accurate to the leading-logarithmic approximation in the collinear limit. Extensions to the next-to-leading logarithmic approximation have been studied in references [162–165].

Recent years have witnessed significant developments related to shower algorithms, including procedures to match parton showers to fixed-order tree-level matrix elements [166–170] and methods to combine parton showers with next-to-leading order matrix elements [171–194]. The shower algorithms in PYTHIA, HERWIG and ARIADNE have been improved [195–197] and new programs like the shower module Apacic++ [198, 199] of SHERPA have become available. Other improvements include the study of uncertainties in parton show-

ers [200–202], as well as showers in the context of the soft-collinear effective theory [203].

Of particular importance is the matching of parton showers with next-to-leading order matrix elements. The pioneering project MC@NLO [180, 204–207] used an existing shower program (HERWIG) and adapted the NLO calculation to the shower algorithm, at the expense of sacrificing the correctness in certain soft limits. It is clear that a better but more labour-intensive approach would adapt the shower algorithm to NLO calculations. Nowadays in NLO computations the dipole subtraction method [145, 148, 208–210] is widely used. Nagy and Soper [184, 185] proposed to build a shower algorithm from the dipole subtraction terms.

In this chapter we report on an implementation of a shower algorithm based on the dipole formalism as suggested by Nagy and Soper. We take the dipole splitting functions as the splitting functions which generate the parton shower. In the dipole formalism, a dipole consists of an emitter–spectator pair, which emits a third particle, soft or collinear to the emitter. The formalism treats initial- and final-state partons on the same footing. In contrast to other shower algorithms, no distinction is made between final- and initial-state showers. The only difference between initial- and final-state particles occurs in the kinematics. In the implementation we have the four cases final–final, final–initial, initial–final and initial–initial corresponding to the possibilities of the particles of the emitter–spectator pair to be in the initial or final state. Because all four cases are included, the shower can be used for hadron colliders and electron–positron colliders. We implemented the shower for massless and massive partons. Initial-state partons are however always assumed to be massless. We use spin-averaged dipole splitting functions. The shower algorithm is correct in the leading-colour approximation. As the evolution variable we use the transverse momentum in the massless case, and a variable suggested in references [196, 211] for the massive case. The variable for the massive case reduces to the transverse momentum in the massless limit. Schumann and Krauss reported on a similar but separate implementation of a parton shower algorithm based on the dipole formalism [212, 213].

This chapter is organised as follows: in section 3.2 we review basic facts about the colour decomposition of QCD amplitudes and the dipole formalism. In section 3.3 we discuss the shower algorithm. In section 3.4 we present numerical results from the parton shower simulation program. Technical details can be found in the appendix. Appendix A.5 discusses the case of a massless final-state emitter and a massless final-state spectator in detail. Appendix A.6 describes the construction of the four-momenta of the $(n+1)$-particle state in all cases. This appendix is also useful in the context of a phase space generator for the real emission part of NLO computations.

3.2 QCD Amplitudes and the Dipole Formalism

In this section we briefly review the colour decomposition of QCD amplitudes and the dipole formalism.

3.2.1 Colour Decomposition

We use the normalisation $\mathrm{Tr}\,(T^a T^b) = {}^1\!/_2\,\delta^{ab}$ for the colour matrices. Amplitudes in QCD may be decomposed into group-theoretical factors (carrying the colour structures) multiplied

by kinematic functions called partial amplitudes [88, 89, 144, 214, 215]. The partial amplitudes are gauge-invariant objects. In the pure gluonic case tree-level amplitudes with n external gluons may be written in the form:

$$\mathcal{A}_n(1,2,\ldots,n) = \left(\frac{g}{\sqrt{2}}\right)^{n-2} \sum_{\sigma\in S_n/Z_n} \delta_{i_{\sigma_1} j_{\sigma_2}} \delta_{i_{\sigma_2} j_{\sigma_3}} \ldots \delta_{i_{\sigma_n} j_{\sigma_1}} A_n(\sigma_1,\ldots,\sigma_n), \tag{3.1}$$

where the sum is over all non-cyclic permutations of the external gluon legs. The quantities $A_n(\sigma_1,\ldots,\sigma_n)$, called the partial amplitudes, contain the kinematic information. They are colour-ordered, e. g. only diagrams with a particular cyclic ordering of the gluons contribute. The choice of the basis for the colour structures is not unique, and several proposals for bases can be found in the literature [216, 217]. Here we use the *colour-flow decomposition* [147, 217]. This basis is obtained by replacing every contraction over an index in the adjoint representation by two contractions over indices i and j in the fundamental representation:

$$V^a E^a = V^a \delta^{ab} E^b = V^a \left(2T^a_{ij} T^b_{ji}\right) E^b = \left(\sqrt{2} T^a_{ij} V^a\right)\left(\sqrt{2} T^b_{ji} E^b\right). \tag{3.2}$$

As a further example we give the colour decomposition for a tree amplitude with a pair of quarks:

$$\mathcal{A}_{n+2}(q,1,2,\ldots,n,\bar{q}) = \left(\frac{g}{\sqrt{2}}\right)^{n} \sum_{S_n} \delta_{i_q j_{\sigma_1}} \delta_{i_{\sigma_1} j_{\sigma_2}} \ldots \delta_{i_{\sigma_n} j_{\bar{q}}} A_{n+2}(q,\sigma_1,\sigma_2,\ldots,\sigma_n,\bar{q}), \tag{3.3}$$

where the sum is over all permutations of the gluon legs. The tree amplitude with a pair of quarks, n gluons and an additional lepton pair has the same colour structure as in equation (3.3). In squaring these amplitudes a colour projector

$$\delta_{i\bar{i}} \delta_{j\bar{j}} - \frac{1}{N_c} \delta_{i\bar{j}} \delta_{j\bar{i}} \tag{3.4}$$

has to applied to each gluon. In these examples we have two basic colour structures, a colour cluster described by the *closed string*

$$\delta_{i_{\sigma_1} j_{\sigma_2}} \delta_{i_{\sigma_2} j_{\sigma_3}} \ldots \delta_{i_{\sigma_n} j_{\sigma_1}} \tag{3.5}$$

and a colour cluster corresponding to the *open string*

$$\delta_{i_q j_{\sigma_1}} \delta_{i_{\sigma_1} j_{\sigma_2}} \ldots \delta_{i_{\sigma_n} j_{\bar{q}}}. \tag{3.6}$$

Born amplitudes with additional pairs of quarks have a decomposition in colour factors, which are products of the two basic colour clusters above. The colour factors in equation (3.1) and equation (3.3) are orthogonal to leading order in $1/N_c$.

3.2.2 The Dipole Formalism

The starting point in the calculation of an observable O in hadron–hadron collisions in perturbation theory is the following formula:

$$\begin{aligned}\langle O\rangle = &\int dx_1 f(x_1) \int dx_2 f(x_2) \frac{1}{2K(\hat{s})} \frac{1}{(2J_1+1)} \frac{1}{(2J_2+1)} \frac{1}{n_1 n_2} \\ &\times \int d\phi_n(p_1,p_2;p_3,\ldots,p_{n+2})\, O(p_1,\ldots,p_{n+2}) \left|\mathcal{A}_{n+2}\right|^2.\end{aligned} \tag{3.7}$$

This equation gives the contribution from the n-parton final state. The two incoming particles are labelled p_1 and p_2, while p_3 to p_{n+2} denote the final-state particles. The function $f(x)$ gives the probability of finding a parton a with momentum fraction x inside the parent hadron h. A sum over all possible partons a is understood implicitly. $2K(s)$ is the flux factor, $1/(2J_1+1)$ and $1/(2J_2+1)$ correspond to an averaging over the initial helicities and n_1 and n_2 are the number of colour degrees of the initial-state particles. The phase space measure $d\phi_n$ for n final-state particles includes (if appropriate) the identical particle factors. The matrix element $|\mathcal{A}_{n+2}|^2$ is calculated perturbatively. At leading and next-to-leading order one has the following contributions:

$$\begin{aligned}\langle O\rangle^{LO} &= \int_n O_n d\sigma^B,\\ \langle O\rangle^{NLO} &= \int_{n+1} O_{n+1} d\sigma^R + \int_n O_n d\sigma^V + \int_n O_n d\sigma^C.\end{aligned} \tag{3.8}$$

Here we used a rather condensed notation. $d\sigma^B$ denotes the Born contribution, while $d\sigma^R$ denotes the real emission contribution, whose matrix element is given by the square of the Born amplitudes with $(n+3)$ partons $|\mathcal{A}^{(0)}_{n+3}|^2$. $d\sigma^V$ gives the virtual contribution, whose matrix element is given by the interference term of the one-loop amplitude $\mathcal{A}^{(1)}_{n+2}$ with $(n+2)$ partons with the corresponding Born amplitude $\mathcal{A}^{(0)}_{n+2}$. $d\sigma^C$ denotes a collinear subtraction term, which subtracts the initial-state collinear singularities. Within the subtraction method one constructs an approximation term $d\sigma^A$ with the same singularity structure as $d\sigma^R$. The NLO contribution is rewritten as:

$$\langle O\rangle^{NLO} = \int_{n+1} \left(O_{n+1} d\sigma^R - O_n d\sigma^A\right) + \int_n \left(O_n d\sigma^V + O_n d\sigma^C + O_n d\sigma^A\right), \tag{3.9}$$

such that the terms inside the two brackets are separately finite. The matrix element corresponding to the approximation term $d\sigma^A$ is given as a sum over dipoles [145, 148, 208–210]:

$$\sum_{\text{pairs } i,j} \sum_{k\neq i,j} \mathcal{D}_{ij,k} + \left[\sum_{\text{pairs } i,j} \mathcal{D}^a_{ij} + \sum_j \sum_{k\neq j} \mathcal{D}^{aj}_k + \sum_j \mathcal{D}^{aj,b} + (a\leftrightarrow b)\right]. \tag{3.10}$$

In equation (3.10) the labels i, j and k denote final-state particles, while a and b denote initial-state particles. The first term describes dipoles where both the emitter and the spectator are in the final state. $\mathcal{D}^a_{ij}$ denotes a dipole where the emitter is in the final state, while the spectator is in the initial state. The reverse situation is denoted by $\mathcal{D}^{aj}_k$: here the emitter is in the initial state and the spectator is in the final state. Finally, $\mathcal{D}^{aj,b}$ denotes a dipole where both the emitter and the spectator are in the initial state. The full complexity is only needed for hadron colliders; for electron–positron annihilation the subtraction terms inside the square bracket are absent. The dipole subtraction terms for a final-state emitter–spectator pair have the following form:

$$\mathcal{D}_{ij,k} = \mathcal{A}^{(0)\,*}_{n+2}\left(p_1,\ldots,\tilde{p}_{(ij)},\ldots,\tilde{p}_k,\ldots\right) \frac{(-\mathbf{T}_k\cdot\mathbf{T}_{ij})}{\mathbf{T}^2_{ij}} \frac{V_{ij,k}}{2p_i\cdot p_j} \mathcal{A}^{(0)}_{n+2}\left(p_1,\ldots,\tilde{p}_{(ij)},\ldots,\tilde{p}_k,\ldots\right). \tag{3.11}$$

The structure of the dipole subtraction terms with initial-state partons is similar. Here $\mathbf{T}_i$ denotes the colour charge operator for parton i and $V_{ij,k}$ is a matrix in the spin space of the emitter parton (ij). In general, the operators $\mathbf{T}_i$ lead to colour correlations, while the $V_{ij,k}$'s lead to spin correlations. The colour charge operators $\mathbf{T}_i$ for a quark, gluon and antiquark in the final state are:

$$\begin{aligned} \text{gluon:} \quad & \mathcal{A}^*(\ldots g^c \ldots)(if^{cab})\mathcal{A}(\ldots g^b \ldots), \\ \text{quark:} \quad & \mathcal{A}^*(\ldots q_i \ldots)(T^a_{ij})\mathcal{A}(\ldots q_j \ldots), \\ \text{antiquark:} \quad & \mathcal{A}^*(\ldots \bar{q}_i \ldots)(-T^a_{ji})\mathcal{A}(\ldots \bar{q}_j \ldots). \end{aligned} \tag{3.12}$$

The corresponding colour charge operators for a quark, gluon and antiquark in the initial state are:

$$\begin{aligned} \text{gluon:} \quad & \mathcal{A}^*(\ldots g^c \ldots)(if^{cab})\mathcal{A}(\ldots g^b \ldots), \\ \text{quark:} \quad & \mathcal{A}^*(\ldots \bar{q}_i \ldots)(-T^a_{ji})\mathcal{A}(\ldots \bar{q}_j \ldots), \\ \text{antiquark:} \quad & \mathcal{A}^*(\ldots q_i \ldots)(T^a_{ij})\mathcal{A}(\ldots q_j \ldots). \end{aligned} \tag{3.13}$$

In the amplitude an incoming quark is denoted as an outgoing antiquark and vice versa.

In this chapter we neglect spin correlations and work to leading order in $1/N_c$. Therefore we replace the splitting functions $V_{ij,k}$ by the spin-averaged splitting functions $V_{ij,k} \to \langle V_{ij,k} \rangle$. In the leading-colour approximation we only have to take into account emitter–spectator pairs, which are adjacent inside a colour cluster. For those pairs we obtain for the colour charge operators

$$\frac{(-\mathbf{T}_k \cdot \mathbf{T}_{ij})}{\mathbf{T}^2_{ij}} = \begin{cases} 1/2 & \text{emitter } (ij) \text{ is a gluon,} \\ 1 & \text{emitter } (ij) \text{ is a quark or antiquark.} \end{cases} \tag{3.14}$$

We introduce the notation

$$\begin{aligned} \mathcal{P}_{ij,k} &= \frac{\langle V_{ij,k} \rangle}{(p_i + p_j)^2 - m^2_{ij}} \cdot \theta\big(\langle V_{ij,k} \rangle\big), \quad \mathcal{P}_{ij,a} = \frac{\langle V^a_{ij} \rangle}{(p_i + p_j)^2 - m^2_{ij}} \cdot \frac{1}{x} \cdot \theta\big(\langle V^a_{ij} \rangle\big), \\ \mathcal{P}_{aj,k} &= \frac{\langle V^{aj}_k \rangle}{\big|2p_a \cdot p_j\big|} \cdot \frac{1}{x} \cdot \theta\big(\langle V^{aj}_k \rangle\big), \quad \mathcal{P}_{aj,b} = \frac{\langle V^{aj,b} \rangle}{\big|2p_a \cdot p_j\big|} \cdot \frac{1}{x} \cdot \theta\big(\langle V^{aj,b} \rangle\big). \end{aligned} \tag{3.15}$$

The functions $\mathcal{P}$ will govern the emission of additional particles in the shower algorithm. The spin-averaged dipole splitting functions $\langle V \rangle$ can be found in references [145, 210]. The Heaviside theta-functions [218] ensure that the functions $\mathcal{P}$ will be non-negative. They are needed for splittings between an initial- and a final-state particle, since the dipole splitting functions $\langle V^a_{ij} \rangle$ and $\langle V^{aj}_k \rangle$ may take negative values in certain regions of phase space. In addition, the spin-averaged dipole splitting functions for massive partons are slightly modified: terms related to the soft singularity are re-arranged between the two dipoles forming an antenna, in order to ensure positivity of the individual dipole splitting functions in the singular limit.

3.3 The Shower Algorithm

In this section we describe the shower algorithm. We first discuss the colour treatment in subsection 3.3.1. The shower algorithm for massless final-state partons is discussed in subsection 3.3.2. The necessary modifications for initial-state partons are discussed in subsection 3.3.3. Finally, massive partons are discussed in subsection 3.3.4.

3.3.1 Colour Treatment

Before starting the parton showers, the partons from the hard matrix element have to be assigned to colour clusters. For the simplest matrix elements, like $e^+e^- \to q\bar{q}$, the choice is unique: the quark–antiquark pair forms a colour cluster. For the parton shower we work in the leading-colour approximation. In the leading-colour approximation we have to take into account only emitter–spectator pairs, which are adjacent inside a colour cluster. We have implemented two options: in the first one, which we call the *strict leading-colour approximation*, we take exactly the terms which are leading in an expansion in $1/N_c$ and only those. As a consequence, all splittings $g \to q\bar{q}$ are ignored, as they are colour-suppressed compared to $g \to gg$. In this approximation C_F is replaced by $3/2$. For the second option, which we call the *modified leading-colour approximation*, we include the splitting $g \to q\bar{q}$ and keep C_F as $(N_c^2-1)/(2N_c)$. In this case, if a gluon in a closed string splits into a quark–antiquark pair, the closed string becomes an open string. If a gluon in an open string splits into a quark–antiquark pair, the open string splits into two open strings.

3.3.2 The Shower Algorithm for Massless Final-State Partons

We first describe the shower algorithm for electron–positron annihilation. The extension to initial-state partons is treated in subsection 3.3.3. For the shower algorithm we use as an evolution variable

$$t = \ln \frac{-k_\perp^2}{Q^2}, \tag{3.16}$$

where Q^2 is a fixed reference scale and $k_\perp$ is the transverse momentum of a splitting. During the shower evolution we move towards smaller (more negative) values of t. We start from a given n-parton configuration. In the dipole formalism, emission of additional partons is described by an emitter–spectator pair. In the leading-colour approximation emitter and spectator are always adjacent in the cyclic order. The probability to evolve from t_1 to t_2 (with $t_1 > t_2$) without any resolvable branching is given by the Sudakov factor [131]. For the algorithm considered here, the Sudakov factor is given as a product of factors corresponding to the no-emission probabilities for individual dipoles' emissions:

$$\Delta(t_1,t_2) = \prod_{\tilde{i},\tilde{k}} \Delta_{\tilde{i},\tilde{k}}(t_1,t_2). \tag{3.17}$$

If parton $\tilde{i}$ can emit different partons, $\Delta_{\tilde{i},\tilde{k}}(t_1,t_2)$ factorises in turn into different contributions:

$$\Delta_{\tilde{i},\tilde{k}}(t_1,t_2) = \prod_j \Delta_{ij,k}(t_1,t_2). \tag{3.18}$$

An example is the possibility of a gluon to split either into two gluons or into a $q\bar{q}$-pair. We denote the emitter before the splitting by $\tilde{i}$, while the emitter after a splitting is denoted by i. This notation takes into account that the emitter might change its "flavour" due to a splitting, like in the case of a $g \to \bar{q}q$ splitting. $\Delta_{ij,k}(t_1,t_2)$ is the probability that the dipole formed by the emitter $\tilde{i}$ and spectator $\tilde{k}$ does not emit a parton j. It is given by:

$$\Delta_{ij,k}(t_1,t_2) = \exp\left(-\int_{t_2}^{t_1} dt\, \mathcal{C}_{\tilde{i},\tilde{k}} \int d\phi_{\text{unres}}\, \delta\left(t - T_{\tilde{i},\tilde{k}}\right) \mathcal{P}_{ij,k}\right), \tag{3.19}$$

where $\mathcal{C}_{\tilde{i},\tilde{k}}$ is a colour factor. In the leading-colour approximation this factor is non-zero only if $\tilde{i}$ and $\tilde{k}$ are adjacent in a colour cluster. Then $\mathcal{C}_{\tilde{i},\tilde{k}}$ is obtained from equation (3.14) and given by:

$$\mathcal{C}_{\tilde{i},\tilde{k}} = \begin{cases} 1/2 & \text{for} \quad \tilde{i} = g, \\ 1 & \text{for} \quad \tilde{i} = q, \bar{q}. \end{cases} \tag{3.20}$$

The dipole phase space is given by:

$$\int d\phi_{\text{unres}} = \frac{(p_{\tilde{i}} + p_{\tilde{k}})^2}{16\pi^2} \int_0^1 d\kappa \int_{z_-(\kappa)}^{z_+(\kappa)} dz \frac{1}{4z(1-z)} \left(1 - \frac{\kappa}{4z(1-z)}\right), \tag{3.21}$$

with

$$z_\pm(\kappa) = \frac{1}{2}\left(1 \pm \sqrt{1-\kappa}\right). \tag{3.22}$$

The variable κ is proportional to the transverse momentum of the splitting:

$$\kappa = 4\frac{(-k_\perp^2)}{(p_{\tilde{i}} + p_{\tilde{k}})^2}. \tag{3.23}$$

$T_{\tilde{i},\tilde{k}}$ depends on the dipole invariant mass $(p_{\tilde{i}} + p_{\tilde{k}})^2$ and the phase space variable κ for the emission of an additional particle and is given by:

$$T_{\tilde{i},\tilde{k}} = \ln \frac{\kappa}{4} \frac{(p_{\tilde{i}} + p_{\tilde{k}})^2}{Q^2}. \tag{3.24}$$

With the help of the delta-function [219] we may perform the integration over κ, while keeping the integration over t and z. Then

$$\kappa(t) = \frac{4Q^2 e^t}{(p_{\tilde{i}} + p_{\tilde{k}})^2}. \tag{3.25}$$

$\mathcal{P}_{ij,k}$ is the dipole splitting function. As an example we quote the splitting function for the $q \to qg$ splitting (others are given in appendix A.5):

$$\mathcal{P}_{q\to qg} = C_F \frac{8\pi\alpha_s(\mu^2)}{(p_{\tilde{i}} + p_{\tilde{k}})^2} \frac{1}{y}\left[\frac{2}{1-z(1-y)} - (1+z)\right], \quad y = \frac{\kappa(t)}{4z(1-z)}. \tag{3.26}$$

α_s is evaluated at the scale $\mu^2 = -k_\perp^2 = \frac{\kappa}{4}(p_{\tilde{i}} + p_{\tilde{k}})^2$.

The probability that a branching occurs at t_2 is given by

$$\sum_{\tilde{i},\tilde{k}} \sum_j \mathcal{C}_{\tilde{i},\tilde{k}} \int d\phi_{\text{unres}} \delta\left(t_2 - T_{\tilde{i},\tilde{k}}\right) \mathcal{P}_{ij,k} \Delta(t_1, t_2). \tag{3.27}$$

We can now state the shower algorithm. Starting from an initial evolution scale t_1 we proceed as follows:

1. Select the next dipole to branch and the scale t_2 at which this occurs. This is done as follows: for each dipole we generate the scale $t_{2,ij,k}$ of the next splitting for this dipole from a uniformly distributed number $r_{1,ij,k}$ in $[0,1]$ by solving (numerically) the equation
$$\Delta_{ij,k}(t_1, t_{2,ij,k}) = r_{1,ij,k}. \tag{3.28}$$
We then set
$$t_2 = \max\left(t_{2,ij,k}\right). \tag{3.29}$$
The dipole which has the maximal value of $t_{2,ij,k}$ is the one which radiates off an additional particle.

2. If t_2 is smaller than a cut-off scale t_{min}, the shower algorithm terminates.

3. Next we have to generate the value of z. Again, using a uniformly distributed random number r_2 in $[0,1]$ we solve:
$$\int_{z_-(t_2)}^{z} dz' J(t_2, z') \mathcal{P}_{ij,k} = r_2 \int_{z_-(t_2)}^{z_+(t_2)} dz' J(t_2, z') \mathcal{P}_{ij,k}, \tag{3.30}$$
where the Jacobian factor $J(t_2, z)$ is given by:
$$J(t_2, z) = \frac{\kappa(t_2)}{4z(1-z)} \left(1 - \frac{\kappa(t_2)}{4z(1-z)}\right). \tag{3.31}$$

4. Select the azimuthal angle ϕ. Finally we generate the azimuthal angle from a uniformly distributed number r_3 in $[0,1]$ as follows:
$$\phi = 2\pi r_3. \tag{3.32}$$

5. With the three kinematical variables t_2, z and ϕ and the information, that parton $\tilde{i}$ emits a parton j, with parton $\tilde{k}$ being the spectator, we insert the new parton j. The momenta $p_{\tilde{i}}$ and $p_{\tilde{k}}$ of the emitter and the spectator are replaced by new momenta p_i and p_k. The details how the new momenta p_i, p_j and p_k are constructed are given in the appendix A.6.

6. Set $t_1 = t_2$ and go to step 1.

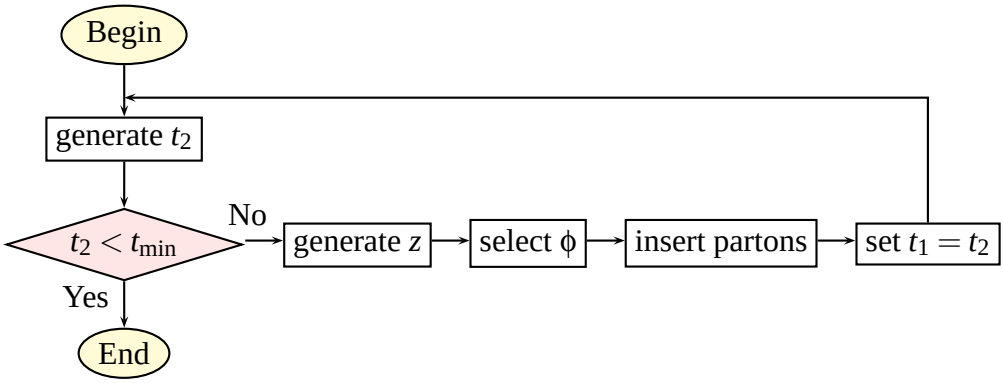

Figure 3.1: *Flowchart of the shower algorithm.*

Remark: step 1 of the algorithm is equivalent to first generating the point t_2 from a uniformly distributed number r_1 in $[0,1]$ by solving (numerically) the equation for the full Sudakov factor

$$\Delta(t_1,t_2) = r_1, \tag{3.33}$$

and then selecting an individual dipole with emitter $\tilde{i}$, emitted particle j and spectator k with probability [220]:

$$P_{ij,k} = \frac{\mathcal{C}_{\tilde{i},\tilde{k}} \int d\phi_{\text{unres}} \delta\left(t_2 - T_{\tilde{i},\tilde{k}}\right) \mathcal{P}_{ij,k}}{\sum\limits_{\tilde{l},\tilde{n}} \sum\limits_{m} \mathcal{C}_{\tilde{l},\tilde{n}} \int d\phi_{\text{unres}} \delta\left(t_2 - T_{\tilde{l},\tilde{n}}\right) \mathcal{P}_{lm,n}}. \tag{3.34}$$

3.3.3 The Shower Algorithm with Initial-State Partons

In this subsection we discuss the necessary modifications for the inclusion of initial-state partons. In the presence of initial-state partons there is no separation into final-state showers and initial-state showers. Initial-state radiation is treated on the same footing as final-state radiation. The algorithm generates initial-state radiation through backward evolution, starting from a hard scale and moving towards softer scales. Therefore the shower evolves in all cases from a hard scale towards lower scales.

Final-state Emitter and Initial-state Spectator

For an initial-state spectator we modify the Sudakov factor in equation (3.19) to:

$$\Delta_{ij,a}(t_1,t_2) = \exp\left(-\int_{t_2}^{t_1} dt \mathcal{C}_{\tilde{i},\tilde{a}} \int d\phi_{\text{unres}} \delta\left(t - T_{\tilde{i},\tilde{a}}\right) \frac{x_a f(x_a,t)}{x_{\tilde{a}} f(x_{\tilde{a}},t)} \mathcal{P}_{ij,a} \right), \tag{3.35}$$

where $x_{\tilde{a}}$ is the momentum fraction of the initial hadron carried by $\tilde{a}$, while x_a is the momentum fraction carried by a. The initial parton of the n-particle state is denoted by $\tilde{a}$, while the

initial parton of the $(n+1)$-particle state is denoted by a. We set:

$$x = \frac{x_{\tilde{a}}}{x_a}. \tag{3.36}$$

The unresolved phase space is given by:

$$\int d\phi_{\text{unres}} = \frac{|2p_{\tilde{i}}p_{\tilde{a}}|}{16\pi^2} \int_{x_{\tilde{a}}}^{1} \frac{dx}{x} \int_0^1 dz. \tag{3.37}$$

The transverse momentum between i and j is expressed as:

$$-k_\perp^2 = \frac{(1-x)}{x} z(1-z)\,(-2p_{\tilde{i}}p_{\tilde{a}}) \tag{3.38}$$

and $T_{\tilde{i},\tilde{a}}$ is therefore given by:

$$T_{\tilde{i},\tilde{a}} = \ln \frac{-k_\perp^2}{Q^2} = \ln \frac{(-2p_{\tilde{i}}p_{\tilde{a}})\,(1-x)z(1-z)}{xQ^2}. \tag{3.39}$$

A subtlety occurs for the emission between a final-state spectator and an initial-state emitter. We discuss this for the splitting $q \to qg$. The spin-averaged splitting function for the $q \to qg$ splitting is given by:

$$\langle V_{qg}^k \rangle = 8\pi\alpha_s\, C_F \left[\frac{2}{1-z+(1-x)} - (1+z) \right]. \tag{3.40}$$

In contrast to the final–final case this function is not a positive function on the complete phase space. It can take negative values in certain (non-singular) regions of phase space. This is not a problem when it is used as a subtraction terms in NLO calculations, but prohibits a straightforward interpretation as a splitting probability for a shower algorithm. However, since negative values occur only in non-singular regions, we can ensure positiveness by modifying the splitting functions through non-singular terms. The simplest choice is to set

$$\mathcal{P}_{ij,a} = \frac{\langle V_{ij}^a \rangle}{(p_i+p_j)^2} \cdot \frac{1}{x} \cdot \theta\left(\langle V_{ij}^a \rangle\right). \tag{3.41}$$

For a final-state emitter we eliminate the x-integration with the help of the delta-function:

$$\int_{x_{\tilde{a}}}^{1} \frac{dx}{x} \delta\left(t - T_{\tilde{i},\tilde{a}}\right) = \frac{1}{1+\frac{4z(1-z)}{\kappa(t)}}, \quad x = \frac{1}{1+\frac{\kappa(t)}{4z(1-z)}}, \quad \kappa(t) = \frac{4Q^2e^t}{(-2p_{\tilde{i}}p_{\tilde{a}})}. \tag{3.42}$$

For the boundaries we obtain:

$$\kappa(t) < \frac{1-x_{\tilde{a}}}{x_{\tilde{a}}}, \quad z_-(t) < z < z_+(t), \quad z_\pm(t) = \frac{1}{2}\left(1 \pm \sqrt{1-\kappa(t)\frac{x_{\tilde{a}}}{1-x_{\tilde{a}}}}\right). \tag{3.43}$$

The modifications to the shower algorithm are as follows: the dipoles for the emission from a final-state emitter with an initial-state spectator are included in the Sudakov factor in equation (3.17). With this modification steps 1 and 2 are as above. Let us define

$$f_{lm,n} = \begin{cases} 1, & \text{if } l \text{ and } n \text{ are final-state particles,} \\ \frac{x_a f(x_a,t)}{x_{\tilde{a}} f(x_{\tilde{a}},t)}, & \text{if } l = a \text{ is an initial-state particle,} \\ \frac{x_b f(x_b,t)}{x_{\tilde{b}} f(x_{\tilde{b}},t)}, & \text{if } n = b \text{ is an initial-state particle and } l \text{ is a final-state particle.} \end{cases} \tag{3.44}$$

In step 2 we replace formula (3.30) by:

$$\int_{z_-(t_2)}^{z} dz' J(t_2,z') f_{ij,a} \mathcal{P}_{ij,a} = r_2 \int_{z_-(t_2)}^{z_+(t_2)} dz' J(t_2,z') f_{ij,a} \mathcal{P}_{ij,a}, \tag{3.45}$$

with the Jacobian

$$J(t,z) = \frac{1}{1+\frac{4z(1-z)}{\kappa(t)}}. \tag{3.46}$$

Steps 4 to 6 proceed as in subsection 3.3.2.

Initial-state Emitter and Final-state Spectator

For an initial-state emitter $\tilde{a}$ with a final-state spectator $\tilde{i}$ the Sudakov factor is given by:

$$\Delta_{aj,i}(t_1,t_2) = \exp\left(-\int_{t_2}^{t_1} dt \mathcal{C}_{\tilde{a},\tilde{i}} \int d\phi_{\text{unres}} \delta\left(t - T_{\tilde{a},\tilde{i}}\right) \frac{x_a f(x_a,t)}{x_{\tilde{a}} f(x_{\tilde{a}},t)} \mathcal{P}_{aj,i} \right). \tag{3.47}$$

The unresolved phase space is again given by equation (3.37). The transverse momentum between a and j is given by:

$$-k_\perp^2 = \frac{(1-x)}{x}(1-z)(-2p_{\tilde{i}}p_{\tilde{a}}) \tag{3.48}$$

and $T_{\tilde{a},\tilde{i}}$ is given by:

$$T_{\tilde{a},\tilde{i}} = \ln \frac{(-2p_{\tilde{i}}p_{\tilde{a}})(1-x)(1-z)}{xQ^2}. \tag{3.49}$$

For a initial-state emitter we eliminate the z-integration with the help of the delta-function:

$$\int_0^1 dz \delta\left(t - T_{\tilde{a},\tilde{i}}\right) = \frac{\kappa(t)}{4}\frac{x}{(1-x)}, \quad z = 1 - \frac{\kappa(t)}{4}\frac{x}{(1-x)}, \quad \kappa(t) = \frac{4Q^2e^t}{(-2p_{\tilde{i}}p_{\tilde{a}})}. \tag{3.50}$$

For the boundaries we obtain:

$$\kappa(t) < 4\frac{1-x_{\tilde{a}}}{x_{\tilde{a}}}, \quad x < x_+(t), \quad x_+(t) = \frac{1}{1+\frac{\kappa(t)}{4}}. \tag{3.51}$$

There are no new modifications to the shower algorithms compared to the case for a final-state emitter and an initial-state spectator, except that in step 3 we now generate the value of x according to:

$$\int_{x_{\tilde{a}}}^{x} dx' J(t_2,x') f_{aj,i} \mathcal{P}_{aj,i} = r_2 \int_{x_{\tilde{a}}}^{x_+(t_2)} dx' J(t_2,x') f_{aj,i} \mathcal{P}_{aj,i}, \tag{3.52}$$

with the Jacobian

$$J(t,x) = \frac{\kappa(t)}{4(1-x)}. \tag{3.53}$$

Initial-state Emitter and Initial-state Spectator

For an initial-state emitter $\tilde{a}$ with an initial-state spectator $\tilde{b}$ the Sudakov factor is given by:

$$\Delta_{aj,b}(t_1,t_2) = \exp\left(-\int_{t_2}^{t_1} dt \mathcal{C}_{\tilde{a},\tilde{b}} \int d\phi_{\text{unres}} \delta\left(t - T_{\tilde{a},\tilde{b}}\right) \frac{x_a f(x_a,t)}{x_{\tilde{a}} f(x_{\tilde{a}},t)} \mathcal{P}_{aj,b} \right). \tag{3.54}$$

In this case we do not rescale the momentum of the spectator, but transform all final-state momenta. Therefore no factor

$$\frac{x_b f(x_b,t)}{x_{\tilde{b}} f(x_{\tilde{b}},t)} \tag{3.55}$$

appears in the Sudakov factor. The unresolved phase space is given by:

$$\int d\phi_{\text{unres}} = \frac{\left|2 p_{\tilde{a}} p_{\tilde{b}}\right|}{16\pi^2} \int_{x_{\tilde{a}}}^{1} \frac{dx}{x} \int_0^{1-x} dv. \tag{3.56}$$

The transverse momentum between a and j is given by:

$$-k_\perp^2 = \frac{(1-x)}{x} v \left(2 p_{\tilde{a}} p_{\tilde{b}}\right) \tag{3.57}$$

and $T_{\tilde{a},\tilde{b}}$ is given by:

$$T_{\tilde{a},\tilde{b}} = \ln \frac{\left(2 p_{\tilde{a}} p_{\tilde{b}}\right)(1-x)v}{xQ^2}. \tag{3.58}$$

We integrate over v with the help of the delta-function:

$$\int_0^{1-x} dv \delta\left(t - T_{\tilde{a},\tilde{b}}\right) = \frac{\kappa(t)}{4} \frac{x}{(1-x)}, \quad v = \frac{\kappa(t)}{4} \frac{x}{(1-x)}, \quad \kappa(t) = \frac{4Q^2 e^t}{\left(2 p_{\tilde{a}} p_{\tilde{b}}\right)}. \tag{3.59}$$

For the boundaries we obtain:

$$\kappa(t) < 4 \frac{(1-x_{\tilde{a}})^2}{x_{\tilde{a}}}, \quad x < x_+(t), \quad x_+(t) = \frac{1}{2}\left(2 + \frac{\kappa(t)}{4} - \sqrt{\kappa(t) + \frac{\kappa(t)^2}{16}}\right). \tag{3.60}$$

In step 3 of the shower algorithm we again select x according to:

$$\int_{x_{\tilde{a}}}^{x} dx' J(t_2,x') f_{aj,b} \mathcal{P}_{aj,b} = r_2 \int_{x_{\tilde{a}}}^{x_+(t_2)} dx' J(t_2,x') f_{aj,b} \mathcal{P}_{aj,b}, \tag{3.61}$$

with the Jacobian

$$J(t,x) = \frac{\kappa(t)}{4(1-x)}. \tag{3.62}$$

3.3.4 The Shower Algorithm for Massive Partons

In this subsection we discuss the modifications of the shower algorithms due to the presence of massive partons. We first address the issue of a splitting of a gluon into a heavy quark pair. This mainly concerns the splitting of a gluon into b-quarks. We will always require that initial-state particles are massless. Therefore for processes with initial-state hadrons we do not consider $g \to q\bar{q}$ splittings. Calculations for initial-state hadrons should be done in the approximation of a massless b-quark. In the case of electron–positron annihilation the parton shower affects only the final state. Here we can consistently allow splittings of a gluon into a pair of massive quarks. As evolution variable we use in the massive case:

$$t = \ln \frac{-k_\perp^2 + (1-z)^2 m_i^2 + z^2 m_j^2}{Q^2}. \tag{3.63}$$

This choice reduces to equation (3.16) in the massless limit and is suggested by dispersion relations for the running coupling [196, 211].

Final-state Emitter and Final-state Spectator

The unresolved phase space is given by:

$$\int d\phi_{\text{unres}} = \frac{(p_{\tilde{i}} + p_{\tilde{k}})^2}{16\pi^2} \left(1 - \mu_i^2 - \mu_j^2 - \mu_k^2\right)^2 \left[\lambda(1, \mu_{ij}^2, \mu_k^2)\right]^{-\frac{1}{2}} \int_{y_-}^{y_+} dy\, (1-y) \int_{z_-(y)}^{z_+(y)} dz, \tag{3.64}$$

where the reduced masses μ_l and the boundaries on the integrations are defined in equations (A.67)–(A.69) in appendix A.6. $T_{\tilde{i},\tilde{k}}$ is given by:

$$T_{\tilde{i},\tilde{k}} = \ln \frac{\left((p_{\tilde{i}} + p_{\tilde{k}})^2 - m_i^2 - m_j^2 - m_k^2\right) yz(1-z)}{Q^2}. \tag{3.65}$$

Again, we have to ensure that the splitting functions are positive. The original spin-averaged dipole splitting functions can take negative values in certain regions of phase space. In the massive case the negative region can extend into the singular region. The problem is related to the soft behaviour of the dipole splitting functions. Since a squared Born matrix element is positive in the soft gluon limit, the negative contribution from a particular dipole is compensated by the contribution from the dipole, where emitter and spectator are exchanged. The

sum of the two contributions is positive in the singular region. Therefore we can cut out the negative region from the first dipole and add it to the second dipole. The second dipole will stay positive.

As in the massless case we eliminate the y-integration:

$$\int_{y_-}^{y_+} dy\,(1-y)\int_{z_-(y)}^{z_+(y)} dz\,\delta\left(t-T_{\tilde{i},\tilde{k}}\right) = \int_{z_{\min}}^{z_{\max}} dz\,y(1-y),$$

$$y = \frac{\kappa(t)}{4z(1-z)},$$

$$\kappa(t) = \frac{4Q^2e^t}{(p_{\tilde{i}}+p_{\tilde{k}})^2-m_i^2-m_j^2-m_k^2}. \tag{3.66}$$

The physical region is defined by:

$$\left(1-\frac{\kappa}{4z(1-z)}\right)^2\left[\frac{\kappa}{4}-(1-z)^2\bar{m}_i^2-z^2\bar{m}_j^2\right]-\left(\frac{\kappa}{4z(1-z)}\right)^2\bar{m}_k^2+4\bar{m}_i^2\bar{m}_j^2\bar{m}_k^2\geq 0, \tag{3.67}$$

with

$$\bar{m}_l^2 = \frac{m_l^2}{(p_{\tilde{i}}+p_{\tilde{k}})^2-m_i^2-m_j^2-m_k^2} \quad \text{for} \quad l\in\{i,j,k\}. \tag{3.68}$$

This equation is solved numerically for $z_{\min}$ and $z_{\max}$. Then z is generated according to:

$$\int_{z_{\min}(t_2)}^{z} dz' J(t_2,z')\mathcal{P}_{ij,k} = r_2\int_{z_{\min}(t_2)}^{z_{\max}(t_2)} dz' J(t_2,z')\mathcal{P}_{ij,k}, \tag{3.69}$$

with the Jacobian

$$J(t,z) = \left(1-\mu_i^2-\mu_j^2-\mu_k^2\right)^2\left[\lambda(1,\mu_{ij}^2,\mu_k^2)\right]^{-\frac{1}{2}}\frac{\kappa(t)}{4z(1-z)}\left(1-\frac{\kappa(t)}{4z(1-z)}\right). \tag{3.70}$$

Final-state Emitter and Initial-state Spectator

The unresolved phase space is given by:

$$\int d\phi_{\text{unres}} = \frac{|2p_{\tilde{i}}p_{\tilde{a}}|}{16\pi^2}\int_{x_{\tilde{a}}}^1\frac{dx}{x}\int_{z_-(x)}^1 dz = \frac{|2p_{\tilde{i}}p_{\tilde{a}}|}{16\pi^2}\int_{z_-(x_{\tilde{a}})}^1 dz\int_{x_{\tilde{a}}}^{x_+(z)}\frac{dx}{x} \tag{3.71}$$

The integration boundary is given by:

$$z_-(x) = \frac{x\tilde{\mu}^2}{1-x(1-\tilde{\mu}^2)}, \quad x_+(z) = \frac{z}{\tilde{\mu}^2+z(1-\tilde{\mu}^2)}, \quad \tilde{\mu}^2 = \frac{m_{\tilde{i}}^2}{|2p_{\tilde{i}}p_{\tilde{a}}|}. \tag{3.72}$$

$T_{\tilde{i},\tilde{a}}$ is given by:

$$T_{\tilde{i},\tilde{a}} = \ln \frac{-k_\perp^2 + (1-z)^2 m_i^2}{Q^2} = \ln \frac{(-2p_{\tilde{i}}p_{\tilde{a}})\,(1-x)z(1-z)}{xQ^2}. \tag{3.73}$$

For a final-state emitter we eliminate the x-integration with the help of the delta-function:

$$\int_{x_{\tilde{a}}}^{1} \frac{dx}{x}\delta\left(t - T_{\tilde{i},\tilde{a}}\right) = \frac{1}{1+\frac{4z(1-z)}{\kappa(t)}}, \quad x = \frac{1}{1+\frac{\kappa(t)}{4z(1-z)}}, \quad \kappa(t) = \frac{4Q^2e^t}{(-2p_{\tilde{i}}p_{\tilde{a}})}. \tag{3.74}$$

For the boundaries we obtain:

$$\begin{aligned} z_+(t) &= \frac{1}{2}\left(1+\sqrt{1-\kappa(t)\frac{x_{\tilde{a}}}{1-x_{\tilde{a}}}}\right), \\ z_-(t) &= \max\left(\frac{x_{\tilde{a}}\tilde{\mu}^2}{1-x_{\tilde{a}}\,(1-\tilde{\mu}^2)}, \frac{1}{2}\left(1-\sqrt{1-\kappa(t)\frac{x_{\tilde{a}}}{1-x_{\tilde{a}}}}\right), 1-\sqrt{\frac{\kappa(t)}{4\tilde{\mu}^2}}\right). \end{aligned} \tag{3.75}$$

The boundary on $\kappa(t)$ is given for $\tilde{\mu}^2 < (1-x_{\tilde{a}})/x_{\tilde{a}}$ by:

$$\kappa(t) < \frac{1-x_{\tilde{a}}}{x_{\tilde{a}}}. \tag{3.76}$$

For $(1-x_{\tilde{a}})/x_{\tilde{a}} < \tilde{\mu}^2$ we have:

$$\kappa(t) < \frac{1-x_{\tilde{a}}}{x_{\tilde{a}}}\left[1-\left(\frac{1-\frac{1-x_{\tilde{a}}}{x_{\tilde{a}}\tilde{\mu}^2}}{1+\frac{1-x_{\tilde{a}}}{x_{\tilde{a}}\tilde{\mu}^2}}\right)^2\right] = \frac{4\tilde{\mu}^2}{\left(1+\frac{x_{\tilde{a}}\tilde{\mu}^2}{1-x_{\tilde{a}}}\right)^2}. \tag{3.77}$$

z is generated according to:

$$\int_{z_-(t_2)}^{z} dz' J(t_2,z')\, f_{ij,a}\mathcal{P}_{ij,a} = r_2 \int_{z_-(t_2)}^{z_+(t_2)} dz' J(t_2,z')\, f_{ij,a}\mathcal{P}_{ij,a}, \tag{3.78}$$

with the Jacobian

$$J(t,z) = \frac{1}{1+\frac{4z(1-z)}{\kappa(t)}}. \tag{3.79}$$

Initial-state Emitter and Final-state Spectator

$T_{\tilde{a},\tilde{i}}$ is given by:

$$T_{\tilde{a},\tilde{i}} = \ln \frac{(-2p_{\tilde{i}}p_{\tilde{a}})\,(1-x)(1-z)}{xQ^2}. \tag{3.80}$$

For an initial-state emitter we eliminate the z-integration with the help of the delta-function:

$$\int_{z_-(x)}^{1} dz\,\delta\left(t - T_{\tilde{a},\tilde{i}}\right) = \frac{\kappa(t)}{4}\frac{x}{(1-x)}, \quad z = 1-\frac{\kappa(t)}{4}\frac{x}{(1-x)}, \quad \kappa(t) = \frac{4Q^2e^t}{(-2p_{\tilde{i}}p_{\tilde{a}})}. \tag{3.81}$$

For the boundaries we obtain:

$$\kappa(t) < \frac{4\,(1-x_{\tilde{a}})^2}{x_{\tilde{a}}\,[1-x_{\tilde{a}}\,(1-\tilde{\mu}^2)]}, \quad x < x_+(t), \quad x_+(t) = \frac{2+\frac{\kappa(t)}{4} - \sqrt{\frac{\kappa(t)^2}{16}+\tilde{\mu}^2\kappa(t)}}{2\left(1+\frac{\kappa(t)}{4}\,(1-\tilde{\mu}^2)\right)}. \tag{3.82}$$

The value of x is generated according to:

$$\int_{x_{\tilde{a}}}^{x} dx' J(t_2,x')\, f_{aj,i}\mathcal{P}_{aj,i} = r_2 \int_{x_{\tilde{a}}}^{x_+(t_2)} dx' J(t_2,x')\, f_{aj,i}\mathcal{P}_{aj,i}, \tag{3.83}$$

with the Jacobian

$$J(t,x) = \frac{\kappa(t)}{4(1-x)}. \tag{3.84}$$

3.4 Numerical Results

In this section we show numerical results obtained from the parton shower. We first discuss observables related to electron–positron annihilation in subsection 3.4.1 and then the shower in hadron collisions in subsection 3.4.2. The shower algorithm depends on two parameters, the strong coupling α_s and the scale $Q_{\min}$. For the strong coupling we use the leading-order formula

$$\alpha_s(\mu) = \frac{4\pi}{\beta_0 \ln\frac{\mu^2}{\Lambda^2}}, \quad \beta_0 = 11 - \frac{2}{3}N_f. \tag{3.85}$$

The cut-off scale $Q_{\min}$ gives the scale at which the shower terminates. As our shower is correct in the leading-colour approximation, we also study the effects of different treatments of subleading colour contributions. As described in subsection 3.3.1 we have implemented two options: the strict leading-colour approximation and the modified leading-colour approximation. Numerical differences from these two options will give an estimate of uncertainties due to subleading colour effects.

3.4.1 Electron–Positron Annihilation

For electron–positron annihilation we use $\alpha_s(m_Z) = 0.118$ corresponding to $\Lambda_5 = 88$ MeV. We start the shower from the $2 \to 2$ hard matrix element $e^+e^- \to q\bar{q}$. We first study the event shape variables thrust, the C-parameter and the D-parameter. The distributions of the first moments of these observables are shown in figure 3.2 for two choices of the cut-off parameter: $Q_{\min} = 1$ GeV and $Q_{\min} = 2$ GeV. The distributions are normalised to unity. The different prescriptions for the colour-treatment do not change the distributions significantly.

In figure 3.3 we show the distributions for the four-jet angles. Again we start from the $2 \to 2$ hard matrix element. The particles in an event are first clustered into jets, defined according to the Durham algorithm [221] with $y_{cut} = 0.008$ and the E-scheme for the recombination. Then events with exactly four jets are selected. We consider the modified

Nachtmann–Reiter angle [222], the Körner–Schierholz–Willrodt angle [223], the Bengtsson–Zerwas angle [224] and the angle α_{34} between the jets with the smallest energy [225]. In the plots we show the results from the different options for the colour treatment for $Q_{\text{min}} = 1\,\text{GeV}$. A variation of the cut-off scale does not change the distributions significantly.

3.4.2 Hadron Colliders

For the Tevatron and the LHC we study Z/γ^*-production. We start from the $2 \to 2$ hard matrix element $q\bar{q} \to Z/\gamma^* \to l^+l^-$. As parton distribution functions we use the CTEQ 6L1 set [226, 227]. For consistency we use here $\alpha_s(m_Z) = 0.130$ corresponding to $\Lambda_5 = 165\,\text{MeV}$. The centre-of-mass energy we set to $\sqrt{s} = 1.96\,\text{TeV}$ for the Tevatron and to $\sqrt{s} = 14\,\text{TeV}$ for the LHC. We require a cut on the invariant mass of the lepton pair of $m_{l^+l^-} > 80\,\text{GeV}$. As cut-off parameter for the parton shower we use $Q_{\text{min}} = 1\,\text{GeV}$. In figure 3.4 we show the transverse momentum distribution and the rapidity distribution of the lepton pair for the Tevatron and the LHC.

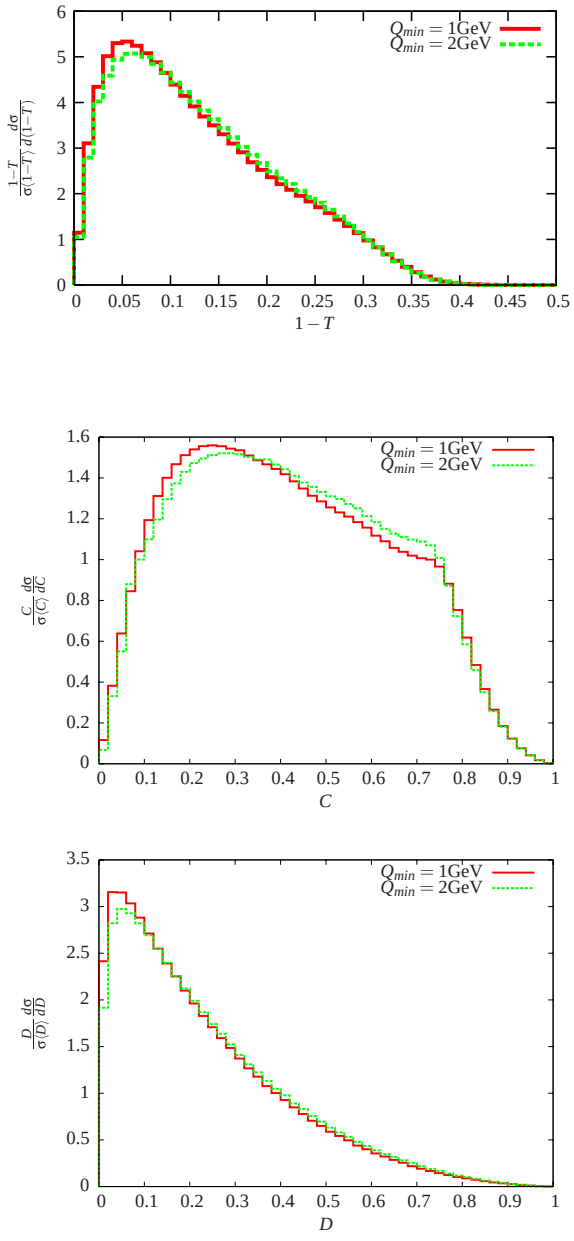

Figure 3.2: *The first moments of the thrust distribution, the C-parameter distribution and the D-parameter distribution. The results are from the parton shower for two different values of the cut-off scale* Q_{min}.

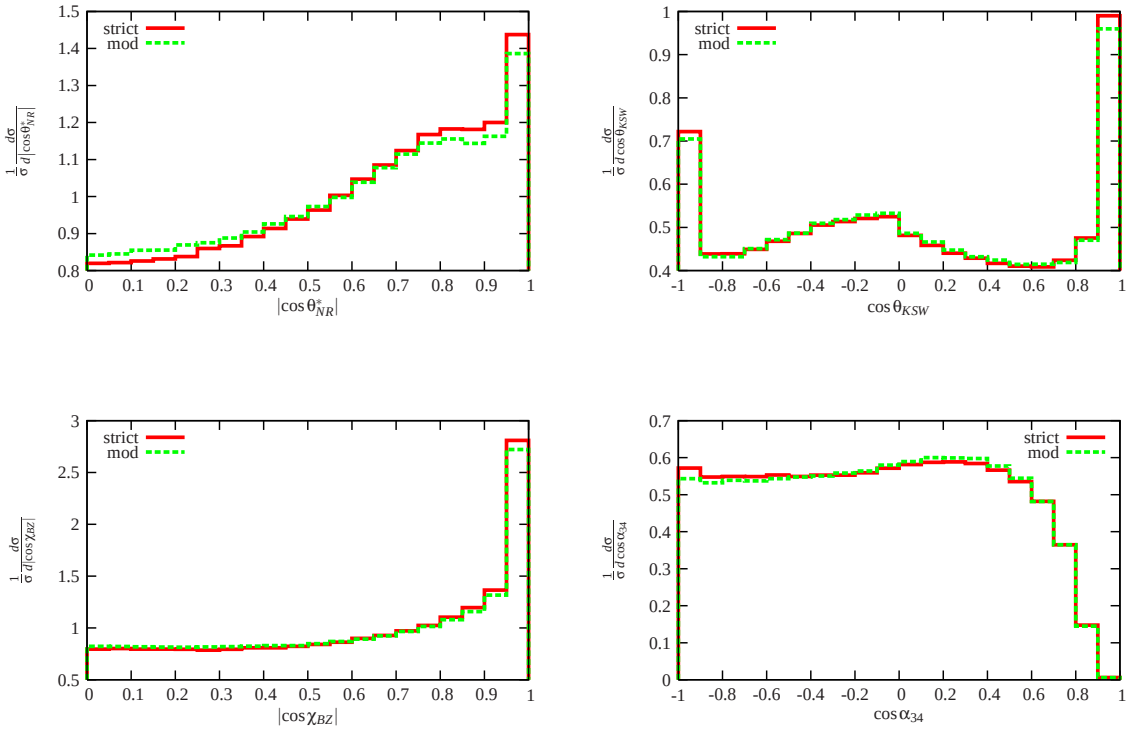

Figure 3.3: *The distributions for the four-jet angles. From top-left to bottom-right: the modified Nachtmann–Reiter angle, the Körner–Schierholz–Willrodt angle, the Bengtsson–Zerwas angle and the angle* α_{34} *between the smallest energy jets. As cut-off parameter* $Q_{\min} = 1\,\text{GeV}$ *is used. Shown are the result from the* strict leading-colour approximation *and the* modified leading-colour approximation.

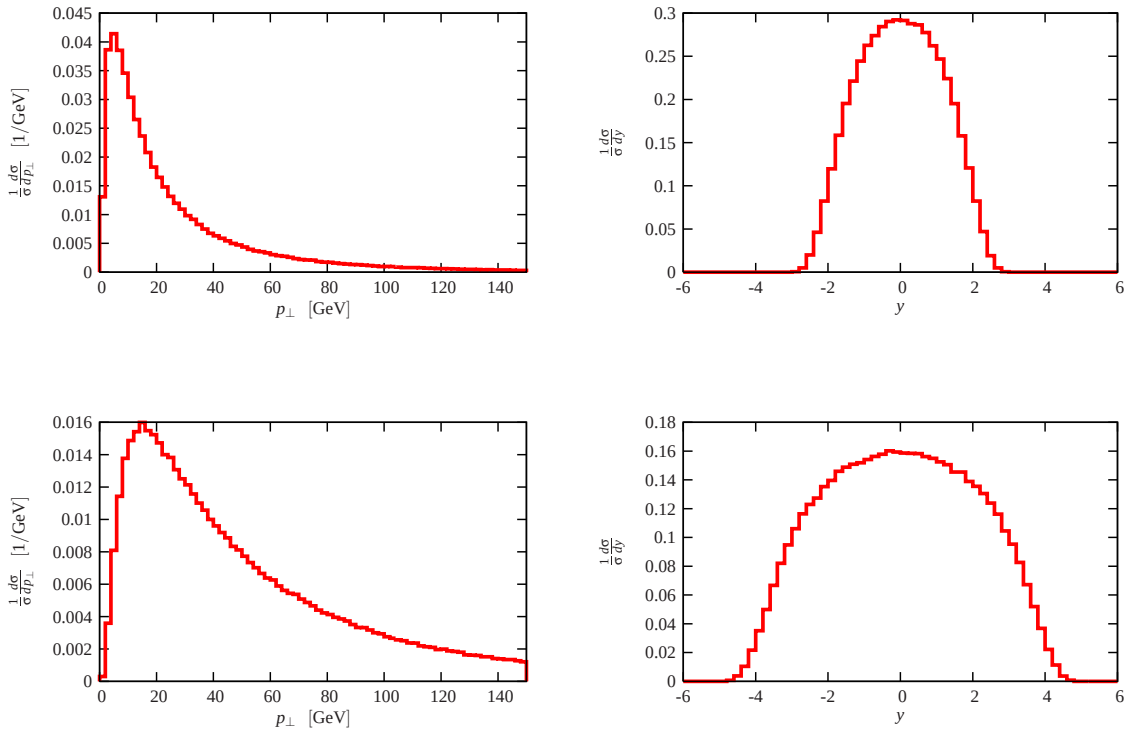

Figure 3.4: *The transverse momentum distribution and the rapidity distribution of the lepton pair for Z/γ^*-production for the Tevatron and the LHC. As cut-off parameter $Q_{\min} = 1$ GeV is used.*

Chapter 4

Summary and Conclusion

The classical way to calculate hard scattering processes in perturbation theory using Feynman diagrams is not efficient enough to calculate all necessary processes – for example for the Large Hadron Collider – to sufficient precision. Two alternatives to order-by-order calculations were investigated in this thesis.

We studied the numerical implementations of four different recursive methods for the computation of Born gluon amplitudes: Berends–Giele recurrence relations, recursive calculations with scalar diagrams, with MHV vertices (Cachazo–Svrček–Witten), and with shifted momenta (Britto–Cachazo–Feng–Witten). From the four methods considered, we found the Berends–Giele method performs best, as the number of external partons increases ($n \geq 8$). However, for a not so large number of external partons ($n < 8$), the on-shell recursion relation (BCFW) offers the best performance. These amplitudes together with corresponding ones, where additional quarks or vector bosons are involved, are relevant for LHC physics. They enter numerical NLO or LO program codes. As these calculations are based on Monte Carlo integration over the phase space, the efficiency of the computation has a direct impact on the running time of the Monte Carlo program. We also investigated the numerical stability and accuracy and found that all methods give satisfactory results.

Duhr, Höche and Maltoni observed exactly the same growth in computation time and improved the CSW calculation [228, 229], to bring it on the same level of complexity as the BCFW calculation. In their implementation the Berends–Giele recurrence relations perform best for the process $gg \to ng$ for $3 \leq n \leq 10$. Gleisberg, Höche, Krauss and Matyszkiewicz addressed the issue of efficiency of the CSW technique when dealing with full cross sections, including summation over colours and helicities, rather than single amplitudes [230].

One possible extension of the tree-level calculations done in this thesis are calculations of loop amplitudes. Some of the methods used in this thesis are similarly useful at loop-level, like the spinor helicity technique, others were generalised to one-loop amplitudes, like colour decomposition [144] and the BCFW recurrence relations [231]. Another approach is the OPP reduction method to compute one-loop amplitudes numerically [232–234].

In the second part of this thesis we presented an implementation of a shower algorithm based on the dipole formalism. The formalism treats initial- and final-state partons on the same footing. The shower can be used for hadron colliders and electron–positron colliders. We also included in the shower algorithm massive partons in the final state. We studied

numerical results for electron–positron annihilation, the Tevatron and the LHC.

Appendix

A.1 Standard Model Lagrangian Density

The most general Standard Model Lagrangian density consists of the following parts: [235]

$$\mathcal{L}_{\mathrm{SM}} = \mathcal{L}_{\mathrm{c}} + \mathcal{L}_{\mathrm{w}} + \mathcal{L}_{\mathrm{f}} + \mathcal{L}_{\mathrm{fc}} + \mathcal{L}_{\mathrm{FPc}} + \mathcal{L}_{\mathrm{FPw}} + \mathcal{L}_{\mathrm{fH}}\,. \tag{A.1}$$

The colour Lagrangian density, describing the gluons of quantum chromodynamics and their mutual interactions

$$\mathcal{L}_{\mathrm{c}} = -\frac{1}{2}\partial_\nu g^a_\mu \partial_\nu g^a_\mu - g_s f^{abc}\partial_\mu g^a_\nu g^b_\mu g^c_\nu - \frac{1}{4}g_s^2 f^{abc} f^{ade} g^b_\mu g^c_\nu g^d_\mu g^e_\nu\,. \tag{A.2}$$

The weak Lagrangian density, describing the vector bosons and their interactions including the interactions with the Higgs system

$$\begin{aligned}
\mathcal{L}_{\mathrm{w}} = {} & -\partial_\nu W^+_\mu \partial_\nu W^-_\mu - M^2 W^+_\mu W^-_\mu - \frac{1}{2}\partial_\nu Z^0_\mu \partial_\nu Z^0_\mu - \frac{1}{2c_w^2}M^2 Z^0_\mu Z^0_\mu - \frac{1}{2}\partial_\mu A_\nu \partial_\mu A_\nu - \frac{1}{2}\partial_\mu H \partial_\mu H \\
& - \frac{1}{2}m_h^2 H^2 - \partial_\mu \phi^+ \partial_\mu \phi^- - M^2 \phi^+ \phi^- - \frac{1}{2}\partial_\mu \phi^0 \partial_\mu \phi^0 - \frac{1}{2c_w^2}M \phi^0 \phi^0 \\
& - \beta_h \left[\frac{2M^2}{g^2} + \frac{2M}{g}H + \frac{1}{2}(H^2 + \phi^0\phi^0 + 2\phi^+\phi^-) \right] + \frac{2M^4}{g^2}\alpha_h \\
& - igc_w \left[\partial_\nu Z^0_\mu \left(W^+_\mu W^-_\nu - W^+_\nu W^-_\mu \right) - Z^0_\nu \left(W^+_\mu \partial_\nu W^-_\mu - W^-_\mu \partial_\nu W^+_\mu \right) \right. \\
& \quad \left. + Z^0_\mu \left(W^+_\nu \partial_\nu W^-_\mu - W^-_\nu \partial_\nu W^+_\mu \right) \right] - \frac{1}{2}g^2 W^+_\mu W^-_\mu W^+_\nu W^-_\nu \\
& - igs_w \left[\partial_\nu A_\mu \left(W^+_\mu W^-_\nu - W^+_\nu W^-_\mu \right) - A_\nu \left(W^+_\mu \partial_\nu W^-_\mu - W^-_\mu \partial_\nu W^+_\mu \right) \right. \\
& \quad \left. + A_\mu \left(W^+_\nu \partial_\nu W^-_\mu - W^-_\nu \partial_\nu W^+_\mu \right) \right] + \frac{1}{2}g^2 W^+_\mu W^-_\nu W^+_\mu W^-_\nu \\
& + g^2 c_w^2 \left(Z^0_\mu W^+_\mu Z^0_\nu W^-_\nu - Z^0_\mu Z^0_\mu W^+_\nu W^-_\nu \right) + g^2 s_w^2 \left(A_\mu W^+_\mu A_\nu W^-_\nu - A_\mu A_\mu W^+_\nu W^-_\nu \right) \\
& + g^2 s_w c_w \left[A_\mu Z^0_\nu \left(W^+_\mu W^-_\nu - W^+_\nu W^-_\mu \right) - 2A_\mu Z^0_\mu W^+_\nu W^-_\nu \right] \\
& - g\alpha_h M \left[H^3 + H\phi^0\phi^0 + 2H\phi^+\phi^- \right] \\
& - \frac{1}{8}g^2 \alpha_h \left[H^4 + (\phi^0)^4 + 4(\phi^+\phi^-)^2 + 4(\phi^0)^2\phi^+\phi^- + 4H^2\phi^+\phi^- + 2(\phi^0)^2 H^2 \right]
\end{aligned}$$

$$
\begin{aligned}
&- gMW_\mu^+ W_\mu^- H - \frac{1}{2}g\frac{M}{c_w^2}Z_\mu^0 Z_\mu^0 H + \frac{1}{2}g\frac{1}{c_w}Z_\mu^0\left(H\partial_\mu\phi^0 - \phi^0\partial_\mu H\right)\\
&- \frac{1}{2}ig\left[W_\mu^+\left(\phi^0\partial_\mu\phi^- - \phi^-\partial_\mu\phi^0\right) - W_\mu^-\left(\phi^0\partial_\mu\phi^+ - \phi^+\partial_\mu\phi^0\right)\right]\\
&+ \frac{1}{2}g\left[W_\mu^+\left(H\partial_\mu\phi^- - \phi^-\partial_\mu H\right) + W_\mu^-\left(H\partial_\mu\phi^+ - \phi^+\partial_\mu H\right)\right]\\
&- ig\frac{s_w^2}{c_w}MZ_\mu^0\left(W_\mu^+\phi^- - W_\mu^-\phi^+\right) + igs_wMA_\mu\left(W_\mu^+\phi^- - W_\mu^-\phi^+\right)\\
&- ig\frac{1-2c_w^2}{2c_w}Z_\mu^0\left(\phi^+\partial_\mu\phi^- - \phi^-\partial_\mu\phi^+\right) + igs_wA_\mu\left(\phi^+\partial_\mu\phi^- - \phi^-\partial_\mu\phi^+\right)\\
&- \frac{1}{4}g^2W_\mu^+W_\mu^-\left[H^2 + (\phi^0)^2 + 2\phi^+\phi^-\right] - \frac{1}{8}g^2\frac{1}{c_w^2}Z_\mu^0Z_\mu^0\left[H^2 + (\phi^0)^2 + 2(2s_w^2-1)^2\phi^+\phi^-\right]\\
&- \frac{1}{2}g^2\frac{s_w^2}{c_w}Z_\mu^0\phi^0\left(W_\mu^+\phi^- + W_\mu^-\phi^+\right) - \frac{1}{2}ig^2\frac{s_w^2}{c_w}Z_\mu^0H\left(W_\mu^+\phi^- - W_\mu^-\phi^+\right)\\
&+ \frac{1}{2}g^2s_wA_\mu\phi^0\left(W_\mu^+\phi^- + W_\mu^-\phi^+\right) + \frac{1}{2}ig^2s_wA_\mu H\left(W_\mu^+\phi^- - W_\mu^-\phi^+\right)\\
&- g^2\frac{s_w}{c_w}\left(2c_w^2-1\right)Z_\mu^0A_\mu\phi^+\phi^- - g^2s_w^2A_\mu A_\mu\phi^+\phi^-\,. \qquad \text{(A.3)}
\end{aligned}
$$

The fermion Lagrangian density, describing the interactions of the fermions with the weak vector bosons

$$
\begin{aligned}
\mathcal{L}_\mathrm{f} = &-\bar{e}^\lambda\left(\gamma\partial + m_e^\lambda\right)e^\lambda - \bar{\nu}^\lambda\gamma\partial\nu^\lambda - \bar{u}_j^\lambda\left(\gamma\partial + m_u^\lambda\right)u_j^\lambda - \bar{d}_j^\lambda\left(\gamma\partial + m_d^\lambda\right)d_j^\lambda\\
&+ igs_wA_\mu\left[-\left(\bar{e}^\lambda\gamma^\mu e^\lambda\right) + \frac{2}{3}\left(\bar{u}_j^\lambda\gamma^\mu u_j^\lambda\right) - \frac{1}{3}\left(\bar{d}_j^\lambda\gamma^\mu d_j^\lambda\right)\right]\\
&+ \frac{ig}{4c_w}Z_\mu^0\left[\left(\bar{\nu}^\lambda\gamma^\mu\left(1+\gamma^5\right)\nu^\lambda\right) + \left(\bar{e}^\lambda\gamma^\mu\left(4s_w^2 - 1 - \gamma^5\right)e^\lambda\right)\right.\\
&\left.+ \left(\bar{d}_j^\lambda\gamma^\mu\left(\frac{4}{3}s_w^2 - 1 - \gamma^5\right)d_j^\lambda\right) + \left(\bar{u}_j^\lambda\gamma^\mu\left(1 - \frac{8}{3}s_w^2 + \gamma^5\right)u_j^\lambda\right)\right]\\
&+ \frac{ig}{2\sqrt{2}}W_\mu^+\left[\left(\bar{\nu}^\lambda\gamma^\mu\left(1+\gamma^5\right)e^\lambda\right) + \left(\bar{u}_j^\lambda\gamma^\mu\left(1+\gamma^5\right)C_{\lambda\kappa}d_j^\kappa\right)\right]\\
&+ \frac{ig}{2\sqrt{2}}W_\mu^-\left[\left(\bar{e}^\lambda\gamma^\mu\left(1+\gamma^5\right)\nu^\lambda\right) + \left(\bar{d}_j^\kappa C_{\lambda\kappa}^\dagger\gamma^\mu\left(1+\gamma^5\right)u_j^\lambda\right)\right]. \qquad \text{(A.4)}
\end{aligned}
$$

The fermion–colour Lagrangian density, describing the interactions of fermions with gluons

$$
\mathcal{L}_\mathrm{fc} = +\frac{1}{2}ig_s^2(\bar{q}_i^\sigma\gamma^\mu q_j^\sigma)g_\mu^a. \qquad \text{(A.5)}
$$

The Faddeev–Popov ghost Lagrangian density of quantum chromodynamics

$$
\mathcal{L}_\mathrm{FPc} = +\bar{G}^a\partial^2G^a + g_sf^{abc}\partial_\mu\bar{G}^aG^bg_\mu^c. \qquad \text{(A.6)}
$$

The Faddeev–Popov ghost Lagrangian density of the weak interactions

$$\begin{aligned}\mathcal{L}_{\mathrm{FPw}} = &+\bar{X}^{+}\left(\partial^2 - M^2\right)X^{+} + \bar{X}^{-}\left(\partial^2 - M^2\right)X^{-} + \bar{X}^{0}\left(\partial^2 - \frac{M^2}{c_w^2}\right)X^{0} + \bar{Y}\partial^2 Y \\ &+ igc_w W_\mu^{+}\left(\partial_\mu \bar{X}^{0}X^{-} - \partial_\mu \bar{X}^{+}X^{0}\right) + igs_w W_\mu^{+}\left(\partial_\mu \bar{Y}X^{-} - \partial_\mu \bar{X}^{+}Y\right) \\ &+ igc_w W_\mu^{-}\left(\partial_\mu \bar{X}^{-}X^{0} - \partial_\mu \bar{X}^{0}X^{+}\right) + igs_w W_\mu^{-}\left(\partial_\mu \bar{X}^{-}Y - \partial_\mu \bar{Y}X^{+}\right) \\ &+ igc_w Z_\mu^{0}\left(\partial_\mu \bar{X}^{+}X^{+} - \partial_\mu \bar{X}^{-}X^{-}\right) + igs_w A_\mu\left(\partial_\mu \bar{X}^{+}X^{+} - \partial_\mu \bar{X}^{-}X^{-}\right) \\ &- \frac{1}{2}gM\left[\bar{X}^{+}X^{+}H + \bar{X}^{-}X^{-}H + \frac{1}{c_w^2}\bar{X}^{0}X^{0}H\right] \\ &+ \frac{1-2c_w^2}{2c_w}igM\left[\bar{X}^{+}X^{0}\phi^{+} - \bar{X}^{-}X^{0}\phi^{-}\right] + \frac{1}{2c_w}igM\left[\bar{X}^{0}X^{-}\phi^{+} - \bar{X}^{0}X^{+}\phi^{-}\right] \\ &+ igMs_w\left[\bar{X}^{-}Y\phi^{-} - \bar{X}^{+}Y\phi^{+}\right] + \frac{1}{2}igM\left[\bar{X}^{+}X^{+}\phi^{0} - \bar{X}^{-}X^{-}\phi^{0}\right]. \end{aligned} \tag{A.7}$$

The fermion–Higgs Lagrangian density, describing the interactions of fermions with the Higgs system

$$\begin{aligned}\mathcal{L}_{\mathrm{fH}} = &+\frac{ig}{2\sqrt{2}}\frac{m_e^{\lambda}}{M}\left[-\phi^{+}\left(\bar{\nu}^{\lambda}\left(1-\gamma^5\right)e^{\lambda}\right) + \phi^{-}\left(\bar{e^{\lambda}}\left(1+\gamma^5\right)\nu^{\lambda}\right)\right] \\ &- \frac{g}{2}\frac{m_e^{\lambda}}{M}\left[H\left(\bar{e^{\lambda}}e^{\lambda}\right) + i\phi^{0}\left(\bar{e^{\lambda}}\gamma^5 e^{\lambda}\right)\right] \\ &+ \frac{ig}{2M\sqrt{2}}\phi^{+}\left[-m_d^{\kappa}\left(\bar{u_j^{\lambda}}C_{\lambda\kappa}\left(1-\gamma^5\right)d_j^{\kappa}\right) + m_u^{\lambda}\left(\bar{u_j^{\lambda}}C_{\lambda\kappa}\left(1+\gamma^5\right)d_j^{\kappa}\right)\right] \\ &+ \frac{ig}{2M\sqrt{2}}\phi^{-}\left[m_d^{\lambda}\left(\bar{d_j^{\lambda}}C_{\lambda\kappa}^{\dagger}\left(1+\gamma^5\right)u_j^{\kappa}\right) - m_u^{\kappa}\left(\bar{d_j^{\lambda}}C_{\lambda\kappa}^{\dagger}\left(1-\gamma^5\right)u_j^{\kappa}\right)\right] \\ &- \frac{g}{2}\frac{m_u^{\lambda}}{M}H\left(\bar{u_j^{\lambda}}u_j^{\lambda}\right) - \frac{g}{2}\frac{m_d^{\lambda}}{M}H\left(\bar{d_j^{\lambda}}d_j^{\lambda}\right) + \frac{ig}{2}\frac{m_u^{\lambda}}{M}\phi^{0}\left(\bar{u_j^{\lambda}}\gamma^5 u_j^{\lambda}\right) - \frac{ig}{2}\frac{m_d^{\lambda}}{M}\phi^{0}\left(\bar{d_j^{\lambda}}\gamma^5 d_j^{\lambda}\right). \end{aligned} \tag{A.8}$$

A.2 Spinors

For the metric we use

$$g_{\mu\nu} = \mathrm{diag}(+1,-1,-1,-1) = \begin{pmatrix} +1 & 0 & 0 & 0 \\ 0 & -1 & 0 & 0 \\ 0 & 0 & -1 & 0 \\ 0 & 0 & 0 & -1 \end{pmatrix}. \tag{A.9}$$

We define the light-cone coordinates as:

$$p_+ = p_0 + p_3, \quad p_- = p_0 - p_3, \quad p_\perp = p_1 + ip_2, \quad p_{\perp^*} = p_1 - ip_2. \tag{A.10}$$

In terms of the light-cone components of a null-vector, the corresponding massless spinors $\langle p^{\pm}|$ and $|p^{\pm}\rangle$ can be chosen as:

$$\left\langle p^{+}\right| = \frac{\exp(-i\frac{\phi}{2})}{\sqrt{|p_+|}}\left(0,0,-p_\perp,p_+\right), \qquad \left\langle p^{-}\right| = \frac{\exp(-i\frac{\phi}{2})}{\sqrt{|p_+|}}\left(p_+,p_{\perp^*},0,0\right),$$

$$\left|p^+\right\rangle = \frac{\exp(-i\frac{\phi}{2})}{\sqrt{|p_+|}} \begin{pmatrix} -p_{\perp^*} \\ p_+ \\ 0 \\ 0 \end{pmatrix}, \qquad \left|p^-\right\rangle = \frac{\exp(-i\frac{\phi}{2})}{\sqrt{|p_+|}} \begin{pmatrix} 0 \\ 0 \\ p_+ \\ p_\perp \end{pmatrix}, \tag{A.11}$$

where the phase ϕ is given by:

$$p_+ = |p_+| \exp(i\phi). \tag{A.12}$$

Spinor products are denoted as:

$$\langle pq\rangle = \langle p^-|q^+\rangle = p^A q_A, \qquad [qp] = \langle q^+|p^-\rangle = q_{\dot{A}} p^{\dot{A}}. \tag{A.13}$$

Here the Weyl–van der Waerden spinor notation was used [236–238]. From the definition in equation (A.11) one immediately sees that products of spinors with the same sign vanish:

$$\langle q^+|p^+\rangle = \langle q^-|p^-\rangle = 0\,. \tag{A.14}$$

The polarisation vectors for positive and negative polarisations are:

$$\varepsilon_\mu^\pm(k_i, q) = \pm \frac{\langle q^\mp|\gamma_\mu|k_i^\mp\rangle}{\sqrt{2}\langle q^\mp|k_i^\pm\rangle}\,, \tag{A.15}$$

where k is the momentum of the vector boson and q is an auxiliary massless vector called reference momentum.
Here the Dirac matrices γ^μ are used. They are defined by the following anticommutation relation:

$$\{\gamma^\mu, \gamma^\nu\} = \gamma^\mu\gamma^\nu + \gamma^\nu\gamma^\mu = 2g^{\mu\nu}\,. \tag{A.16}$$

One specific choice of them is:

$$\gamma^\mu = \begin{pmatrix} 0 & \sigma^\mu \\ \bar{\sigma}^\mu & 0 \end{pmatrix}, \qquad \gamma^5 = \begin{pmatrix} -\mathbb{1} & 0 \\ 0 & \mathbb{1} \end{pmatrix}, \tag{A.17}$$

with

$$\sigma^\mu = (1, \sigma^1, \sigma^2, \sigma^3)\,, \tag{A.18}$$

where the Pauli matrices [239]

$$\sigma^1 = \begin{pmatrix} 0 & 1 \\ 1 & 0 \end{pmatrix}, \quad \sigma^2 = \begin{pmatrix} 0 & -i \\ i & 0 \end{pmatrix}, \quad \sigma^3 = \begin{pmatrix} 1 & 0 \\ 0 & -1 \end{pmatrix} \tag{A.19}$$

are used.
Complex conjugation reverses the helicity:

$$\left(\varepsilon^\pm\right)^* = \varepsilon^\mp\,. \tag{A.20}$$

Polarisation vectors are normalised:

$$\begin{aligned} \varepsilon^\pm \cdot \left(\varepsilon^\pm\right)^* &= \varepsilon^\pm\varepsilon^\mp = -1\,, \\ \varepsilon^\pm \cdot \left(\varepsilon^\mp\right)^* &= \varepsilon^\pm\varepsilon^\pm = 0\,. \end{aligned} \tag{A.21}$$

There are some properties that make the calculations with polarisation vectors especially easy:

$$\begin{aligned}
\varepsilon^{\pm}(k,q)\cdot k &= 0\,,\\
\varepsilon^{\pm}(k,q)\cdot q &= 0\,,\\
\varepsilon^{+}(k_i,q)\cdot\varepsilon^{+}(k_j,q) &= \varepsilon^{-}(k_i,q)\cdot\varepsilon^{-}(k_j,q) = 0\,,\\
\varepsilon^{+}(k_i,k_j)\cdot\varepsilon^{-}(k_j,q) &= \varepsilon^{+}(k_i,q)\cdot\varepsilon^{-}(k_j,k_i) = 0\,,\\
\not{\varepsilon}^{+}(k_i,k_j)|k_j^{+}\rangle &= \not{\varepsilon}^{-}(k_i,k_j)|k_j^{-}\rangle = 0\,,\\
\langle k_j^{+}|\not{\varepsilon}^{-}(k_i,k_j) &= \langle k_j^{-}|\not{\varepsilon}^{+}(k_i,k_j) = 0\,.
\end{aligned} \tag{A.22}$$

Convenient abbreviations for spinor products are:

$$\begin{aligned}
\langle jl\rangle &= \langle k_j k_l\rangle = \langle k_j^{-}|k_l^{+}\rangle,\\
[jl] &= [k_j k_l] = [k_j^{-}|k_l^{+}].
\end{aligned} \tag{A.23}$$

The spinor products are antisymmetric:

$$\begin{aligned}
\langle jl\rangle &= -\langle l\,j\rangle,\\
[jl] &= -[l\,j]\,,
\end{aligned} \tag{A.24}$$

they fulfil the Schouten identity [240]:

$$\langle 12\rangle\langle 34\rangle = \langle 14\rangle\langle 32\rangle + \langle 13\rangle\langle 24\rangle, \tag{A.25}$$

and the Fierz identity [241, 242]:

$$\langle 1^{-}|\gamma^{\mu}|2^{-}\rangle\langle 3^{+}|\gamma_{\mu}|4^{+}\rangle = 2\langle 14\rangle\,[32]\,. \tag{A.26}$$

In addition there is charge conjugation of current:

$$\langle 1^{+}|\gamma^{\mu}|2^{+}\rangle = \langle 2^{-}|\gamma^{\mu}|1^{-}\rangle \tag{A.27}$$

and the following property:

$$\langle j\,j\rangle = [j\,j] = 0\,. \tag{A.28}$$

A.3 Splitting Functions

In the collinear limit the all-gluon tree-level partial amplitudes factorise according to:

$$A_{n+1}(\ldots,k_a,k_b,\ldots) \xrightarrow{k_a\|k_b} \sum_{\lambda=+/-} \mathrm{Split}_{-\lambda}(k_a^{\lambda_a},k_b^{\lambda_b})A_n(\ldots,K^{\lambda},\ldots), \tag{A.29}$$

where k_a and k_b are the momenta of two adjacent legs, $K = k_a + k_b$, $k_a = zK$ and $k_b = (1-z)K$. λ, λ_a and λ_b denote the corresponding helicities. The splitting functions are:

$$\begin{aligned}
&\mathrm{Split}_{g^+}(g^+,g^+) = 0, && \mathrm{Split}_{g^-}(g^-,g^-) = 0,\\
&\mathrm{Split}_{g^+}(g^+,g^-) = \sqrt{2}\frac{(1-z)^{\frac{3}{2}}}{\sqrt{z}\langle ab\rangle}, && \mathrm{Split}_{g^-}(g^-,g^+) = -\sqrt{2}\frac{(1-z)^{\frac{3}{2}}}{\sqrt{z}[ab]},\\
&\mathrm{Split}_{g^+}(g^-,g^+) = \sqrt{2}\frac{z^{\frac{3}{2}}}{\sqrt{(1-z)}\langle ab\rangle}, && \mathrm{Split}_{g^-}(g^+,g^-) = -\sqrt{2}\frac{z^{\frac{3}{2}}}{\sqrt{(1-z)}[ab]},\\
&\mathrm{Split}_{g^+}(g^-,g^-) = -\sqrt{2}\frac{1}{\sqrt{z(1-z)}[ab]}, && \mathrm{Split}_{g^-}(g^+,g^+) = \sqrt{2}\frac{1}{\sqrt{z(1-z)}\langle ab\rangle}.
\end{aligned} \tag{A.30}$$

A.4 Feynman Rules

A.4.1 Feynman Rules in the Standard Model

The Feynman rules for external lines:

incoming photon		$\varepsilon_\mu(\lambda)$
outgoing photon		$\varepsilon^*_\mu(\lambda)$
incoming gluon	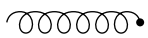	$\varepsilon_\mu(\lambda)$
outgoing gluon	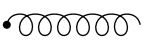	$\varepsilon^*_\mu(\lambda)$
incoming fermion		$u(p,s)$
outgoing fermion		$\bar{u}(p,s)$
incoming antifermion		$\bar{v}(p,s)$
outgoing antifermion	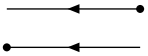	$v(p,s)$

The Feynman rules for internal lines (propagators) in Feynman gauge:

Photon	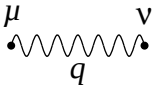	$-i\,\frac{g_{\mu\nu}}{q^2}$
Gluon	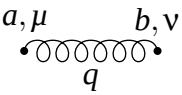	$-i\delta_{ab}\frac{g_{\mu\nu}}{q^2}$
massless Fermion	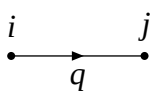	$i\delta_{ij}\frac{\not{q}}{q^2}$

Here the Feynman slash was used

$$\not{q} \equiv q\cdot\gamma = g_{\mu\nu}q^\mu\gamma^\nu\,. \tag{A.31}$$

The Feynman rules for vertices:

photon-fermion 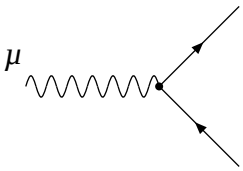

$-iee_f\gamma_\mu$

gluon-quark 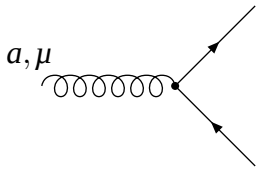

$-ig_s\gamma_\mu T^c_{jk}$

The conventional three- and four-point Feynman vertices are

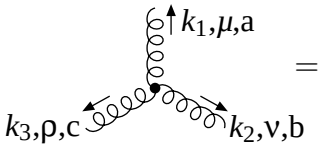

$$= -gf^{abc}\left[g^{\mu\nu}\left(k_1^\rho - k_2^\rho\right) + g^{\nu\rho}\left(k_2^\mu - k_3^\mu\right) + g^{\rho\mu}\left(k_3^\nu - k_1^\nu\right)\right],$$

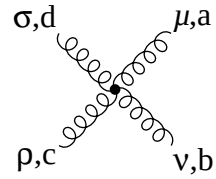

$$= \begin{cases} -ig^2\left[f^{abe}f^{cde}(g^{\mu\rho}g^{\nu\sigma} - g^{\mu\sigma}g^{\nu\rho})\right. \\ \quad + f^{ace}f^{bde}(g^{\mu\nu}g^{\rho\sigma} - g^{\mu\sigma}g^{\nu\rho}) \\ \quad \left. + f^{ade}f^{bce}(g^{\mu\nu}g^{\rho\sigma} - g^{\mu\rho}g^{\nu\sigma})\right], \\ \end{cases}$$

where the f^{abc} are the structure constants defined by

$$[T^a, T^b] = if^{abc}T^c\ . \tag{A.32}$$

The only non-zero elements (up to permutations) of the totally antisymmetric tensor are:

$$\begin{aligned} 1 &= f_{123} = 2f_{147} = 2f_{246} = 2f_{257} = 2f_{345} \\ &= -2f_{156} = -2f_{367} = \frac{2}{\sqrt{3}}f_{458} = \frac{2}{\sqrt{3}}f_{678}. \end{aligned} \tag{A.33}$$

The Gell-Mann matrices [243] are the generators of the Lie algebra of the group $SU(3)$:

$$\lambda_1 = \begin{pmatrix} 0 & 1 & 0 \\ 1 & 0 & 0 \\ 0 & 0 & 0 \end{pmatrix}, \quad \lambda_2 = \begin{pmatrix} 0 & -i & 0 \\ i & 0 & 0 \\ 0 & 0 & 0 \end{pmatrix}, \quad \lambda_3 = \begin{pmatrix} 1 & 0 & 0 \\ 0 & -1 & 0 \\ 0 & 0 & 0 \end{pmatrix},$$

$$\lambda_4 = \begin{pmatrix} 0 & 0 & 1 \\ 0 & 0 & 0 \\ 1 & 0 & 0 \end{pmatrix}, \quad \lambda_5 = \begin{pmatrix} 0 & 0 & -i \\ 0 & 0 & 0 \\ i & 0 & 0 \end{pmatrix}, \quad \lambda_6 = \begin{pmatrix} 0 & 0 & 0 \\ 0 & 0 & 1 \\ 0 & 1 & 0 \end{pmatrix},$$

$$\lambda_7 = \begin{pmatrix} 0 & 0 & 0 \\ 0 & 0 & -i \\ 0 & i & 0 \end{pmatrix}, \quad \lambda_8 = \frac{1}{\sqrt{3}}\begin{pmatrix} 1 & 0 & 0 \\ 0 & 1 & 0 \\ 0 & 0 & -2 \end{pmatrix}. \tag{A.34}$$

They are correlated to the T^a by:

$$T^a = \frac{\lambda^a}{2}\,. \tag{A.35}$$

A.4.2 Colour-Ordered Feynman Rules

The Feynman rules for colour-ordered partial amplitudes read:

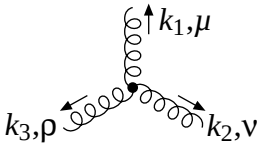

$$= i\left[g^{\mu\nu}\left(k_1^\rho - k_2^\rho\right) + g^{\nu\rho}\left(k_2^\mu - k_3^\mu\right) + g^{\rho\mu}\left(k_3^\nu - k_1^\nu\right)\right],$$

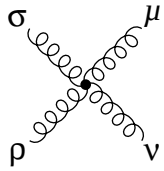

$$= i\left[2g^{\mu\rho}g^{\nu\sigma} - g^{\mu\nu}g^{\rho\sigma} - g^{\mu\sigma}g^{\nu\rho}\right]. \tag{A.36}$$

A.4.3 Scalar Diagrammatic Rules

The non-vanishing primitive vertices involving only gluons are:

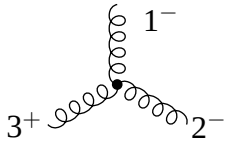

$$= V_3(k_1^-,k_2^-,k_3^+) = i\sqrt{2}\langle 12\rangle\frac{[3q]^2}{[1q][2q]} = i\sqrt{2}\frac{\langle 12\rangle^4}{\langle 12\rangle\langle 23\rangle\langle 31\rangle},$$

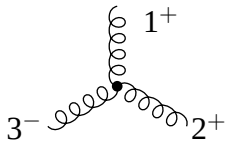

$$= V_3(k_1^+,k_2^+,k_3^-) = i\sqrt{2}[21]\frac{\langle 3q\rangle^2}{\langle 1q\rangle\langle 2q\rangle} = i\sqrt{2}\frac{[21]^4}{[32][21][13]},$$

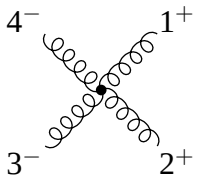

$$\begin{aligned} &= V_4(k_1^+,k_2^+,k_3^-,k_4^-) \\ &= i\frac{[1q][2q]\langle 3q\rangle\langle 4q\rangle}{\langle 1q\rangle\langle 2q\rangle[3q][4q]}\left(1 + \frac{\langle q^-|2-3|q^-\rangle\,\langle q^-|4-1|q^-\rangle}{\langle q^-|2+3|q^-\rangle\,\langle q^-|4+1|q^-\rangle}\right), \end{aligned}$$

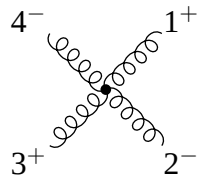

$$
\begin{aligned}
&= V_4(k_1^+, k_2^-, k_3^+, k_4^-) \\
&= i\frac{[1q]\langle 2q\rangle[3q]\langle 4q\rangle}{\langle 1q\rangle[2q]\langle 3q\rangle[4q]}\left(\frac{\langle q^-|1-2|q^-\rangle\langle q^-|3-4|q^-\rangle}{\langle q^-|1+2|q^-\rangle\langle q^-|3+4|q^-\rangle}\right. \\
&\quad \left. + \frac{\langle q^-|2-3|q^-\rangle\langle q^-|4-1|q^-\rangle}{\langle q^-|2+3|q^-\rangle\langle q^-|4+1|q^-\rangle} - 2\right).
\end{aligned} \tag{A.37}
$$

A.5 Sudakov Factors for Massless Final-State Partons

In this appendix we discuss in more detail the Sudakov factors for massless final-state partons. This case is simple enough that one integration can be done analytically. The spin-averaged dipole splitting functions in four dimensions are:

$$
\begin{aligned}
\mathcal{P}_{q\to qg} &= C_F \frac{8\pi\alpha_s(\mu^2)}{s_{ijk}}\frac{1}{y}\left[\frac{2}{1-z(1-y)} - (1+z)\right], \\
\mathcal{P}_{g\to gg} &= C_A \frac{8\pi\alpha_s(\mu^2)}{s_{ijk}}\frac{1}{y}\left[\frac{2}{1-z(1-y)} + \frac{2}{1-(1-z)(1-y)} - 4 + 2z(1-z)\right], \\
\mathcal{P}_{g\to q\bar{q}} &= T_R \frac{8\pi\alpha_s(\mu^2)}{s_{ijk}}\frac{1}{y}\left[1-2z(1-z)\right],
\end{aligned} \tag{A.38}
$$

where

$$
s_{ijk} = \left(p_i + p_j + p_k\right)^2 = (p_{\tilde{i}} + p_{\tilde{k}})^2. \tag{A.39}
$$

The dipole phase space measure is:

$$
\int d\phi_{\text{unres}} = \frac{s_{ijk}}{16\pi^2}\int_0^1 d\kappa \int_{z_-(\kappa)}^{z_+(\kappa)} dz \frac{1}{4z(1-z)}\left(1 - \frac{\kappa}{4z(1-z)}\right), \tag{A.40}
$$

where

$$
z_\pm(\kappa) = \frac{1}{2}\left(1 \pm \sqrt{1-\kappa}\right). \tag{A.41}
$$

The strong coupling is evaluated at the scale $\mu^2 = -k_\perp^2$:

$$
\alpha_s(\mu^2) = \alpha_s\left(\frac{1}{4}\kappa s_{ijk}\right). \tag{A.42}
$$

The Sudakov factor is given by:

$$
\Delta_{ij,k}(t_1,t_2) = \exp\left(-\int_{t_2}^{t_1} dt\, \mathcal{C}_{\tilde{i},\tilde{k}} \int d\phi_{\text{unres}}\, \delta\left(t - T_{\tilde{i},\tilde{k}}\right)\mathcal{P}_{ij,k}\right). \tag{A.43}
$$

For the splitting $q \to qg$ we obtain:

$$\Delta_{ij,k}(t_1,t_2) = \exp\left\{ -\mathcal{C}_{\tilde{i},\tilde{k}} C_F \int_{\kappa_-}^{\kappa_+} \frac{d\kappa}{\kappa} \frac{\alpha_s(\mu^2)}{2\pi} \int_{z_-(\kappa)}^{z_+(\kappa)} dz\,(1-y)\left[\frac{2}{1-z(1-y)} - (1+z)\right] \right\}, \tag{A.44}$$

where

$$\kappa_- = 4\frac{Q^2}{s_{ijk}} e^{t_2}, \quad \kappa_+ = \min\left(1, 4\frac{Q^2}{s_{ijk}} e^{t_1}\right), \quad y = \frac{\kappa}{4z(1-z)}, \mu^2 = \frac{1}{4}\kappa s_{ijk}. \tag{A.45}$$

The integration over z can be done analytically:

$$\begin{aligned} \int dz\,(1-y)\left[\frac{2}{1-z(1-y)} - (1+z)\right] &= -\frac{1}{2}z^2 - z + \frac{\kappa}{4}\left[\ln z - 2\ln(1-z)\right] \\ &\quad - \frac{4}{4+\kappa}\left[\frac{1}{2}\kappa \ln z + \ln\left(\kappa + 4(1-z)^2\right) + \sqrt{\kappa}\arctan\left(\frac{2}{\sqrt{\kappa}}(1-z)\right)\right]. \end{aligned} \tag{A.46}$$

The same holds for the other splittings. Therefore we obtain for the Sudakov factors:

$$\Delta_{ij,k}(t_1,t_2) = \exp\left\{ -\mathcal{C}_{\tilde{i},\tilde{k}} C \int_{\kappa_-}^{\kappa_+} \frac{d\kappa}{\kappa} \frac{\alpha_s\left(\frac{1}{4}\kappa s_{ijk}\right)}{2\pi} \left(\mathcal{V}_{ij,k}(\kappa, z_+) - \mathcal{V}_{ij,k}(\kappa, z_-)\right) \right\}, \tag{A.47}$$

where C is a colour factor and equal to:

$$C = \begin{cases} C_F & \text{for} \quad q \to qg, \\ C_A & \text{for} \quad g \to gg, \\ T_R & \text{for} \quad g \to q\bar{q}. \end{cases} \tag{A.48}$$

The functions $\mathcal{V}_{ij,k}(\kappa, z)$ are given by:

$$\begin{aligned} \mathcal{V}_{qg,k}(\kappa,z) &= -\frac{1}{2}z^2 - z + \frac{\kappa}{4}\left[\ln z - 2\ln(1-z)\right] \\ &\quad - \frac{4}{4+\kappa}\left[\frac{1}{2}\kappa\ln z + \ln\left(\kappa + 4(1-z)^2\right) - \sqrt{\kappa}\arctan\left(\frac{2}{\sqrt{\kappa}}(1-z)\right)\right], \\ \mathcal{V}_{gg,k}(\kappa,z) &= -\frac{2}{3}z^3 + z^2 - 4z - \frac{1}{2}\kappa z + \kappa \ln\frac{z}{1-z} + \frac{4}{4+\kappa}\left[\frac{1}{2}\kappa\ln\frac{1-z}{z}\right. \\ &\quad \left. + \ln\frac{\kappa+4z^2}{\kappa+4(1-z)^2} - \sqrt{\kappa}\arctan\left(\frac{2z}{\sqrt{\kappa}}\right) + \sqrt{\kappa}\arctan\left(\frac{2(1-z)}{\sqrt{\kappa}}\right)\right], \\ \mathcal{V}_{gq,k}(\kappa,z) &= \frac{2}{3}z^3 - z^2 + z + \frac{\kappa}{2}z - \frac{\kappa}{4}\ln\frac{z}{1-z}. \end{aligned} \tag{A.49}$$

A.6 Insertion of Emitted Particles

In this appendix we list the relevant formulæ for the insertion of one additional four-vector into a set of n four-vectors. This insertion satisfies momentum conservation and can be considered as the inverse of the $(n+1) \to n$ phase space mapping of Catani and Seymour. These

insertion mappings are also useful for an efficient phase space integration of the real emission contribution in NLO calculations. Therefore we quote in addition the relevant phase space weights. For the shower algorithm, these weights are not needed, as they are taken into account through the generation of the shower.

A.6.1 Insertion for Final-State Particles

The Massless Case

We start with the simplest case, where both the emitter and the spectator are in the final state and all particles involved in the dipole splitting are massless. The insertion procedure is identical to the one used in references [146]. Given the four-vectors $\tilde{p}_{ij}$ and $\tilde{p}_k$ together with the three variables y, z and ϕ_s we would like to construct p_i, p_j and p_k, such that

$$p_i + p_j + p_k = \tilde{p}_{ij} + \tilde{p}_k, \quad p_i^2 = p_j^2 = p_k^2 = 0. \tag{A.50}$$

In four dimensions we have for the phase space measure:

$$d\phi_{\text{unres}} = \frac{s_{ijk}}{32\pi^3} \int_0^1 dy\ (1-y) \int_0^1 dz \int_0^{2\pi} d\phi_s, \tag{A.51}$$

where $s_{ijk} = (\tilde{p}_{ij} + \tilde{p}_k)^2 = (p_i + p_j + p_k)^2$. It is convenient to work in the rest frame of $P = \tilde{p}_{ij} + \tilde{p}_k = p_i + p_j + p_k$. We shall orient the frame in such a way, that the spatial components of $\tilde{p}_k$ are along the z-direction. When used as a phase space generator we set:

$$y = u_1, \quad z = u_2, \quad \phi_s = 2\pi u_3, \tag{A.52}$$

where u_1, u_2 and u_3 are three uniformly distributed random numbers in $[0,1]$. From

$$y = \frac{s_{ij}}{s_{ij} + s_{ik} + s_{jk}}, \quad z = \frac{s_{ik}}{s_{ik} + s_{jk}} \tag{A.53}$$

we obtain:

$$s_{ij} = yP^2, \quad s_{ik} = z(1-y)P^2, \quad s_{jk} = (1-z)(1-y)P^2. \tag{A.54}$$

If $s_{ij} < s_{jk}$ we want to have $p_k' \to p_k$ as $s_{ij} \to 0$. Define

$$E_i = \frac{s_{ij} + s_{ik}}{2\sqrt{s_{ijk}}}, \qquad E_j = \frac{s_{ij} + s_{jk}}{2\sqrt{s_{ijk}}}, \qquad E_k = \frac{s_{ik} + s_{jk}}{2\sqrt{s_{ijk}}}, \tag{A.55}$$

$$\theta_{ik} = \arccos\left(1 - \frac{s_{ik}}{2E_iE_k}\right), \quad \theta_{jk} = \arccos\left(1 - \frac{s_{jk}}{2E_jE_k}\right). \tag{A.56}$$

In our coordinate system we have:

$$\begin{aligned} p_i' &= E_i(1, \sin\theta_{ik}\cos(\phi_s + \pi), \sin\theta_{ik}\sin(\phi_s + \pi), \cos\theta_{ik}), \\ p_j' &= E_j(1, \sin\theta_{jk}\cos\phi_s, \sin\theta_{jk}\sin\phi_s, \cos\theta_{jk}), \\ p_k' &= E_k(1, 0, 0, 1)\,. \end{aligned} \tag{A.57}$$

The momenta p_i', p_j' and p_k' are related to the momenta p_i, p_j and p_k by a sequence of Lorentz transformations back to the original frame:

$$p_i = \Lambda_{\text{boost}} \Lambda_{xy}(\phi) \Lambda_{xz}(\theta) p_i' \tag{A.58}$$

and analogously for the other two momenta. The explicit formulæ for the Lorentz transformations are obtained as follows: let $|P| = \sqrt{(\tilde{p}_{ij} + \tilde{p}_k)^2}$ and denote by $\hat{p}_k$ the coordinates of the hard momentum $\tilde{p}_k$ in the centre of mass system of $\tilde{p}_{ij} + \tilde{p}_k$. $\hat{p}_k$ is given by:

$$\hat{p}_k = \left(\frac{E_P}{|P|} \tilde{E}_k - \frac{\vec{\tilde{p}}_k \cdot \vec{P}}{|P|}, \vec{\tilde{p}}_k + \left(\frac{\vec{\tilde{p}}_k \cdot \vec{P}}{|P|(E_P + |P|)} - \frac{\tilde{E}_k}{|P|} \right) \vec{P} \right). \tag{A.59}$$

The angles are then given by:

$$\theta = \arccos \left(\frac{2\hat{E}_k E_k' - 2\hat{p}_k \cdot p_k'}{2 \left| \vec{\hat{p}}_k \right| \left| \vec{p}_k' \right|} \right), \quad \phi = \arctan \left(\frac{\hat{p}_k^y}{\hat{p}_k^x} \right). \tag{A.60}$$

For the case considered here particle k is massless and the formula for θ reduces to:

$$\theta = \arccos \left(1 - \frac{2\hat{p}_k \cdot p_k'}{2\hat{p}_k^t p_k^{t'}} \right). \tag{A.61}$$

The explicit form of the rotations is:

$$\Lambda_{xz}(\theta) = \begin{pmatrix} 1 & 0 & 0 & 0 \\ 0 & \cos\theta & 0 & \sin\theta \\ 0 & 0 & 1 & 0 \\ 0 & -\sin\theta & 0 & \cos\theta \end{pmatrix}, \quad \Lambda_{xy}(\phi) = \begin{pmatrix} 1 & 0 & 0 & 0 \\ 0 & \cos\phi & -\sin\phi & 0 \\ 0 & \sin\phi & \cos\phi & 0 \\ 0 & 0 & 0 & 1 \end{pmatrix}. \tag{A.62}$$

The boost $p = \Lambda_{\text{boost}} q$ is given by:

$$p = \left(\frac{E_P}{|P|} E_q + \frac{\vec{q} \cdot \vec{P}}{|P|}, \vec{q} + \left(\frac{\vec{q} \cdot \vec{P}}{|P|(E_P + |P|)} + \frac{E_q}{|P|} \right) \vec{P} \right). \tag{A.63}$$

The weight is given by:

$$w = \frac{s_{ijk}}{16\pi^2} (1 - y). \tag{A.64}$$

The Massive Case

We now consider the case of final-state particles with arbitrary masses:

$$\tilde{p}_{ij}^2 = m_{ij}^2, \quad p_i^2 = m_i^2, \quad p_j^2 = m_j^2, \quad \tilde{p}_k^2 = p_k^2 = m_k^2. \tag{A.65}$$

The dipole phase space reads [210]:

$$d\phi_{\text{unres}} = \frac{s_{ijk}}{32\pi^3} \left(1 - \mu_i^2 - \mu_j^2 - \mu_k^2\right)^2 \left[\lambda\left(1, \mu_{ij}^2, \mu_k^2\right)\right]^{-\frac{1}{2}} \int_{y_-}^{y_+} dy \, (1-y) \int_{z_-}^{z_+} dz \int_0^{2\pi} d\phi_s, \tag{A.66}$$

where

$$s_{ijk} = \left(\tilde{p}_{ij} + \tilde{p}_k\right)^2, \quad \mu_l = \frac{m_l}{\sqrt{s_{ijk}}}, \quad \lambda(x,y,z) = x^2 + y^2 + z^2 - 2xy - 2yz - 2zy. \tag{A.67}$$

The integration boundaries are given by:

$$\begin{aligned} y_+ &= 1 - \frac{2\mu_k(1-\mu_k)}{1-\mu_i^2-\mu_j^2-\mu_k^2}, \quad y_- = \frac{2\mu_i\mu_j}{1-\mu_i^2-\mu_j^2-\mu_k^2}, \\ z_\pm &= \frac{2\mu_i^2 + \left(1-\mu_i^2-\mu_j^2-\mu_k^2\right)y}{2\left[\mu_i^2+\mu_j^2+\left(1-\mu_i^2-\mu_j^2-\mu_k^2\right)y\right]}\left(1 \pm v_{ij,i}v_{ij,k}\right). \end{aligned} \tag{A.68}$$

The general formula for the relative velocities is $v_{p,q} = \sqrt{1-p^2q^2/(pq)}$. In our case the relative velocities are given by:

$$\begin{aligned} v_{ij,k} &= \frac{\sqrt{\left[2\mu_k^2 + \left(1-\mu_i^2-\mu_j^2-\mu_k^2\right)(1-y)\right]^2 - 4\mu_k^2}}{\left(1-\mu_i^2-\mu_j^2-\mu_k^2\right)(1-y)}, \\ v_{ij,i} &= \frac{\sqrt{\left(1-\mu_i^2-\mu_j^2-\mu_k^2\right)^2 y^2 - 4\mu_i^2\mu_j^2}}{\left(1-\mu_i^2-\mu_j^2-\mu_k^2\right)y + 2\mu_i^2}. \end{aligned} \tag{A.69}$$

For the phase space generation we set:

$$y = (y_+ - y_-)\,u_1 + y_-, \quad z = (z_+ - z_-)\,u_2 + z_-, \quad \phi_s = 2\pi u_3. \tag{A.70}$$

We again work in the rest frame of $P = \tilde{p}_{ij} + \tilde{p}_k = p_i + p_j + p_k$, such that the spatial components of $\tilde{p}_k$ are along the z-direction:

$$\tilde{p}_{ij} = \left(\tilde{E}_{ij}, 0, 0, -\left|\vec{\tilde{p}}_k\right|\right), \quad \tilde{p}_k = \left(\tilde{E}_k, 0, 0, \left|\vec{\tilde{p}}_k\right|\right). \tag{A.71}$$

For the invariants we have:

$$\begin{aligned} 2p_ip_j &= y\left(P^2 - m_i^2 - m_j^2 - m_k^2\right), \\ 2p_ip_k &= z(1-y)\left(P^2 - m_i^2 - m_j^2 - m_k^2\right), \\ 2p_jp_k &= (1-z)(1-y)\left(P^2 - m_i^2 - m_j^2 - m_k^2\right). \end{aligned} \tag{A.72}$$

The invariants are related to y and z as follows:

$$y = \frac{2p_ip_j}{2p_ip_j + 2p_ip_k + 2p_jp_k}, \quad z = \frac{2p_ip_k}{2p_ip_k + 2p_jp_k}. \tag{A.73}$$

In our chosen frame

$$\begin{aligned} p_i' &= |\vec{p}_i|\,(\frac{E_i}{|\vec{p}_i|}, \sin\theta_{ik}\cos(\phi_s+\pi), \sin\theta_{ik}\sin(\phi_s+\pi), \cos\theta_{ik}), \\ p_j' &= \left|\vec{p}_j\right|(\frac{E_j}{\left|\vec{p}_j\right|}, \sin\theta_{jk}\cos\phi_s, \sin\theta_{jk}\sin\phi_s, \cos\theta_{jk}), \\ p_k' &= |\vec{p}_k|\,(\frac{E_k}{|\vec{p}_k|}, 0, 0, 1)\,. \end{aligned} \tag{A.74}$$

The energies are obtained from the invariants as follows:

$$\begin{aligned} E_i &= \frac{s_{ijk} - 2p_j p_k + m_i^2 - m_j^2 - m_k^2}{2\sqrt{s_{ijk}}}, \\ E_j &= \frac{s_{ijk} - 2p_i p_k - m_i^2 + m_j^2 - m_k^2}{2\sqrt{s_{ijk}}}, \\ E_k &= \frac{s_{ijk} - 2p_i p_j - m_i^2 - m_j^2 + m_k^2}{2\sqrt{s_{ijk}}}. \end{aligned} \tag{A.75}$$

For the angles we have:

$$\theta_{ik} = \arccos\left(\frac{2E_iE_k - 2p_ip_k}{2\left|\vec{p}_i\right|\left|\vec{p}_k\right|}\right), \quad \theta_{jk} = \arccos\left(\frac{2E_jE_k - 2p_jp_k}{2\left|\vec{p}_j\right|\left|\vec{p}_k\right|}\right). \tag{A.76}$$

The momenta p_i', p_j' and p_k' are related to the momenta p_i, p_j and p_k by the same sequence of Lorentz transformations as in equation (A.58). The weight is:

$$w = \frac{s_{ijk}}{16\pi^2}\left(1 - \mu_i^2 - \mu_j^2 - \mu_k^2\right)^2 \left[\lambda\left(1, \mu_{ij}^2, \mu_k^2\right)\right]^{-\frac{1}{2}} (1-y)\,(y_+ - y_-)\,(z_+ - z_-)\,. \tag{A.77}$$

A.6.2 Insertion for an Antenna Between an Initial State and a Final State

The Massless Case

Here the $(n+1)$-particle phase space is given by a convolution:

$$d\phi_{n+1} = \int_0^1 dx\, d\phi_n(xp_a)\, d\phi_{\text{dipole}}. \tag{A.78}$$

The dipole phase space reads:

$$d\phi_{\text{dipole}} = \frac{\left|2\tilde{p}_{ij}p_a\right|}{32\pi^3}\int_0^1 dz \int_0^{2\pi} d\phi_s. \tag{A.79}$$

The angle ϕ_s parametrises the solid angle perpendicular to $\tilde{p}_{ij}$ and xp_a. Therefore we can treat the case of a final-state emitter with an initial-state spectator as well as the case of an initial-state emitter with a final-state spectator at the same time. x and z are related to the invariants as follows:

$$x = \frac{-2p_ip_a - 2p_jp_a - 2p_ip_j}{-2p_ip_a - 2p_jp_a}, \quad z = \frac{-2p_ip_a}{-2p_ip_a - 2p_jp_a}. \tag{A.80}$$

For the phase space generation we set:

$$x = 1 - u_1, \quad z = u_2, \quad \phi_s = 2\pi u_3. \tag{A.81}$$

We denote $Q = \tilde{p}_{ij} + x p_a = p_i + p_j + p_a$. It is convenient to work in the rest frame of $P = p_i + p_j = Q - p_a$ and to orient the frame such that p_a is along the z-axis. For the invariants we have:

$$2p_i p_j = \left(-Q^2\right) \frac{1-x}{x}, \quad 2p_i p_a = \frac{z}{x} Q^2, \quad 2p_j p_a = \frac{1-z}{x} Q^2. \tag{A.82}$$

In this frame

$$\begin{aligned} p_i' &= E_i(1, \sin\theta_{ia}\cos\phi_s, \sin\theta_{ia}\sin\phi_s, \cos\theta_{ia}), \\ p_j' &= E_i(1, -\sin\theta_{ia}\cos\phi_s, -\sin\theta_{ia}\sin\phi_s, -\cos\theta_{ia}), \\ p_a' &= \left(-|E_a|, 0, 0, |E_a|\,\mathrm{sign}(p_a^{z\prime})\right). \end{aligned} \tag{A.83}$$

We have

$$E_i = \frac{1}{2}|P|, \quad E_a = \frac{1}{|P|}(P \cdot p_a), \quad \theta_{ia} = \arccos\left[\mathrm{sign}(p_a^{z\prime})\left(-1 + \frac{2p_i p_a}{2E_i E_a}\right)\right]. \tag{A.84}$$

The momenta p_i', p_j' are again related to the momenta p_i, p_j by a sequence of Lorentz transformations as in equation (A.58). The weight is given by:

$$w = \frac{\left|Q^2\right|}{16\pi^2 x}. \tag{A.85}$$

The Massive Case

The dipole phase space now reads:

$$d\phi_{\text{dipole}} = \frac{\left|2\tilde{p}_{ij}p_a\right|}{32\pi^3} \int_{z_-}^{z_+} dz \int_0^{2\pi} d\phi_s. \tag{A.86}$$

The integration boundaries are given by:

$$z_+ = 1, \quad z_- = \frac{\mu^2}{1 - x + \mu^2}, \tag{A.87}$$

where

$$\mu^2 = \frac{m_i^2}{\left|2\tilde{p}_{ij}p_a\right|} = \frac{x m_i^2}{\left|Q^2 - m_i^2\right|}. \tag{A.88}$$

We consider only the case where $m_{\tilde{ij}} = m_i = m$ and all other masses are zero. For the phase space generation we set:

$$x = 1 - u_1, \quad z = (z_+ - z_-)\,u_2 + z_-, \quad \phi_s = 2\pi u_3. \tag{A.89}$$

For the invariants we have now:

$$2p_i p_j = \left(-Q^2 + m_i^2\right) \frac{1-x}{x}, \quad 2p_i p_a = \frac{z}{x}\left(Q^2 - m_i^2\right), \quad 2p_j p_a = \frac{1-z}{x}\left(Q^2 - m_i^2\right). \tag{A.90}$$

We parametrise the momenta as:

$$\begin{aligned} p_i' &= |\vec{p}_i|\,(\frac{E_i}{|\vec{p}_i|}, \sin\theta_{ia}\cos\phi_s, \sin\theta_{ia}\sin\phi_s, \cos\theta_{ia}), \\ p_j' &= |\vec{p}_i|\,(1, -\sin\theta_{ia}\cos\phi_s, -\sin\theta_{ia}\sin\phi_s, -\cos\theta_{ia}), \\ p_a' &= (-|E_a|, 0, 0, |E_a|\,\mathrm{sign}(p_a^{z\prime}))\,. \end{aligned} \tag{A.91}$$

Then

$$E_i = \frac{P^2+m_i^2}{2|P|}, \quad E_a = \frac{1}{|P|}(P\cdot p_a), \quad \theta_{ia} = \arccos\left[\mathrm{sign}(p_a^{z\prime})\frac{(2E_iE_a - 2p_ip_a)}{2|\vec{p}_i|\,(-E_a)}\right]. \tag{A.92}$$

The momenta p_i', p_j' are again related to the momenta p_i, p_j by a sequence of Lorentz transformations as in equation (A.58). The weight is given by:

$$w = \frac{\left|Q^2 - m_i^2\right|}{16\pi^2 x}(z_+ - z_-)\,. \tag{A.93}$$

A.6.3 Insertion for an Initial-State Antenna

Here we only have to consider the case where all particles are massless. In this case we transform all the final-state momenta. The $(n+1)$-particle phase space is given by a convolution:

$$d\phi_{n+1} = \int_0^1 dx\, d\phi_n(xp_a)\, d\phi_{\mathrm{dipole}}. \tag{A.94}$$

The dipole phase space reads:

$$d\phi_{\mathrm{dipole}} = \frac{|2p_ap_b|}{32\pi^3}\int_0^{1-x} dv \int_0^{2\pi} d\phi_s. \tag{A.95}$$

The variable v is given by:

$$v = \frac{-2p_ap_i}{2p_ap_b}. \tag{A.96}$$

For the phase space generation we set:

$$x = 1-u_1, \quad v = (1-x)(1-u_2), \quad \phi_s = 2\pi u_3. \tag{A.97}$$

We denote

$$K = -p_a - p_b - p_i, \quad \tilde{K} = -\tilde{p}_{ai} - p_b. \tag{A.98}$$

We have

$$\begin{aligned} p_a &= \frac{1}{x}\tilde{p}_{ai}, \\ p_i &= \Lambda_{\mathrm{boost}} E_i\,(1, \sin\theta_{ia}\cos\phi_s, \sin\theta_{ia}\sin\phi_s, \cos\theta_{ia})\,, \\ p_b &= p_b, \end{aligned} \tag{A.99}$$

with E_i and θ_{ia} given in the rest frame of $p_a + p_b$ by:

$$\begin{aligned} E_a &= -\frac{1}{2}\sqrt{2p_a p_b}\,, \\ E_i &= \frac{\tilde{K}^2 - 2p_a p_b}{4E_a}\,, \\ \theta_{ia} &= \arccos\left[\mathrm{sign}(\hat{p}_a^z)\left(-1 + \frac{2p_i p_a}{2E_i E_a}\right)\right]. \end{aligned} \tag{A.100}$$

$\hat{p}_a$ denotes p_a in the rest frame of $p_a + p_b$. Λ_{boost} transforms from the rest frame of $p_a + p_b$ to the lab frame. All other final-state momenta are transformed with:

$$\Lambda^{-1} = g^{\mu\nu} - 2\frac{\left(K+\tilde{K}\right)^{\mu}\left(K+\tilde{K}\right)^{\nu}}{\left(K+\tilde{K}\right)^2} + 2\frac{K^{\mu}\tilde{K}^{\nu}}{K^2}. \tag{A.101}$$

The weight is given by:

$$w = \frac{\left|\tilde{K}^2\right|}{16\pi^2 x}(1-x). \tag{A.102}$$

Bibliography

[1] C.P. Burgess and G.D. Moore, *The Standard Model: A Primer* (Cambridge, UK, 2007), 542 p.

[2] M.E. Peskin and D.V. Schroeder, *An Introduction to Quantum Field Theory* (Boulder, Colorado, 1995), 842 p.

[3] H. Fritzsch and M. Gell-Mann, *Current Algebra: Quarks and What Else?*, in J. D. Jackson and A. Roberts (ed.), *Proceedings of the XVI International Conference on High Energy Physics, Chicago, 1972*, Volume 2, pp. 135–165, arXiv: hep-ph/0208010

[4] H. Fritzsch and M. Gell-Mann, *Scale Invariance and the Light Cone*, in M. Dal Cin, G. J. Iverson and A. Perlmutter (ed.), *Broken Scale Invariance and the Light Cone* (New York, 1971), pp. 1–42

[5] H. Fritzsch, M. Gell-Mann and H. Leutwyler, *Advantages of the Color Octet Gluon Picture*, Phys. Lett. B47 (1973) pp. 365–368, introduced the term "color"

[6] D.J. Gross and F. Wilczek, *Ultraviolet Behavior of Non-Abelian Gauge Theories*, Phys. Rev. Lett. 30 (1973) pp. 1343–1346

[7] H.D. Politzer, *Reliable Perturbative Results for Strong Interactions?*, Phys. Rev. Lett. 30 (1973) pp. 1346–1349

[8] S.L. Glashow, *Partial-Symmetries of Weak Interactions*, Nucl. Phys. 22 (1961) pp. 579–588

[9] S. Weinberg, *A Model of Leptons*, Phys. Rev. Lett. 19 (1967) pp. 1264–1266

[10] A. Salam, *Weak and Electromagnetic Interactions*, in N. Svartholm (ed.): *Elementary Particle Theory, Relativistic Groups and Analyticity, Proceedings of the Nobel Symposium Held 1968 at Lerum, Sweden* (Stockholm, 1968), pp. 367–377

[11] T. Nakano and K. Nishijima, *Charge Independence for V-Particles*, Prog. Theor. Phys. 10 (1953) pp. 581–582

[12] K. Nishijima, *Charge Independence Theory of V Particles*, Prog. Theor. Phys. 13 (1955) pp. 285–304

[13] M. Gell-Mann, *The Interpretation of the New Particles as Displaced Charge Multiplets*, Nuovo Cim. 4 (1956) pp. 848–866

[14] M. Gell-Mann, *A Schematic Model of Baryons and Mesons*, Phys. Lett. 8 (1964) pp. 214–215, quarks as constituents of baryons and mesons were introduced. Shoichi Sakata proposed that proton, neutron and Λ form a fundamental triplet. Baryons are made of three of them and mesons from particle-antiparticle pairs (*On a Composite Model for the New Particles*, Prog. Theor. Phys. 16 (1956) pp. 686–688).

[15] G. Zweig, *An SU_3 Model for Strong Interaction Symmetry and its Breaking*, (1964), CERN-TH-401 and CERN-TH-412, also in D.B. Lichtenberg, S.P. Rosen (ed.), *Developments in the Quark Theory of Hadrons*, vol. 1, (Nonantum, Mass., 1980), pp. 22–101, Zweig called the constituents "aces"

[16] Particle Data Group, K. Nakamura et al., *Review of Particle Physics*, J. Phys. G37 (2010) 075021, online version available at `http://pdg.lbl.gov/`

[17] L.D. Faddeev and V.N. Popov, *Feynman Diagrams for the Yang–Mills Field*, Phys. Lett. B25 (1967) pp. 29–30

[18] N. Cabibbo, *Unitary Symmetry and Leptonic Decays*, Phys. Rev. Lett. 10 (1963) pp. 531–533

[19] M. Kobayashi and T. Maskawa, *CP-Violation in the Renormalizable Theory of Weak Interaction*, Prog. Theor. Phys. 49 (1973) pp. 652–657

[20] B. Pontecorvo, *Mesonium and Antimesonium*, Sov. Phys. JETP 6 (1957) pp. 429–431

[21] B. Pontecorvo, *Inverse Beta Processes and Nonconservation of Lepton Charge*, Sov. Phys. JETP 7 (1958) pp. 172–173, for Pontecorvo's contributions to neutrino physics see U. Dore and L. Zanello, *Bruno Pontecorvo and Neutrino Physics*, (2009), arXiv: 0910.1657

[22] Z. Maki, M. Nakagawa and S. Sakata, *Remarks on the Unified Model of Elementary Particles*, Prog. Theor. Phys. 28 (1962) pp. 870–880

[23] J. Wess and B. Zumino, *Supergauge Transformations in Four Dimensions*, Nucl. Phys. B70 (1974) pp. 39–50

[24] S. Dimopoulos and H. Georgi, *Softly Broken Supersymmetry and SU(5)*, Nucl. Phys. B193 (1981) pp. 150–162

[25] S. Dimopoulos and D.W. Sutter, *The Supersymmetric Flavor Problem*, Nucl. Phys. B452 (1995) pp. 496–512, arXiv: hep-ph/9504415, they counted 110 physical parameters for the supersymmetric $SU(3) \times SU(2) \times U(1)$ theory with minimal particle content and general soft supersymmetry breaking terms.

[26] S. Weinberg, *Implications of Dynamical Symmetry Breaking*, Phys. Rev. D13 (1976) pp. 974–996

[27] S. Weinberg, *Implications of Dynamical Symmetry Breaking: An Addendum*, Phys. Rev. D19 (1979) pp. 1277–1280

[28] L. Susskind, *Dynamics of Spontaneous Symmetry Breaking in the Weinberg–Salam Theory*, Phys. Rev. D20 (1979) pp. 2619–2625

[29] K. Lane, *Two Lectures on Technicolor*, (2002), arXiv: hep-ph/0202255, review article

[30] N. Arkani-Hamed, S. Dimopoulos and G.R. Dvali, *The Hierarchy Problem and New Dimensions at a Millimeter*, Phys. Lett. B429 (1998) pp. 263–272, arXiv: hep-ph/9803315

[31] I. Antoniadis, N. Arkani-Hamed, S. Dimopoulos and G.R. Dvali, *New Dimensions at a Millimeter to a Fermi and Superstrings at a TeV*, Phys. Lett. B436 (1998) pp. 257–263, arXiv: hep-ph/9804398

[32] N. Arkani-Hamed, S. Dimopoulos and G.R. Dvali, *Phenomenology, Astrophysics, and Cosmology of Theories with Submillimeter Dimensions and TeV Scale Quantum Gravity*, Phys. Rev. D59 (1999) 086004, arXiv: hep-ph/9807344

[33] L. Randall and R. Sundrum, *Large Mass Hierarchy from a Small Extra Dimension*, Phys. Rev. Lett. 83 (1999) pp. 3370–3373, arXiv: hep-ph/9905221

[34] L. Randall and R. Sundrum, *An Alternative to Compactification*, Phys. Rev. Lett. 83 (1999) pp. 4690–4693, arXiv: hep-th/9906064

[35] T. Kaluza, *Zum Unitätsproblem der Physik*, Sitzungsber. Preuss. Akad. Wiss. Berlin (1921) pp. 966–972

[36] O. Klein, *Quantentheorie und fünfdimensionale Relativitätstheorie*, Z. Phys. 37 (1926) pp. 895–906

[37] S.D. Drell and T.M. Yan, *Massive Lepton-Pair Production in Hadron–Hadron Collisions at High Energies*, Phys. Rev. Lett. 25 (1970) pp. 316–320, erratum ibid. p. 902

[38] ATLAS collaboration, *ATLAS Detector and Physics Performance. Technical Design Report. Vol. 2*, CERN-LHCC-99-15

[39] CMS collaboration, G.L. Bayatian et al., *CMS Physics Technical Design Report, Volume II: Physics Performance*, J. Phys. G34 (2007) pp. 995–1579

[40] F. Englert and R. Brout, *Broken Symmetry and the Mass of Gauge Vector Mesons*, Phys. Rev. Lett. 13 (1964) pp. 321–323, received 26 June 1964, published 31 August 1964

[41] P.W. Higgs, *Broken Symmetries, Massless Particles and Gauge Fields*, Phys. Lett. 12 (1964) pp. 132–133, received 27 July 1964, published 15 September 1964

[42] P.W. Higgs, *Broken Symmetries and the Masses of Gauge Bosons,* Phys. Rev. Lett. 13 (1964) pp. 508–509, received 31 August 1964, published 19 October 1964

[43] G.S. Guralnik, C.R. Hagen and T.W.B. Kibble, *Global Conservation Laws and Massless Particles,* Phys. Rev. Lett. 13 (1964) pp. 585–587, received 12 October 1964, published 16 November 1964, see also G. S. Guralnik, *The History of the Guralnik, Hagen and Kibble development of the Theory of Spontaneous Symmetry Breaking and Gauge Particles*, IJMPA 24 (2009) pp. 2601–2627, arXiv: 0907.3466

[44] LEP Working Group for Higgs Boson Searches, R. Barate et al., *Search for the Standard Model Higgs Boson at LEP*, Phys. Lett. B565 (2003) pp. 61–75, arXiv: hep-ex/0306033

[45] L. Evans and P. Bryant (ed.), *LHC Machine,* JINST 3 (2008) S08001

[46] *LHC The Guide,* (2009), see `http://cdsweb.cern.ch/record/1165534/files/CERN-Brochure-2009-003-Eng.pdf` (a brochure of the interested public)

[47] O.S. Brüning (ed.) et al., *LHC Design Report. Vol. I: The LHC Main Ring,* CERN-2004-003-V-1, `http://lhc.web.cern.ch/LHC/LHC-DesignReport.html`

[48] M.J. Syphers, *Analytical Description of Tevatron Integrated Luminosity,* Presented at Particle Accelerator Conference (PAC 09), Vancouver, BC, Canada, 4–8 May 2009, available at `http://trshare.triumf.ca/~pac09proc/Proceedings/papers/we6pfp033.pdf`

[49] F. Gianotti et al., *Physics Potential and Experimental Challenges of the LHC Luminosity Upgrade*, Eur. Phys. J. C39 (2005) pp. 293–333, arXiv: hep-ph/0204087

[50] D. Bortoletto, *The ATLAS and CMS Plans for the LHC Luminosity Upgrade*, (2008), arXiv: 0809.0671

[51] VLHC Design Study Group, G. Ambrosio et al., *Design Study for a Staged Very Large Hadron Collider,* (2001), SLAC-R-591

[52] J. Brau (ed.) et al., *International Linear Collider Reference Design Report. 1: Executive Summary. 2: Physics at the ILC. 3: Accelerator. 4: Detectors*, ILC-REPORT-2007-001, (2009), `http://ilcdoc.linearcollider.org/record/6321?ln=en`, see also Barry Barish, *A Technically Driven Timeline for the ILC,* (2007), `http://www.linearcollider.org/cms/?pid=1000422`

[53] CLIC Physics Working Group, E. Accomando et al., *Physics at the CLIC Multi-TeV Linear Collider*, (2004), arXiv: hep-ph/0412251, see also `http://clic-study.web.cern.ch/clic-study/`

[54] C.M. Ankenbrandt et al., *Status of Muon Collider Research and Development and Future Plans,* Phys. Rev. ST Accel. Beams 2 (1999) 081001, arXiv: physics/9901022

[55] W. Fischer, *Run Overview of the Relativistic Heavy Ion Collider*, (2009), http://www.agsrhichome.bnl.gov/RHIC/Runs/

[56] ATLAS collaboration, *ATLAS Detector and Physics Performance. Technical Design Report. Vol. 1*, CERN-LHCC-99-14, for the technical design reports of the single subdetectors see http://www.slac.stanford.edu/spires/find/hep/www?rawcmd=find+title+ATLAS+technical+design+report

[57] CMS collaboration, G.L. Bayatian et al., *CMS Physics: Technical Design Report. Volume I: Detector Performance and Software*, CERN-LHCC-2006-001, for the technical design reports of the single subdetectors see http://www.slac.stanford.edu/spires/find/ hep/www?rawcmd=find+title+CMS+technical+design+report

[58] LHCb collaboration, S. Amato et al., *LHCb Technical Proposal*, CERN-LHCC-98-04, for the subdetectors' TDRs see http://www.slac.stanford.edu/spires/find/hep/www?rawcmd=find+title+LHCb+technical+design+report

[59] TOTEM collaboration, V. Berardi et al., *TOTEM: Technical Design Report. Total Cross Section, Elastic Scattering and Diffraction Dissociation at the Large Hadron Collider at CERN*, CERN-LHCC-2004-002 and CERN-LHCC-2004-020

[60] ALICE collaboration, *ALICE: Technical Proposal for A Large Ion Collider Experiment at the CERN LHC*, CERN-LHCC-95-71, for the technical design reports of the single subdetectors see http://www.slac.stanford.edu/spires/find/hep/www?rawcmd=find+title+ALICE+technical+design+report

[61] LHCf collaboration, O. Adriani et al., *Technical Design Report of the LHCf Experiment: Measurement of Photons and Neutral Pions in the Very Forward Region of LHC*, CERN-LHCC-2006-004

[62] T. Kinoshita, *Mass Singularities of Feynman Amplitudes*, J. Math. Phys. 3 (1962) pp. 650–677

[63] T.D. Lee and M. Nauenberg, *Degenerate Systems and Mass Singularities*, Phys. Rev. 133 (1964) pp. B1549–B1562

[64] G. 't Hooft and M.J.G. Veltman, *Regularization and Renormalization of Gauge Fields*, Nucl. Phys. B44 (1972) pp. 189–213

[65] C.G. Bollini and J.J. Giambiagi, *Lowest Order "Divergent" Graphs in* ν*-Dimensional Space*, Phys. Lett. B40 (1972) pp. 566–568

[66] J.F. Ashmore, *A Method of Gauge-Invariant Regularization*, Lett. Nuovo Cim. 4 (1972) pp. 289–290

[67] G.M. Cicuta and E. Montaldi, *Analytic Renormalization via Continuous Space Dimension*, Nuovo Cim. Lett. 4 (1972) pp. 329–332

[68] W. Pauli and F. Villars, *On the Invariant Regularization in Relativistic Quantum Theory*, Rev. Mod. Phys. 21 (1949) pp. 434–444

[69] S. Tomonaga, *On a Relativistically Invariant Formulation of the Quantum Theory of Wave Fields*, Prog. Theor. Phys. 1 (1946) pp. 27–42

[70] J.S. Schwinger, *Quantum Electrodynamics. I. A Covariant Formulation*, Phys. Rev. 74 (1948) pp. 1439–1461

[71] R.P. Feynman, *The Theory of Positrons*, Phys. Rev. 76 (1949) pp. 749–759

[72] R.P. Feynman, *Space-Time Approach to Quantum Electrodynamics*, Phys. Rev. 76 (1949) pp. 769–789, some of Feynman's ideas (like space–time diagrams for processes such as Compton scattering and positrons as electrons travelling backwards in time) were already published by Zisman in 1940 and 1941, see Г. А. Зисман, *Теория Позитрона*, ЖЭТФ 10 (1940) pp. 1163–1167 and 11 (1941) pp. 631–641

[73] F.J. Dyson, *The Radiation Theories of Tomonaga, Schwinger, and Feynman*, Phys. Rev. 75 (1949) pp. 486–502

[74] F.J. Dyson, *The S Matrix in Quantum Electrodynamics*, Phys. Rev. 75 (1949) pp. 1736–1755

[75] H.A. Bethe, *The Electromagnetic Shift of Energy Levels*, Phys. Rev. 72 (1947) pp. 339–341

[76] J.S. Schwinger, *On Quantum-Electrodynamics and the Magnetic Moment of the Electron*, Phys. Rev. 73 (1948) pp. 416–417

[77] F.J. Dyson, *Divergence of Perturbation Theory in Quantum Electrodynamics*, Phys. Rev. 85 (1952) pp. 631–632

[78] L.N. Lipatov, *Divergence of the Perturbation-Theory Series and the Quasiclassical Theory*, Sov. Phys. JETP 45 (1977) pp. 216–223, also in J. C. Le Guillou and J. Zinn-Justin (ed.), *Large-Order Behaviour of Perturbation Theory* (Amsterdam, 1990), pp. 83–90

[79] J. Zinn-Justin, *Quantum Field Theory and Critical Phenomena* (Oxford, 1996), third edition, 1008 p. (Int. Ser. Monogr. Phys., 92), especially chapter 41 *Perturbation Theory at Large Orders and Instantons. The Summation Problem*, pp. 871–889

[80] U. Jentschura and G. Soff, *Divergence of Perturbation Theory and Resummation*, in U. Grundinger (ed.), *GSI Scientific Report 2000* (Darmstadt, 2000), p. 110, see also `http://www.gsi.de/informationen/wti/library/scientificreport2000/`

[81] I.M. Suslov, *Divergent Perturbation Series*, J. Exp. Theor. Phys. 100 (2005) pp. 1188–1233, arXiv: hep-ph/0510142

[82] A.V. Semenov, *LanHEP – a Package for the Automatic Generation of Feynman Rules in Field Theory. Version 3.0,* Comput. Phys. Commun. 180 (2009) pp. 431–454, arXiv: 0805.0555, see also `http://theory.npi.msu.su/~semenov/lanhep.html`

[83] J. Küblbeck, M. Böhm and A. Denner, *Feyn Arts – Computer-Algebraic Generation of Feynman Graphs and Amplitudes,* Comput. Phys. Commun. 60 (1990) pp. 165–180

[84] K.G. Chetyrkin, B.A. Kniehl and M. Steinhauser, *GEFICOM: Automated Generation and Computation of Feynman Diagrams in Quantum Chromodynamics up to Three Loops*, in T. Plesser (ed.), *Forschung und wissenschaftliches Rechnen* (Göttingen, 1998), pp. 127–142, see also `http://www.billingpreis.mpg.de/hbp97/inhalt97.htm`

[85] R. Harlander and M. Steinhauser, *Automatic Computation of Feynman Diagrams,* Prog. Part. Nucl. Phys. 43 (1999) pp. 167–228, arXiv: hep-ph/9812357

[86] S. Heinemeyer, *The Road Towards the International Linear Collider: Higgs, Top/Quantum Chromodynamics, Loops,* Pramana 69 (2007) pp. 727–733, arXiv: hep-ph/0611374

[87] R. Kleiss and H. Kuijf, *Multigluon Cross Sections and 5-Jet Production at Hadron Colliders,* Nucl. Phys. B312 (1989) pp. 616–644

[88] F.A. Berends and W. Giele, *The Six-Gluon Process as an Example of Weyl-van der Waerden Spinor Calculus,* Nucl. Phys. B294 (1987) pp. 700–732

[89] M.L. Mangano, S.J. Parke and Z. Xu, *Duality and Multi-Gluon Scattering,* Nucl. Phys. B298 (1988) pp. 653–672

[90] M.L. Mangano and S.J. Parke, *Multi-Parton Amplitudes in Gauge Theories,* Phys. Rept. 200 (1991) pp. 301–367, arXiv: hep-th/0509223

[91] F.A. Berends et al., *Single Bremsstrahlung Processes in Gauge Theories,* Phys. Lett. B103 (1981) pp. 124–128

[92] P. De Causmaecker, R. Gastmans, W. Troost and T.T. Wu, *Helicity Amplitudes for Massless QED,* Phys. Lett. B105 (1981) pp. 215–218

[93] P. De Causmaecker, R. Gastmans, W. Troost and T.T. Wu, *Multiple Bremsstrahlung in Gauge Theories at High Energies. (I). General Formalism for Quantum Electrodynamics,* Nucl. Phys. B206 (1982) pp. 53–60

[94] R. Kleiss and W.J. Stirling, *Spinor Techniques for Calculating $p\bar{p} \to W^{\pm}/Z^0$ + Jets,* Nucl. Phys. B262 (1985) pp. 235–262

[95] Z. Xu, D.H. Zhang and L. Chang, *Helicity Amplitudes for Multiple Bremsstrahlung in Massless Non-Abelian Gauge Theories,* Nucl. Phys. B291 (1987) pp. 392–428

[96] J.F. Gunion and Z. Kunszt, *Improved Analytic Techniques for Tree Graph Calculations and the $ggq\bar{q}l\bar{l}$ Subprocess,* Phys. Lett. B161 (1985) pp. 333–340

[97] R. Gastmans and T.T. Wu, *The Ubiquitous Photon: Helicity Method for QED and QCD* (Oxford, UK, 1990), 648 p. (International Series of Monographs on Physics, 80), gives a pedagogical introduction to the helicity method and – in the preface – a historical remark

[98] F.A. Berends and W.T. Giele, *Recursive Calculations for Processes with n Gluons*, Nucl. Phys. B306 (1988) pp. 759–808

[99] D.A. Kosower, *Light-Cone Recurrence Relations for QCD Amplitudes*, Nucl. Phys. B335 (1990) pp. 23–44

[100] R. Penrose, *Twistor Algebra*, J. Math. Phys. 8 (1967) pp. 345–366

[101] R. Penrose, *On the Origins of Twistor Theory*, in W. Rindler and A. Trautman (ed.), *Gravitation and Geometry: A Volume in Honour of Ivor Robinson* (Naples, 1987), pp. 341–361; see `http://users.ox.ac.uk/~tweb/00001/`

[102] R.S. Ward and R.O. Wells, *Twistor Geometry and Field Theory* (Cambridge, UK, 1990), 520 p.

[103] E. Witten, *Perturbative Gauge Theory as a String Theory in Twistor Space*, Commun. Math. Phys. 252 (2004) pp. 189–258, arXiv: hep-th/0312171

[104] F. Cachazo and P. Svrček, *Lectures on Twistor String Theory and Perturbative Yang–Mills Theory*, PoS RTN2005 (2005) 004, arXiv: hep-th/0504194

[105] F. Cachazo, P. Svrček and E. Witten, *MHV Vertices and Tree Amplitudes in Gauge Theory*, JHEP 09 (2004) 006, arXiv: hep-th/0403047

[106] K. Risager, *A Direct Proof of the CSW Rules*, JHEP 12 (2005) 003, arXiv: hep-th/0508206

[107] S.J. Parke and T.R. Taylor, *Amplitude for n-Gluon Scattering*, Phys. Rev. Lett. 56 (1986) pp. 2459–2460

[108] R. Britto, F. Cachazo and B. Feng, *New Recursion Relations for Tree Amplitudes of Gluons*, Nucl. Phys. B715 (2005) pp. 499–522, arXiv: hep-th/0412308

[109] R. Britto, F. Cachazo, B. Feng and E. Witten, *Direct Proof of the Tree-Level Scattering Amplitude Recursion Relation in Yang–Mills Theory*, Phys. Rev. Lett. 94 (2005) 181602, arXiv: hep-th/0501052

[110] P.D. Draggiotis, R.H.P. Kleiss, A. Lazopoulos and C.G. Papadopoulos, *Diagrammatic Proof of the BCFW Recursion Relation for Gluon Amplitudes in QCD*, Eur. Phys. J. C46 (2006) pp. 741–750, arXiv: hep-ph/0511288

[111] D. Vaman and Y.P. Yao, *QCD Recursion Relations from the Largest Time Equation*, JHEP 04 (2006) 030, arXiv: hep-th/0512031

[112] S.D. Badger, E.W.N. Glover, V.V. Khoze and P. Svrček, *Recursion Relations for Gauge Theory Amplitudes with Massive Particles*, JHEP 07 (2005) 025, arXiv: hep-th/0504159

[113] J. Bedford, A. Brandhuber, B.J. Spence and G. Travaglini, *A Recursion Relation for Gravity Amplitudes*, Nucl. Phys. B721 (2005) pp. 98–110, arXiv: hep-th/0502146

[114] C. Schwinn and S. Weinzierl, *On-shell Recursion Relations for all Born QCD Amplitudes*, JHEP 04 (2007) 072, arXiv: hep-ph/0703021

[115] R.K. Ellis, W.J. Stirling and B.R. Webber, *QCD and Collider Physics* (Cambridge, 1996), 435 p., (Camb. Monogr. Part. Phys. Nucl. Phys. Cosmol., 8), especially chapter 5 *Parton Branching and Jet Simulation*, pp. 157–192, see `http://www.hep.phy.cam.ac.uk/theory/webber/QCDupdates.html` for a list of updates and corrections

[116] S. Brandt, C. Peyrou, R. Sosnowski and A. Wroblewski, *The Principal Axis of Jets – An Attempt to Analyze High-Energy Collisions as Two-Body Processes*, Phys. Lett. 12 (1964) pp. 57–61

[117] E. Farhi, *Quantum Chromodynamics Test for Jets*, Phys. Rev. Lett. 39 (1977) pp. 1587–1588

[118] N. Metropolis and S. Ulam, *The Monte Carlo Method*, J. Amer. Statistical Assoc. 44 (1949) pp. 335–341, see also S. Ulam, R. D. Richtmyer and J. von Neumann, *Statistical Methods in Neutron Diffusion*, Los Alamos Scientific Laboratory report LAMS-551 (1947), published in A.R. Bednarek and F. Ulam (ed.), *Analogies Between Analogies. The Mathematical Reports of S.M. Ulam and his Los Alamos Collaborators* (Berkeley, 1990), pp. 17–36; see also N. Metropolis, *The Beginning of the Monte Carlo Method*, Los Alamos Science, No. 15 (1970) pp. 125–130

[119] T. Sjöstrand, S. Mrenna and P. Skands, *PYTHIA 6.4 Physics and Manual*, JHEP 05 (2006) 026, arXiv: hep-ph/0603175

[120] T. Sjöstrand, S. Mrenna and P. Skands, *A Brief Introduction to PYTHIA 8.1*, Comput. Phys. Commun. 178 (2008) pp. 852–867, arXiv: 0710.3820, see also `http://home.thep.lu.se/~torbjorn/Pythia.html`

[121] G. Corcella et al., *HERWIG 6.5: An Event Generator for Hadron Emission Reactions with Interfering Gluons (Including Supersymmetric Processes)*, JHEP 01 (2001) 010, arXiv: hep-ph/0011363, see also `http://hepwww.rl.ac.uk/theory/seymour/herwig/`

[122] S. Gieseke et al., *Herwig++ 1.0: An Event Generator for e^+e^- Annihilation*, JHEP 02 (2004) 005, arXiv: hep-ph/0311208

[123] M. Bähr et al., *Herwig++ 2.3 Release Note*, (2008), arXiv: 0812.0529, see also `http://projects.hepforge.org/herwig/`

[124] F.E. Paige, S.D. Protopopescu, H. Baer and X. Tata, *ISAJET 7.69: A Monte Carlo Event Generator for pp, $\bar{p}p$, and e^+e^- Reactions*, (2003), arXiv: hep-ph/0312045, see also http://www.nhn.ou.edu/∼isajet/

[125] T. Gleisberg et al., *SHERPA 1.α, a Proof-of-Concept Version*, JHEP 02 (2004) 056, arXiv: hep-ph/0311263, see also http://www.sherpa-mc.de/

[126] L. Lönnblad, *Ariadne Version 4 – A Program for Simulation of QCD Cascades Implementing the Colour Dipole Model*, Comput. Phys. Commun. 71 (1992) pp. 15–31, see also http://home.thep.lu.se/∼leif/ariadne/index.html

[127] M.L. Mangano et al., *ALPGEN, a Generator for Hard Multiparton Processes in Hadronic Collisions*, JHEP 07 (2003) 001, arXiv: hep-ph/0206293, see also http://mlm.home.cern.ch/mlm/alpgen/

[128] G. Altarelli and G. Parisi, *Asymptotic Freedom in Parton Language*, Nucl. Phys. B126 (1977) pp. 298–318

[129] Y.L. Dokshitzer, *Calculation of the Structure Functions for Deep-Inelastic Scattering and e^+e^- Annihilation by Perturbation Theory in Quantum Chromodynamics*, Sov. Phys. JETP 46 (1977) pp. 641–653

[130] V.N. Gribov and L.N. Lipatov, *Deep Inelastic ep Scattering in Perturbation Theory*, Sov. J. Nucl. Phys. 15 (1972) pp. 438–450

[131] V.V. Sudakov, *Vertex Parts at Very High Energies in Quantum Electrodynamics*, Sov. Phys. JETP 3 (1956) pp. 65–71

[132] R.D. Field and R.P. Feynman, *Quark Elastic Scattering as a Source of High-Transverse-Momentum Mesons*, Phys. Rev. D15 (1977) pp. 2590–2616

[133] R.D. Field and R.P. Feynman, *A Parametrization of the Properties of Quark Jets*, Nucl. Phys. B136 (1978) pp. 1–76

[134] X. Artru and G. Mennessier, *String Model and Multiproduction*, Nucl. Phys. B70 (1974) pp. 93–115

[135] M.G. Bowler, *e^+ e^- Production of Heavy Quarks in the String Model*, Zeit. Phys. C11 (1981) pp. 169–174

[136] B. Andersson, G. Gustafson and B. Soderberg, *A General Model for Jet Fragmentation*, Z. Phys. C20 (1983) pp. 317–329

[137] B. Andersson, G. Gustafson, G. Ingelman and T. Sjöstrand, *Parton Fragmentation and String Dynamics*, Phys. Rept. 97 (1983) pp. 31–145

[138] T. Sjöstrand, *Jet Fragmentation of Multiparton Configurations in a String Framework*, Nucl. Phys. B248 (1984) pp. 469–502

[139] D. Amati and G. Veneziano, *Preconfinement as a Property of Perturbative QCD*, Phys. Lett. B83 (1979) pp. 87–92

[140] A. Bassetto, M. Ciafaloni and G. Marchesini, *Color Singlet Distributions and Mass Damping in Perturbative QCD*, Phys. Lett. B83 (1979) pp. 207–212

[141] T. Sjöstrand, *A Model for Initial State Parton Showers*, Phys. Lett. B157 (1985) pp. 321–325

[142] G. Marchesini and B.R. Webber, *Monte Carlo Simulation of General Hard Processes with Coherent QCD Radiation*, Nucl. Phys. B310 (1988) pp. 461–526

[143] M. Dinsdale, M. Ternick and S. Weinzierl, *A Comparison of Efficient Methods for the Computation of Born Gluon Amplitudes*, JHEP 03 (2006) 056, arXiv: hep-ph/0602204

[144] Z. Bern and D.A. Kosower, *Color Decomposition of One-Loop Amplitudes in Gauge Theories*, Nucl. Phys. B362 (1991) pp. 389–448

[145] S. Catani and M.H. Seymour, *A General Algorithm for Calculating Jet Cross Sections in NLO QCD*, Nucl. Phys. B485 (1997) pp. 291–419, arXiv: hep-ph/9605323

[146] S. Weinzierl and D.A. Kosower, *QCD Corrections to Four-Jet Production and Three-Jet Structure in e^+e^- Annihilation*, Phys. Rev. D60 (1999) 054028, arXiv: hep-ph/9901277

[147] S. Weinzierl, *Automated Computation of Spin- and Colour-Correlated Born Matrix Elements*, Eur. Phys. J. C45 (2006) pp. 745–757, arXiv: hep-ph/0510157

[148] S. Catani and M.H. Seymour, *Erratum to "A General Algorithm for Calculating Jet Cross Sections in NLO QCD" [Nucl. Phys. B485 (1997) 291–419]*, Nucl. Phys. B510 (1998) pp. 503–504

[149] Z. Bern, *String-Based Perturbative Methods for Gauge Theories*, (1992), arXiv: hep-ph/9304249

[150] L.J. Dixon, *Calculating Scattering Amplitudes Efficiently*, (1996), arXiv: hep-ph/9601359

[151] C. Schwinn and S. Weinzierl, *Scalar Diagrammatic Rules for Born Amplitudes in QCD*, JHEP 05 (2005) 006, arXiv: hep-th/0503015

[152] C. Schwinn and S. Weinzierl, *Born Amplitudes in QCD from Scalar Diagrams*, Nucl. Phys. Proc. Suppl. 164 (2007) pp. 54–59, arXiv: hep-th/0510054

[153] D.A. Kosower, *Next-to-Maximal Helicity Violating Amplitudes in Gauge Theory*, Phys. Rev. D71 (2005) 045007, arXiv: hep-th/0406175

[154] I. Bena, Z. Bern and D.A. Kosower, *Twistor-Space Recursive Formulation of Gauge-Theory Amplitudes*, Phys. Rev. D71 (2005) 045008, arXiv: hep-th/0406133

[155] M. Dinsdale, M. Ternick and S. Weinzierl, *Parton Showers from the Dipole Formalism*, Phys. Rev. D76 (2007) 094003, arXiv: 0709.1026

[156] G. Marchesini and B.R. Webber, *Simulation of QCD Jets Including Soft Gluon Interference*, Nucl. Phys. B238 (1984) pp. 1–29

[157] B.R. Webber, *A QCD Model for Jet Fragmentation Including Soft Gluon Interference*, Nucl. Phys. B238 (1984) pp. 492–528

[158] G. Gustafson, *Dual Description of a Confined Colour Field*, Phys. Lett. B175 (1986) pp. 453–456

[159] G. Gustafson and U. Pettersson, *Dipole Formulation of QCD Cascades*, Nucl. Phys. B306 (1988) pp. 746–758

[160] B. Andersson, G. Gustafson and L. Lönnblad, *Gluon Splitting in the Colour Dipole Cascades*, Nucl. Phys. B339 (1990) pp. 393–405

[161] B. Andersson, G. Gustafson, L. Lönnblad and U. Pettersson, *Coherence Effects in Deep Inelastic Scattering*, Z. Phys. C43 (1989) pp. 625–632

[162] K. Kato and T. Munehisa, *Monte Carlo Approach to QCD Jets in the Next-to-Leading-Logarithmic Approximation*, Phys. Rev. D36 (1987) pp. 61–82

[163] K. Kato and T. Munehisa, *Double-Cascade Scheme for QCD Jets in e^+e^- Annihilation*, Phys. Rev. D39 (1989) pp. 156–162

[164] K. Kato and T. Munehisa, *NLLjet: A Monte Carlo Code for e^+e^- QCD Jets Including Next-to-Leading Order Terms*, Comput. Phys. Commun. 64 (1991) pp. 67–97

[165] H. Tanaka, T. Sugiura and Y. Wakabayashi, *Factorization Algorithm for Parton Showers Beyond the Leading Logarithmic Order of QCD*, Prog. Theor. Phys. 114 (2005) pp. 477–486, arXiv: hep-ph/0510185

[166] S. Catani, F. Krauss, R. Kuhn and B.R. Webber, *QCD Matrix Elements + Parton Showers*, JHEP 11 (2001) 063, arXiv: hep-ph/0109231

[167] F. Krauss, *Matrix Elements and Parton Showers in Hadronic Interactions*, JHEP 08 (2002) 015, arXiv: hep-ph/0205283

[168] A. Schälicke and F. Krauss, *Implementing the ME+PS Merging Algorithm*, JHEP 07 (2005) 018, arXiv: hep-ph/0503281

[169] M.L. Mangano, M. Moretti and R. Pittau, *Multijet Matrix Elements and Shower Evolution in Hadronic Collisions: $Wbb+n$ Jets as a Case Study*, Nucl. Phys. B632 (2002) pp. 343–362, arXiv: hep-ph/0108069

[170] S. Mrenna and P. Richardson, *Matching Matrix Elements and Parton Showers with HERWIG and PYTHIA*, JHEP 05 (2004) 040, arXiv: hep-ph/0312274

[171] H. Baer and M.H. Reno, *Complete $\mathcal{O}(\alpha_s)$ Event Generator for $p\bar{p} \to W^+X \to e^+\nu X$ with Parton Showering*, Phys. Rev. D44 (1991) pp. R3375–R3378

[172] H. Baer and M.H. Reno, *W and Z Production at $p\bar{p}$ Colliders: Parton Showers Merged with $\mathcal{O}(\alpha_s)$ Monte Carlo Approach*, Phys. Rev. D45 (1992) pp. 1503–1511

[173] C. Friberg and T. Sjöstrand, *Some Thoughts on how to Match Leading Log Parton Showers with NLO Matrix Elements*, (1999), arXiv: hep-ph/9906316

[174] S. Mrenna, *Higher Order Corrections to Parton Showering from Resummation Calculations*, (1999), arXiv: hep-ph/9902471

[175] B. Pötter, *Combining QCD Matrix Elements at Next-to-Leading Order with Parton Showers in Electroproduction*, Phys. Rev. D63 (2001) 114017, arXiv: hep-ph/0007172

[176] B. Pötter and T. Schörner, *Matching Parton Showers to the QCD-Improved Parton Model in Deep-Inelastic e P Scattering*, Phys. Lett. B517 (2001) pp. 86–92, arXiv: hep-ph/0104261, the preprint had another title

[177] M. Dobbs, *Incorporating Next-to-Leading Order Matrix Elements for Hadronic Diboson Production in Showering Event Generators*, Phys. Rev. D64 (2001) 034016, arXiv: hep-ph/0103174

[178] M. Dobbs, *Phase Space Veto Method for Next-to-Leading Order Event Generators in Hadronic Collisions*, Phys. Rev. D65 (2002) 094011, arXiv: hep-ph/0111234

[179] J. Collins, *Monte Carlo Event Generators at Nonleading Order*, Phys. Rev. D65 (2002) 094016, arXiv: hep-ph/0110113

[180] S. Frixione and B.R. Webber, *Matching NLO QCD Computations and Parton Shower Simulations*, JHEP 06 (2002) 029, arXiv: hep-ph/0204244

[181] M. Krämer and D.E. Soper, *Next-to-Leading Order QCD Calculations with Parton Showers. I. Collinear Singularities*, Phys. Rev. D69 (2004) 054019, arXiv: hep-ph/0306222

[182] D.E. Soper, *Next-to-Leading Order QCD Calculations with Parton Showers. II. Soft Singularities*, Phys. Rev. D69 (2004) 054020, arXiv: hep-ph/0306268

[183] P. Nason, *A new Method for Combining NLO QCD with Shower Monte Carlo Algorithms*, JHEP 11 (2004) 040, arXiv: hep-ph/0409146

[184] Z. Nagy and D.E. Soper, *Matching Parton Showers to NLO Computations*, JHEP 10 (2005) 024, arXiv: hep-ph/0503053

[185] Z. Nagy and D.E. Soper, *A new Parton Shower Algorithm: Shower Evolution, Matching at Leading and Next-to-Leading Order Level*, (2006), arXiv: hep-ph/0601021

[186] Z. Nagy and D.E. Soper, *Parton Showers with Quantum Interference*, JHEP 09 (2007) 114, arXiv: 0706.0017

[187] M. Krämer, S. Mrenna and D.E. Soper, *Next-to-Leading Order QCD Jet Production with Parton Showers and Hadronization*, Phys. Rev. D73 (2006) 014022, arXiv: hep-ph/0509127

[188] Y. Kurihara et al., *QCD Event Generators with Next-to-Leading Order Matrix-Elements and Parton Showers*, Nucl. Phys. B654 (2003) pp. 301–319, arXiv: hep-ph/0212216

[189] S. Odaka and Y. Kurihara, *Initial-State Parton Shower Kinematics for NLO Event Generators*, Eur. Phys. J. C51 (2007) pp. 867–873, arXiv: hep-ph/0702138

[190] W.T. Giele, D.A. Kosower and P.Z. Skands, *A Simple Shower and Matching Algorithm*, Phys. Rev. D78 (2008) 014026, arXiv: 0707.3652

[191] S. Frixione, P. Nason and G. Ridolfi, *The POWHEG-hvq Manual Version 1.0*, (2007), arXiv: 0707.3081, see also `http://moby.mib.infn.it/~nason/POWHEG/`

[192] S. Frixione, P. Nason and G. Ridolfi, *A Positive-Weight Next-to-Leading-Order Monte Carlo for Heavy Flavour Hadroproduction*, JHEP 09 (2007) 126, arXiv: 0707.3088

[193] O. Latunde-Dada, S. Gieseke and B. Webber, *A Positive-Weight Next-to-Leading-Order Monte Carlo for e^+e^- Annihilation to Hadrons*, JHEP 02 (2007) 051, arXiv: hep-ph/0612281

[194] O. Latunde-Dada, *Herwig++ Monte Carlo at Next-to-Leading Order for e^+e^- Annihilation and Lepton Pair Production*, JHEP 11 (2007) 040, arXiv: 0708.4390

[195] T. Sjöstrand and P.Z. Skands, *Transverse-Momentum-Ordered Showers and Interleaved Multiple Interactions*, Eur. Phys. J. C39 (2005) pp. 129–154, arXiv: hep-ph/0408302

[196] S. Gieseke, P. Stephens and B. Webber, *New Formalism for QCD Parton Showers*, JHEP 12 (2003) 045, arXiv: hep-ph/0310083

[197] L. Lönnblad, *Correcting the Colour-Dipole Cascade Model with Fixed Order Matrix Elements*, JHEP 05 (2002) 046, arXiv: hep-ph/0112284

[198] F. Krauss, R. Kuhn and G. Soff, *AMEGIC++ 1.0: A Matrix Element Generator in C++*, JHEP 02 (2002) 044, arXiv: hep-ph/0109036

[199] F. Krauss, A. Schälicke and G. Soff, *APACIC++ 2.0: A Parton Cascade in C++*, Comput. Phys. Commun. 174 (2006) pp. 876–902, arXiv: hep-ph/0503087

[200] S. Gieseke, *Uncertainties of Sudakov Form Factors*, JHEP 01 (2005) 058, arXiv: hep-ph/0412342

[201] P. Stephens and A. van Hameren, *Propagation of Uncertainty in a Parton Shower*, (2007), arXiv: hep-ph/0703240

[202] C.W. Bauer and F.J. Tackmann, *Gaining Analytic Control of Parton Showers*, Phys. Rev. D76 (2007) 114017, arXiv: 0705.1719

[203] C.W. Bauer and M.D. Schwartz, *Event Generation from Effective Field Theory*, Phys. Rev. D76 (2007) 074004, arXiv: hep-ph/0607296

[204] S. Frixione, P. Nason and B.R. Webber, *Matching NLO QCD and Parton Showers in Heavy Flavour Production*, JHEP 08 (2003) 007, arXiv: hep-ph/0305252

[205] S. Frixione, E. Laenen, P. Motylinski and B.R. Webber, *Single-Top Production in MC@NLO*, JHEP 03 (2006) 092, arXiv: hep-ph/0512250

[206] S. Frixione, E. Laenen, P. Motylinski and B.R. Webber, *Angular Correlations of Lepton Pairs from Vector Boson and Top Quark Decays in Monte Carlo Simulations*, JHEP 04 (2007) 081, arXiv: hep-ph/0702198

[207] S. Frixione and B.R. Webber, *The MC@NLO 3.4 Event Generator*, (2008), arXiv: 0812.0770, see also `http://www.hep.phy.cam.ac.uk/theory/webber/MCatNLO/`

[208] S. Dittmaier, *A General Approach to Photon Radiation off Fermions*, Nucl. Phys. B565 (2000) pp. 69–122, arXiv: hep-ph/9904440

[209] L. Phaf and S. Weinzierl, *Dipole Formalism with Heavy Fermions*, JHEP 04 (2001) 006, arXiv: hep-ph/0102207

[210] S. Catani, S. Dittmaier, M.H. Seymour and Z. Trócsányi, *The Dipole Formalism for Next-to-Leading Order QCD Calculations with Massive Partons*, Nucl. Phys. B627 (2002) pp. 189–265, arXiv: hep-ph/0201036

[211] Y.L. Dokshitzer, G. Marchesini and B.R. Webber, *Dispersive Approach to Power-Behaved Contributions in QCD Hard Processes*, Nucl. Phys. B469 (1996) pp. 93–142, arXiv: hep-ph/9512336

[212] S. Schumann and F. Krauss, *A Parton Shower Algorithm Based on Catani–Seymour Dipole Factorisation*, JHEP 03 (2008) 038, arXiv: 0709.1027

[213] S. Schumann, *Simulation of Signal and Background Processes for Collider Experiments*, Ph.D. thesis, University of Dresden (2008), see `http://deposit.ddb.de/cgi-bin/dokserv?idn=988337630`

[214] P. Cvitanović, P.G. Lauwers and P.N. Scharbach, *Gauge Invariance Structure of Quantum Chromodynamics*, Nucl. Phys. B186 (1981) pp. 165–186

[215] D. Kosower, B.H. Lee and V.P. Nair, *Multi Gluon Scattering: A String-Based Calculation*, Phys. Lett. B201 (1988) pp. 85–89

[216] V. Del Duca, L.J. Dixon and F. Maltoni, *New Color Decompositions for Gauge Amplitudes at Tree and Loop Level*, Nucl. Phys. B571 (2000) pp. 51–70, arXiv: hep-ph/9910563

[217] F. Maltoni, K. Paul, T. Stelzer and S. Willenbrock, *Color-Flow Decomposition of QCD Amplitudes*, Phys. Rev. D67 (2003) 014026, arXiv: hep-ph/0209271

[218] O. Heaviside, *On Operators in Physical Mathematics. Part I*, Proc. Roy. Soc. Lond. 52 (1892–1893) pp. 504–529, especially p. 513

[219] P.A.M. Dirac, *The Physical Interpretation of the Quantum Dynamics*, Proc. Roy. Soc. Lond. A113 (1927) pp. 621–641, for the history of the delta-function before Dirac, see B. van der Pol and H. Bremmer, *Operational Calculus* (New York, 1987), third edition, chapter V.4 *History of the Impulse Function*, pp. 62–66; see also K.-H. Peters, *Der Zusammenhang von Mathematik und Physik am Beispiel der Geschichte der Distributionen*, Ph.D. thesis, University of Hamburg (2003), available at `http://deposit.d-nb.de/cgi-bin/dokserv?idn=972150358`, also published as *Schönheit, Exaktheit, Wahrheit. Der Zusammenhang von Mathematik und Physik am Beispiel der Geschichte der Distributionen* (Berlin, 2004), ISBN 3-928186-74-4

[220] M.H. Seymour, *Matrix-Element Corrections to Parton Shower Algorithms*, Comp. Phys. Commun. 90 (1995) pp. 95–101, arXiv: hep-ph/9410414

[221] W.J. Stirling, *Hard QCD Working Group: Theory Summary*, J. Phys. G17 (1991) pp. 1567–1574

[222] O. Nachtmann and A. Reiter, *A Test for the Gluon Selfcoupling in the Reactions $e^+e^- \to$ 4 Jets and $Z^0 \to$ 4 Jets*, Z. Phys. C16 (1982) pp. 45–54

[223] J.G. Körner, G. Schierholz and J. Willrodt, *QCD Predictions for Four-Jet Final States in e^+e^- Annihilation. (II.) Angular Correlations as a Test of the Triple-Gluon Coupling*, Nucl. Phys. B185 (1981) pp. 365–381

[224] M. Bengtsson and P.M. Zerwas, *Four-Jet Events in e^+e^- Annihilation: Testing the Three-Gluon Vertex*, Phys. Lett. B208 (1988) pp. 306–308

[225] DELPHI collaboration, P. Abreu et al., *Experimental Study of the Triple-Gluon Vertex*, Phys. Lett. B255 (1991) pp. 466–476

[226] J. Pumplin et al., *New Generation of Parton Distributions with Uncertainties from Global QCD Analysis*, JHEP 07 (2002) 012, arXiv: hep-ph/0201195

[227] D. Stump et al., *Inclusive Jet Production, Parton Distributions, and the Search for New Physics*, JHEP 10 (2003) 046, arXiv: hep-ph/0303013

[228] C. Duhr, S. Höche and F. Maltoni, *Color-Dressed Recursive Relations for Multi-Parton Amplitudes*, JHEP 08 (2006) 062, arXiv: hep-ph/0607057

[229] S. Höche, *Perturbative QCD in Event Generation*, Ph.D. thesis, University of Durham (2009), see `http://www.freacafe.de/dnl/diss/diss_stefan.pdf`

[230] T. Gleisberg, S. Höche, F. Krauss and R. Matyszkiewicz, *How to Calculate Colourful Cross Sections Efficiently*, (2008), arXiv: 0808.3672

[231] Z. Bern, L.J. Dixon and D.A. Kosower, *On-shell Recurrence Relations for One-Loop QCD Amplitudes*, Phys. Rev. D71 (2005) 105013, arXiv: hep-th/0501240

[232] G. Ossola, C.G. Papadopoulos and R. Pittau, *Reducing Full One-Loop Amplitudes to Scalar Integrals at the Integrand Level*, Nucl. Phys. B763 (2007) pp. 147–169, arXiv: hep-ph/0609007

[233] G. Ossola, C.G. Papadopoulos and R. Pittau, *Numerical Evaluation of Six-Photon Amplitudes*, JHEP 07 (2007) 085, arXiv: 0704.1271

[234] G. Ossola, C.G. Papadopoulos and R. Pittau, *CutTools: A Program Implementing the OPP Reduction Method to Compute One-Loop Amplitudes*, JHEP 03 (2008) 042, arXiv: 0711.3596

[235] M. Veltman, *Diagrammatica: The Path to Feynman Rules* (Cambridge, UK, 1994), 284 p. (Cambridge lecture notes in physics, 4), *Appendix E*, especially pp. 249–257

[236] B.L. van der Waerden, *Spinoranalyse*, Nachr. Ges. Wiss. Gött. Math.-Phys. Kl. (1929) pp. 100–109, see also H. Weyl, *Gruppentheorie und Quantenmechanik* (Leipzig, 1928); B.L. van der Waerden, *Die gruppentheoretische Methode in der Quantenmechanik* (Berlin, 1932), pp. 78–87

[237] A. Kersch and F. Scheck, *Amplitude and Trace Reduction Using Weyl-van der Waerden Spinors: Pion Pair Decay* $\pi^+ \to e^+e^-e^+\nu_e$, Nucl. Phys. B263 (1986) pp. 475–492

[238] S. Dittmaier, *Weyl–van der Waerden Formalism for Helicity Amplitudes of Massive Particles*, Phys. Rev. D59 (1999) 016007, arXiv: hep-ph/9805445

[239] W. Pauli, *Zur Quantenmechanik des magnetischen Elektrons*, Z. Phys. 43 (1927) pp. 601–623

[240] J.A. Schouten, *Ueber die geometrische Deutung von gewöhnlichen p-Vektoren und W-p-Vektoren und den korrespondierenden Dichten*, Proc. Kon. Ned. Akad. v. Wet. 41 (1938) pp. 709–716, see also J.A. Schouten, *Tensor Analysis for Physicists* (Oxford, 1951), p. 66

[241] M. Fierz, *Zur Fermischen Theorie des* β*-Zerfalls*, Z. Phys. 104 (1937) pp. 553–565

[242] C.C. Nishi, *Simple Derivation of General Fierz-Type Identities*, Am. J. Phys. 73 (2005) pp. 1160–1163, arXiv: hep-ph/0412245

[243] M. Gell-Mann, *The Eightfold Way: A Theory of Strong Interaction Symmetry*, California Institute of Technology Synchrotron Laboratory Report CTSL-20 (1961), unpublished, available at `http://www.osti.gov/accomplishments/gellmann.html` reproduced in M. Gell-Mann and Y. Ne'eman, *The Eightfold Way. A Review with a Collection of Reprints* (New York, 1964), pp. 11–57

Acknowledgement

First of all I thank my supervisor Prof. Dr. Stefan Weinzierl for giving me the chance to work on a hot topic in high energy physics, for continuous support of any kind, and for taking time to answer all my questions patiently. His door is literally always open, and likewise his mind. I thank Prof. Dr. Hartmut Wittig for being the second reviewer. I thank Prof. Dr. Jürgen Körner for relaying my application for his group to my later thesis advisor. I thank Prof. Dr. Martin Reuter for writing an assessment in a very short amount of time, when I needed it urgently. I thank Prof. Dr. Hubert Spiesberger for solving any kind of computer related problems. I thank Michael Dinsdale Ph.D., a former postdoc in the group of Prof. Weinzierl. I thank Dr. Sven-Olaf Moch: I profited a lot from the things I learned while writing my diploma thesis under his supervision, and still do.

I thank Florian Jung for help with LaTeX and emacs, for the regular tea after lunch and for an introduction to the theory of Go. Dr. Alimjan Kadeer and Florian Jung I thank for carefully reading the manuscript and making many valuable remarks. For interesting discussions I thank Dr. Alimjan Kadeer, Dr. Martin Fischer, Dr. Stefan Groote, Christian Hundt, Florian Jung, Dr. Markus Knodel, Dr. Mikhail Rogal, and Dr. Erick Tuiran, as well as my office mates Mohammad Assadsolimani, Sebastian Becker and Sebastian Buchta, and everyone else in the group of Theoretical High Energy Physics at the University of Mainz.

I thank the German Research Foundation (Deutsche Forschungsgemeinschaft), whose postgraduate programme *Gauge theories – experimental tests and theoretical foundations* I had the honour to be a member of. The DFG scholarship does not only gave me the possibility to write this thesis, but also to attend NRW phenomenology meeting in Bad Honnef, Germany, January 13–14, 2006, where I had the opportunity to give a talk[1]; the KET-Workshop on QCD and electroweak physics at the LHC, October 16–17, 2006, at DESY Hamburg; the International School of Theoretical Physics, *New Physics at the LHC: from model building to event generation* in Parma, Italy, September 3–8, 2007; and the DPG Spring Meeting 2008 in Freiburg, Germany, March 3–7, 2008, where I also had the pleasure to present my work.

I thank the University of Mainz for a scholarship and for giving the access to research literature, may it be through online subscribing the most important scientific journals, through hard copies in the library or through ordering hard to find papers like the Russian ones in reference [72].

[1] available at `http://www.th.physik.uni-bonn.de/th/People/dreiner/HOME-PAGE/RESEARCH/NRW-PHENO/TALKS-06/Ternick.pdf`